Passive Damping Mechanism of Herschel-Quincke Tubes for Pressure Pulsations in Piping Systems

by

Thomas Lato

A Thesis Submitted in Partial Fulfillment
of the Requirements for the Degree of

Master of Applied Science

in
The Faculty of Engineering and Applied Science
Mechanical Engineering

University of Ontario Institute of Technology
Oshawa, Ontario, Canada

December, 2018

THESIS EXAMINATION INFORMATION

Submitted by: **Thomas Lato**

Master of Applied Science in **Mechanical Engineering**

Thesis title: Passive Damping Mechanism of Herschel-Quincke Tubes for Pressure Pulsations in Piping Systems

An oral defense of this thesis took place on December 3rd 2018 in front of the following examining committee:

Examining Committee:

Chair of Examining Committee	Dr. Haoxiang Lang
Research Supervisor	Dr. Atef Mohany
Research Co-supervisor	N/A
Examining Committee Member	Dr. Brendan MacDonald
Examining Committee Member	N/A
University Examiner	N/A
External Examiner	Dr. Moustafa El-Gindy, UOIT - Department of Automotive Engineering

The above committee determined that the thesis is acceptable in form and content and that a satisfactory knowledge of the field covered by the thesis was demonstrated by the candidate during an oral examination. A signed copy of the Certificate of Approval is available from the School of Graduate and Postdoctoral Studies.

Abstract

The acoustic pressure pulsations in industrial piping systems can induce fluctuating loads on inline equipment which may cause fatigue failure and in severe cases, initiate a phenomenon known as acoustic resonance. Passive damping devices such as the Herschel-Quincke (HQ) Tube can be implemented into a resonant system to mitigate the pressure pulsations. Some practical considerations have been clarified in the current work which include the normalization of the transmission loss with respect to the HQ tube to pipeline diameter ratio and the change in attenuation when placing an HQ device at different locations along the standing wave formed in the pipeline. The attenuation mechanism of the HQ device was clarified for the application to resonant piping systems. It was found that the second acoustic mode of an open-open pipe is excited within the device. A Computational Aeroacoustic simulation was performed to visualize the acoustic state variables within the HQ device.

Dedication

I would like to dedicate this work to my family as they were always a strong supporter of me throughout this important journey of my life. To my Mother Joanne, Sister Daniella, Father Tom, Nicolette and my grandparents.

Acknowledgment

I would like to take this opportunity to express my thanks and appreciation for my supervisor Dr. Atef Mohany, for his support, guidance and lessons which I hold in the highest regard. I believe that your encouraging words and endless shared knowledge have helped me to succeed through my goals and aspirations achieved throughout my undergraduate and MASc thesis experience. I look forward to future years of graduate studies with you. Thank you to the members of the Aeroacoustics and Noise Control Laboratory (ANCL) for your unconditional help and support. Dr. Nadim Arafa, Mahmoud Shaaban, Omar Sadek, Moamen Abdelmwgoud, Mohammed Alziadeh, Karim Sachedina and Rashidul Islam, you have all been so kind and I enjoyed our work efforts within the laboratory very much.

Thank you to the CANDU Owners Group (COG), the University Network of Excellence in Nuclear Engineering (UNENE), the Natural Sciences and Engineering Research Council of Canada (NSERC) and the University for the much appreciated financial support throughout this thesis.

To my closest friends, especially Timothy Batty, Adam McGilvray, Mark Manning, Jerome Arrieta, Michael Lambrou and Alexander Lopez, thank you for your dearest friendship and highly esteemed advice.

Finally, I would like to extend my most sincerest acknowledgement to my family. To my loving and kind mother, Joanne Lato and my beloved father, Tom Lato, thank you for your endless love, support and faith in me as I am so lucky to have such great parents to learn from your experience. To my sister Daniella Lato who is a PhD candidate at McMaster University, thank you for your support and guidance. You are the best sister I could hope for, your advice has been so helpful. Nicolette, Thank you for your love and encouragement as you have been so close to me during this crucial point in my life. I could have never, and would have never completed any of this without you by my side.

Contents

Abstract **iii**

Dedication **iv**

Acknowledgements **v**

Table of Contents **vi**

Nomenclature **ix**

List of Tables **xi**

List of Figures **xii**

1 Introduction **1**

1.1 Background and Motivation 1

1.2 Scope of the Work 2

1.3 Outline of the Thesis 4

2 Literature Review **5**

2.1 Sources of Acoustic Pressure Pulsations in Industrial Pipelines 5

2.1.1 Valves and Piping Components - Self-sustained Oscillations & Flow-induced Noise/Vibration 5

2.1.2 Centrifugal or Reciprocating Turbomachinery 8

2.2 Natural Damping of Acoustic Waves in Pipeline Systems 12
2.3 Amplification of Pressure Pulsations in Pipelines through Acoustic Resonance 13
2.4 Acoustic Damping Devices 21
2.4.1 Active Devices 21
2.4.2 Passive Devices 24
2.5 The Herschel-Quincke Tube 27
2.5.1 Conventional Mechanisms of Attenuation 28
2.5.2 Analytical Modeling 29
2.5.3 Applications with Mean Flow 38
2.5.4 Higher Order Modes 41
2.6 Summary and Research Needs 43

3 Experimental Setup **46**
3.1 The Test Setup 46
3.2 Herschel-Quincke Tube Design and Manufacturing 49
3.3 Measurement Techniques 50
3.3.1 Transmission Loss 51
3.3.2 Insertion Loss 54
3.3.3 Acoustic Reflection Coefficient, Specific Acoustic Impedance Ratio 54
3.3.4 Acoustic Pressure Signal Phase Measurements 56
3.4 Experimental Validation 57

4 Passive Damping of a Resonant Piping System **61**
4.1 Relative Diameter Ratio (d/D) 62
4.2 Axial Location of an HQ Device 70
4.3 Implementation of Multiple HQ Devices 73
4.4 Mean Flow and Directionality Effects 76

4.5 Summary and Conclusions 80

5 Attenuation Mechanism During Resonant Conditions 82

5.1 Acoustic Response of an HQ Device Under Resonant Conditions 83

5.2 Change in Specific Acoustic Impedance Ratio and the Acoustic Reflection Coefficient 88

5.3 Computational Aeroacoustic (CAA) Simulations 92

5.3.1 Simulation Setup, Mesh and Validation 92

5.3.2 HQ Device Simulation Results 101

5.4 Summary and Conclusions 107

6 Passive Damping of a Travelling Wave System 109

6.1 Relative Diameter Ratio (d/D) & Proximity to Adjacent Piping Components 110

6.2 Summary and Conclusions 116

7 Conclusions 118

7.1 Summary and Conclusions 118

7.2 Research Contributions 122

7.3 Recommendations for Future Work 123

7.4 Supporting Publications 124

Bibliography 125

Nomenclature

A,B,C,D	Four pole parameters
c	Speed of sound
CFL	Acoustic Courant-Fridrick-Lewy number
d	Diameter of HQ tube side branch
D	Diameter of HQ tube main branch
F	Froud number
f	Frequency
H	Transfer Function
$H^{'}$	Heaviside Function
h	Cross sectional area ratio for an expansion chamber
IL	Insertion Loss
i, j	Imaginary unit
k_0	Wavenumber
l	Spacing between microphones
L	Pipeline length
L_1	Length of Reactive Muffler
L_2	Length of HQ tube side branch
L_3	Length of HQ tube main branch
L_4	Length between the closest microphone and the test element
L_{Eff}	Effective Length
M	Mach number
m, n	Integer
N	Number of impeller blades
Pr	Prandtl number
PPW	Points per wavelength criteria
p	Acoustic Pressure

Nomenclature

R	Complex Reflection Coefficient
S	Cross sectional area of pipe
s	Shear number
SPL	Sound pressure level
TL	Transmission Loss
V	Volume
v	Velocity
$y\rho c$	Specific acoustic admittance ratio
$\frac{z}{\rho c}$	Specific acoustic impedance ratio
Z_0	Characteristic acoustic impedance

Greek letters

α	Pressure attenuation constant
δ, ϵ	Transmission loss coefficient
γ	Heat capacity ratio
λ	Wavelength
ω	Angular velocity of pump/compressor
ρ	Density of the fluid

Subscripts

i, j	Integers

List of Tables

2.1 Pressure measurement parameters for the set-up outlined in Fig. 9 Rzentkowski and Zbroja [21]. 15

4.1 Measured and analytically predicted shift in the 150 Hz resonant frequency of the total acoustic response of the piping system. HQ devices with d/D=0.25, 0.5 66

4.2 Measured and analytically predicted shift in the 150 Hz resonant frequency of the total acoustic response of the piping system for multiple HQ devices 68

5.1 Measured and simulated comparison of the acoustic pressure signal measured at various microphone locations outlined in the experimental set-up 97

List of Figures

1.1 Schematic of the Herschel-Quincke Device (HQ). 2

2.1 Design Guideline for SRV Valves, picture courtesy of Baldwin and Simmons [7]. 6

2.2 Steam Control Valve - Venturi Type, Yonezawa [10]. 7

2.3 Experimental set-up for investigating the acoustic source caused by the BPF of centrifugal pumps, Morgenroth & Weaver [12]. 9

2.4 Flow visualization at 40% nominal flow rate, 500 rpm - (left): sharp tip; (right): 5mm rounded tip (Morgenroth & Weaver) [12]. 9

2.5 Divided acoustic cells for determination of the sound emission from an ideal source, Keller et al. [14]. 10

2.6 Amplitude of the pressure fluctation at the blade passing frequency along the volute for several nominal flow rates. Circles: Experimental Data, Squares: Prediction from Ideal Sources Model, Keller et al. [14]. 12

2.7 Acoustic pressure distribution of an open-open pipe and a closed-open pipe. Pressure anti-nodes denoted as AN and pressure nodes denoted as N. 14

2.8 Experimental setup for the test-loop designed by Rzentkowski and Zbroja [21]. 15

2.9 Pressure spectrum of the pump discharge T=265 degree Celsius Rzentkowski and Zbroja [21]. 16

2.10 Pressure pulsations extracted at the blade passing frequency for several temperatures. Thick line: Discharge, Thin line: Suction Rzentkowski and Zbroja [21]. 17
2.11 Pressure pulsations extracted at the blade passing frequency for several axial locations along the test-loop (265 degrees Celsius) Rzentkowski and Zbroja [21]. 18
2.12 Open end test-loop experimental setup constructed for the work of Chatergoon and Li [22]. 19
2.13 A comparison of the turbulent flow and no flow cases for the open end test loop, Chatergoon and Li [22]. 20
2.14 a) Schematic of pipe-cavity with instrumentation and feedback loop b)Cross section of the cavity; $D_p = 0.14$ m, $D_0 = 0.067$ m and $L_c = 0.075$ m, Huang and Weaver [24]. 22
2.15 Hot-wire spectra compared with the shear layer visualization under the no control, enhancement and suppression conditions, Huang and Weaver [24]. 23
2.16 Experimental setup for the active noise control in a duct, Zimmer et al. [25]. 23
2.17 Schematic of a Helmholtz Resonator (HR) and its corresponding natural frequency of acoustic resonance. 25
2.18 Schematic of a Quarter Wave Resonator (QWR) and its corresponding natural frequency of acoustic resonance. 26
2.19 Schematic of a Herschel-Quincke Tube (HQ) 28
2.20 Experimental result and Analytical model comparison for the transmission of an HQ device, Stewart [39] 30
2.21 Schematic of an HQ device developed for the theoretical model created by Selamet [40] 30
2.22 Theoretical, computational and experimental comparison of the work done by Selamet [40] (d_1=d_2=4.859 cm, d_3=4.674 cm, l_2=39.85 cm, l_3=78.45cm). 32

2.23 Schematic of an Adaptive HQ Tube [43] 33
2.24 Transmission loss of the adaptive PVDF membrane HQ device for constant geometric parameters and changing values of applied voltage [43] 34
2.25 Schematic of adaptive HQ tubes using the a) ball and b) diaphragm devices [44] 34
2.26 Model of a straight wave guide with a single constriction [44] 35
2.27 Model of a straight wave guide with a smooth variable constriction [44] . . 36
2.28 Schematic of the experimental apparatus [44] 36
2.29 Impedance matrix coefficients for the diaphragm HQ tube. Applied pressure is 4.0 psi [44] 37
2.30 Frequency adaptation of resonance frequencies for ball-in HQ tube (left) and diaphragm HQ tube (right) [44] 37
2.31 Transmission loss contours: $l_1 = 2l_2$. Top M=0; bottom M=0.15 [45] 39
2.32 Simulated and measured transmission loss at a) M=0 and b) M=0.15 for an HQ device with $d/D = 1$ [47] 40

3.1 Schematic of the experimental set-up for the air loop pipeline system . . . 48
3.2 Schematic of the setup for the a) downstream and b) upstream incident acoustic wave configuration 48
3.3 Schematic of the moulding jig utilized during the manufacturing process of a PVC HQ device using thermoplastic heat treatment 50
3.4 Schematic of the two microphone wave decomposition set-up utilize to determine the acoustic reflection coefficient and specific acoustic impedance ratio 55
3.5 Schematic of the acoustic pressure signal phase measurements conducted within the HQ device and main piping system 57
3.6 Measured and theoretical[53], [54] comparison of the transmission loss of a reactive muffler: h=0.13 ,L_1=609.6 mm 58

3.7 Measured and theoretical[40] comparison of the transmission loss of a HQ tube with d/D=0.25 59
3.8 Measured and theoretical[55] comparison of the specific acoustic admittance ratio of an open unflanged circular pipe 60

4.1 Transmission loss measured for several HQ devices with varying diameter ratio 63
4.2 Extracted transmission loss peaks at the 150 Hz Type I peak normalized by relative diameter ratio 64
4.3 Natural acoustic response measured at a pressure antinode within the main piping system without and with HQ devices of varying relative diameter ratio 65
4.4 Natural acoustic response measured at a pressure antinode within the main piping system without and with multiple HQ devices 69
4.5 Transmission loss measured for various HQ device locations along the axial direction of the main piping system 71
4.6 Insertion loss measured for various HQ device locations along the axial direction of the main piping system 72
4.7 Comparison of multiple HQ devices attached to an acoustic pressure antinode on the measured transmission loss 74
4.8 Measured insertion loss for multiple HQ devices attached to a single acoustic pressure antinode 75
4.9 Schematic of two HQ devices of $d/D = 0.25$ attached to either a single acoustic pressure antinode (left) or different acoustic pressure antinodes (right) 76
4.10 Measured insertion loss for two HQ devices of $d/D = 0.25$ attached to either a single acoustic pressure antinode or different acoustic pressure antinodes 76

4.11 Comparison of mean flow with the measured transmission loss for an HQ device of d/D=0.25 78

4.12 Mean flow effect on the transmission loss measured for a downstream incident acoustic propagating wave, HQ device of d/D=0.25 79

4.13 Mean flow effect on the transmission loss measured for an upstream incident acoustic propagating wave, HQ device of d/D=0.25 80

5.1 Acoustic response measured within an HQ device subjected to a resonant piping system excited by a 150 Hz pulse signal 84

5.2 Transmission loss vs Length of the HQ device normalized by the targeted wavelength of attenuation. The second, third and fourth acoustic mode excited within the HQ device is studied. 86

5.3 Schematic of the operating mechanism of a Quarter Wave Resonator (QWR) 87

5.4 Imaginary component of the specific acoustic impedance ratio for a straight pipe module and subsequently for the addition of HQ devices with several relative diameter ratios 90

5.5 Measured acoustic reflection coefficient for an incident acoustic wave subjected to both an HQ device and QWR 91

5.6 Simulation domain and imposed boundary conditions for the CAA simulation conducted in ANSYS Fluent 93

5.7 Velocity inlet profile generated by Equation 5.1 to be implemented at the velocity inlet boundary condition located at the speaker diaphragm. 94

5.8 3D Structured/Unstructured Mesh used for ANSYS Fluent Simulation (interior elements not shown 95

5.9 Experimental and Simulated comparison of the acoustic pressure spectra measured at Microphone 1 location. Excitation source for both the simulation and experiment was set to a 150 Hz pulse signal 96

5.10 Simulated comparison of the acoustic pressure distribution along the pipeline at different points along the 150 Hz cycle. Excitation source was set to a 150 Hz pulse signal 99
5.11 Simulated comparison of the Top: acoustic pressure, $\phi = 0°$ and Bottom: acoustic particle velocity distribution, $\phi = 0°$ along the pipeline. Excitation source was set to a 150 Hz pulse signal 100
5.12 Top: Experimental and Bottom: Simulated comparison of the time signals for several locations along the HQ device 102
5.13 Experimental and Simulated comparison of the acoustic pressure spectra measured at the AN2 location within the HQ device. Excitation source for both the simulation and experiment was set to a 150 Hz pulse signal . . 103
5.14 Simulated comparison of the acoustic pressure contours along the HQ device for different time instances along the 150 Hz cycle. 104
5.15 Simulated acoustic particle total velocity contour within the HQ device. $\phi = 0°$ 105
5.16 Simulated comparison of the acoustic particle u-velocity contours along the HQ device at different points along the 150 Hz cycle. 106

6.1 Change in transmission loss for HQ devices applied to a resonant and travelling wave piping system 112
6.2 Resonant and travelling wave piping system comparison for insertion loss of an HQ device at multiple locations along the pipeline axis 113
6.3 Change in insertion loss with HQ device placement for multiple locations along a travelling wave piping system including an end termination located at a multiple of $\frac{\lambda}{2}$ away 114
6.4 Change in insertion loss with HQ device placement for multiple locations along a travelling wave piping system including an open T-connection located at a multiple of $\frac{\lambda}{2}$ away 115

Chapter 1

Introduction

1.1 Background and Motivation

Pressure pulsations in piping systems have been known to cause the failure of critical components within industrial pipelines [1]. If the energy provided by the pulsations emitted from equipment such as a centrifugal pump or compressor is sufficiently large enough to overcome the natural damping in the piping system, the coincidence between one of the natural frequencies of the piping system and this pulsation frequency may initiate acoustic resonance. The vibrations and noise caused by such a phenomenon has been observed in heat exchanger tube bundles [2] [3] as well as the flow over cavities found in HVAC, piping and aerospace applications [4] [5]. The pressure pulsations could be caused by dynamic instability of the unsteady flow or as a result of reciprocating or centrifugal equipment. Several studies have been performed in the literature to date to further understand the pressure pulsations emitted from centrifugal or reciprocating turbo machinery, the amplification of pressure pulsations in pipelines through acoustic resonance and the active and passive damping techniques which can be applied to mitigate such pulsations. However, there have been several practical considerations for industrial implementation of the Herschel-Quincke tube, shown in Figure 1.1, which have not yet

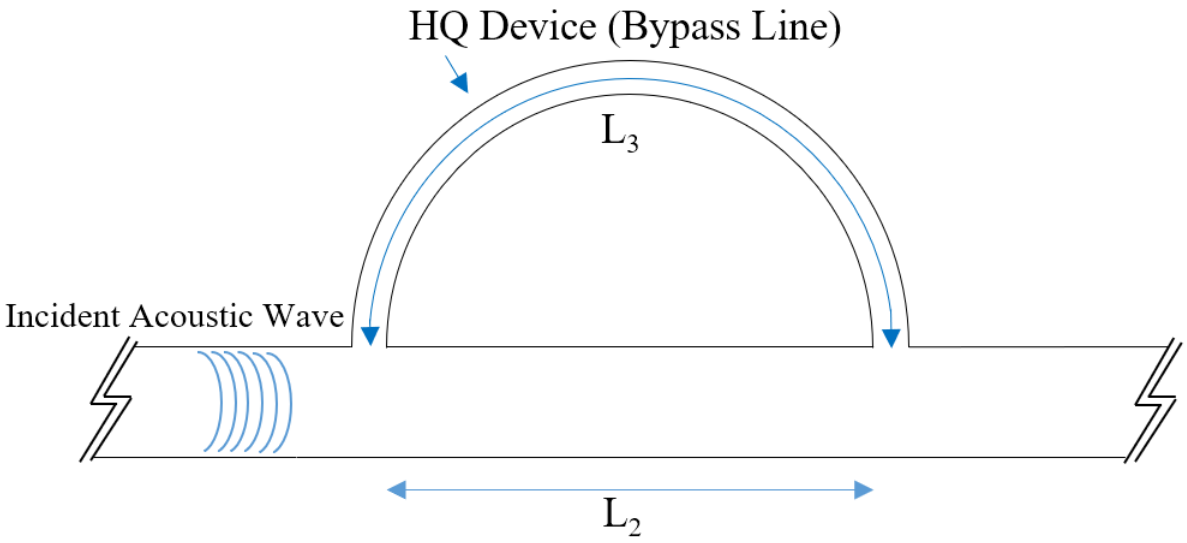

Figure 1.1: Schematic of the Herschel-Quincke Device (HQ).

been investigated, nor has the HQ device been applied to a resonant piping system. Therefore, the main objective of this thesis is to investigate the mechanism of attenuation of the HQ device applied to resonant piping systems. The secondary objective is to clarify the practical considerations for the application of an HQ device to a resonant piping system which have not been investigated in the literature to date.

1.2 Scope of the Work

In order to carry out the objectives of this thesis, several HQ devices were manufactured for testing the effect of the relative diameter ratio and the length of the device on its damping mechanism. The HQ device was tuned to target the 150 Hz frequency of interest chosen for a specific industrial application. The test apparatus consisted of a piping system whose length allows for the 5^{th} acoustic mode of an open-open pipe to coincide with the 150 Hz frequency. The 5^{th} acoustic mode was selected in order to allow for the formation of multiple acoustic pressure anti-nodes which are required to study

the different axial locations of the HQ device along the piping system, as well as the implementation of multiple HQ devices at different axial locations along the pipeline. A strong acoustic resonance is initiated within the test apparatus to study various practical considerations such as the relative diameter ratio of the HQ device to the main piping system, the effect of the HQ device on the total response of the piping system, the implementation of an HQ device at different locations along the axial direction of the piping system, investigating multiple HQ devices attached at a single or multiple locations and the mean flow/directionality effect on the attenuation of the HQ device.

Secondly, the mechanism of attenuation of an HQ device in a resonant pipeline is studied by first experimentally measuring the acoustic response within the HQ device when subjected to a resonant piping system. Acoustic pressure signal phase measurements are also conducted in order to verify the behaviour and phenomenon taking place within the HQ device. The observed experimental trends are then reinforced by the use of Computational Aeroacoustic (CAA) simulations of the experimental setup. The observed phenomenon is simulated to further understand the mechanism of attenuation as well as to visualize the changing acoustic state variables (acoustic pressure and particle velocity) with time and space.

The third portion of this thesis studies a travelling wave piping system, whereby the length of the main pipeline is adjusted such that the targeted 150 Hz frequency of attenuation is an anti-resonant frequency of the main pipeline. This prevents the formulation of acoustic resonance within the piping system to study the application of the HQ device to a travelling wave scenario. The study of the HQ device diameter ratio is compared with that of the resonant piping system to see how the magnitude of attenuation is changed. The HQ device placement is also investigated for different locations relative to other adjacent piping components or boundary conditions in order to determine if this has some effect on the attenuation performance of the HQ device. Multiple HQ devices will provide the flexibility to implement in industrial applications

where the main piping system diameter is very large and therefore, the division of a large HQ device into several smaller devices will be considered.

1.3 Outline of the Thesis

The current thesis is divided into seven chapters. Chapter (1) presents an introduction to the current work including the background and motivation and the scope of work. Chapter (2) provides a detailed review of the literature to date including topics such as sources of acoustic pressure pulsations in industrial pipelines, natural damping and amplification of pressure pulsations in pipelines, acoustic damping devices and the Herschel-Quincke (HQ) Tube along with a summary and outline of the research needs. Chapter (3) describes the experimental setup utilized throughout the entire work including the test setup, design and manufacturing of the HQ tubes, the measurement techniques and finally, the experimental validation. Chapter (4) presents the results and discussion of the passive damping of a resonant piping system using HQ tubes of different relative diameter ratios, axial locations along the piping system, multiple devices and mean flow/directionality effects. Chapter (5) investigates the attenuation mechanism of the HQ device under resonant conditions by means of measuring the acoustic response of the HQ device, the measurement of the specific acoustic impedance ratio and acoustic reflection coefficient, and a computational aeroacoustic (CAA) simulation performed in ANSYS Fluent to further understand and visualize the experimentally observed phenomenon. Chapter (6) outlines the observed trends in a travelling wave system which show significant differences to that seen in the resonant piping system, including the relative diameter ratio and the proximity of the HQ device to adjacent piping components. Chapter (7) summarizes and concludes the main findings of this work along with the research contributions which have been made and the recommendations for future work.

Chapter 2

Literature Review

2.1 Sources of Acoustic Pressure Pulsations in Industrial Pipelines

2.1.1 Valves and Piping Components - Self-sustained Oscillations & Flow-induced Noise/Vibration

A common mechanism of acoustic pressure pulsations exhibited in pipeline systems is self-sustained oscillations. In industry, a geometry that exists in several piping components (such as steam relief valves and gate valves) is a side branch cavity. As outlined by Rockwell and Naudascher [6], during high flow velocities, the unsteady shear layer separation caused by the leading edge of the cavity may induce periodic vortices to be shed downstream. These vortices interact with the downstream edge to produce pressure fluctuations which will in turn interact with the upstream edge, acting as a feedback mechanism to enhance and amplify the shear layer oscillations. This is what is known as fluid-dynamic oscillations. In some conditions, the vortex shedding frequency caused by the separation over the leading edge of the cavity may coincide with one of the acoustic natural frequencies of the side branch causing severe noise or vibration. Such phenomenon

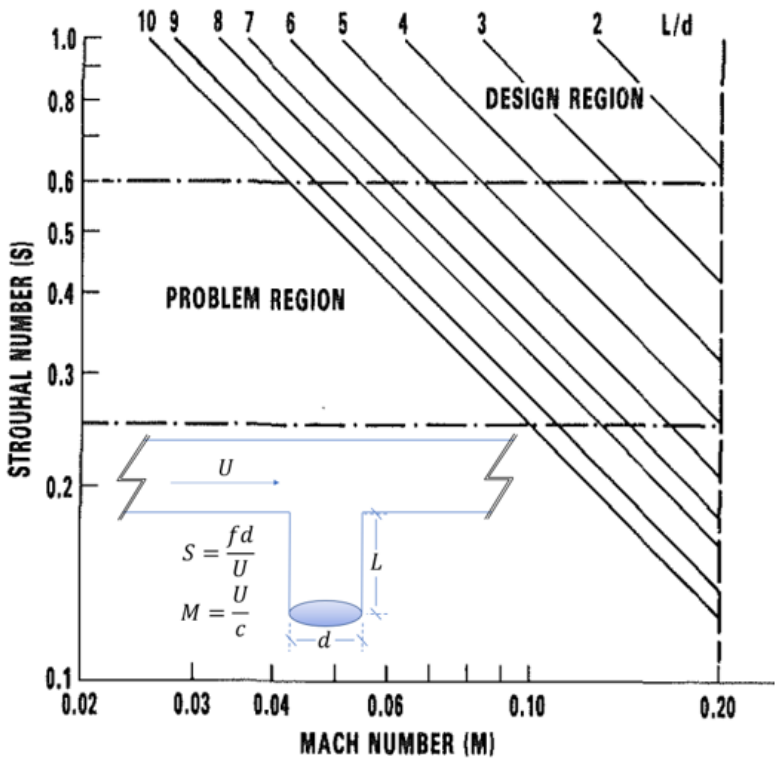

Figure 2.1: Design Guideline for SRV Valves, picture courtesy of Baldwin and Simmons [7].

is known as fluid-resonant oscillations. The work of Baldwin and Simmons [7] developed a design procedure for safety relief valve (SRV) stubs based on field data in order to avoid such a problem for existing or newly installed SRV valves.

This is particularly useful as it allows for designers to ensure that the detrimental coincidence between the natural frequency of the side branch and the vortex shedding frequency is avoided. Figure 2.1 illustrates a design guideline developed to ensure that a sufficient stub length to diameter ratio is achieved for a given Mach number in order to eliminate flow-acoustic coupling.

The flow-induced vibration observed in Venturi-type valves is another industrial issue faced in piping systems, specifically the main steam control valves for nuclear and thermal powerplants. These valves control the flow by moving a valve head toward or away

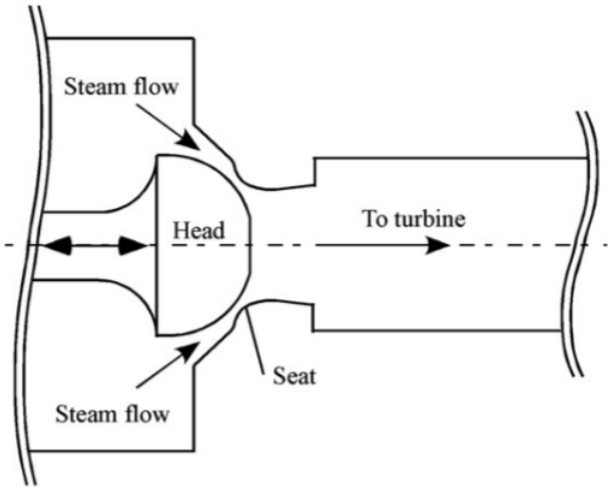

Figure 2.2: Steam Control Valve - Venturi Type, Yonezawa [10].

from the seat as shown in Figure 2.2. The flow pattern around the valve results in flow fluctuations and unsteady pressure oscillations. The fluctuations in the flow can cause random pressure fluctuations on the surface of the valve head and valve seat. The longitudinal acoustic mode was seen to be excited by the flow fluctuations in the work of Widel [8] which caused severe damage to the venturi valve. A similar phenomenon was also investigated by Shioyama et al. [9] whereby severe noise and vibrations were caused by the excitation of the acoustic mode of the downstream pipe. This coupling phenomenon with the downstream pipe is of critical importance as any in-line components will be affected by the amplified pressure waves which propagate through the pipe, leading to fatigue and the potential failure of critical components.

2.1.2 Centrifugal or Reciprocating Turbomachinery

The focus of the current work is on the acoustic pressure pulsations in pipelines that originate from centrifugal or reciprocating turbomachinery. In particular, a significant source of acoustic pressure pulsations will occur at the blade passing frequency (BPF) which is a product of the number of impeller blades and the rotational frequency of the impeller (Brennan [11]). For centrifugal pumps under constant operating conditions, the acoustic pulsations are created due to the interaction between the impeller and the volute of the pump. The detailed work of Morgenroth & Weaver [12] allowed for a clear understanding of the mechanism of sound generation by the impeller – volute interaction along with the effects of flow rate and cut-water geometry on the resonant peak acoustic pressure amplitudes.

The experimental set-up shown in Figure 2.3 consists of a centrifugal pump connected to a closed loop pipeline supplied by a head tank. Thermocouples were utilized to monitor the water temperature in the loop and a flow meter was mounted upstream of the pump. This experiment focused also on the resonant condition created by coupling the blade passing frequency with the natural frequency of the pipeline and so eight piezoelectric pressure transducers were mounted at equally spaced intervals throughout the pipeline. The speed of sound was determined by introducing a sound source and measuring the time elapsed for the acoustic wave to travel from one pressure transducer to another.

An important aspect of the work from Morgenroth & Weaver [12] was flow visualization inside the pump housing with a particular focus on a window showing the cutwater and blade interaction. Figure 2.4 illustrates the flow effect of changing the geometry of the cutwater from a sharp tip (left) to a 5mm rounded tip (right). It was found that the amplitude of the acoustic pressure fluctuations were significantly reduced without having any large effect on the performance of the pump. The point of the flow separation of the sharp cut-water is fixed, while the rounded cut-water allows for the stagnation point to move during the cycle of the blade, ultimately reducing the unsteady vortices which are

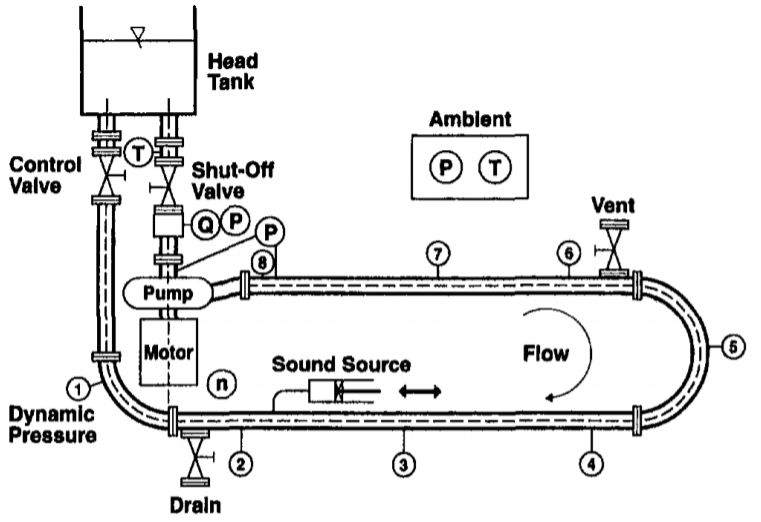

Figure 2.3: Experimental set-up for investigating the acoustic source caused by the BPF of centrifugal pumps, Morgenroth & Weaver [12].

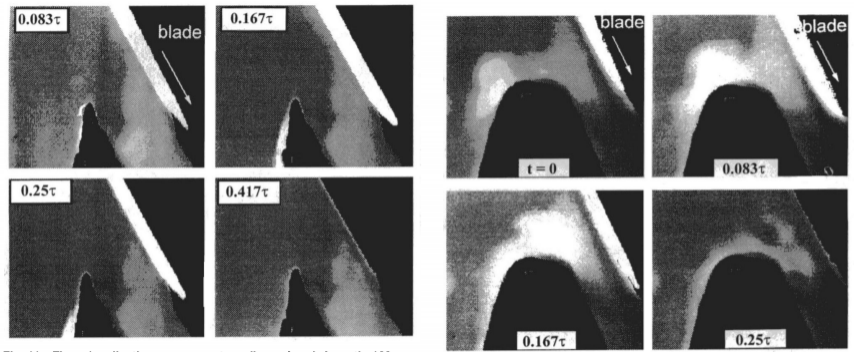

Figure 2.4: Flow visualization at 40% nominal flow rate, 500 rpm - (left): sharp tip; (right): 5mm rounded tip (Morgenroth & Weaver) [12].

produced.

The work of Morgenroth & Weaver [12] also confirmed the observations of Brownell et al. [13] whereby the stagnation point located at the cut-water was altered to the recirculation side (as opposed to the discharge side) as the flow rate increased. It was also noted that the stagnation point was located directly at the tip for the 100% nominal flow rate case. The acoustic emission from the blade-tongue interaction was investigated in a different approach by Keller et al. [14] by modeling the blade-tongue interaction as ideal sound sources located at various positions in the region of the tongue. This allowed for the determination of the acoustic emission of the pump based on the impedance imposed by a connected pipeline of arbitrary geometry. The volute was divided up into several cells in order to predict the plane waves propagating along the volute in both the positive and negative direction as shown in Figure 2.5 where by the relation between the incoming and exiting pressure wave is represented by the transmission matrix shown in Eqn. 2.1

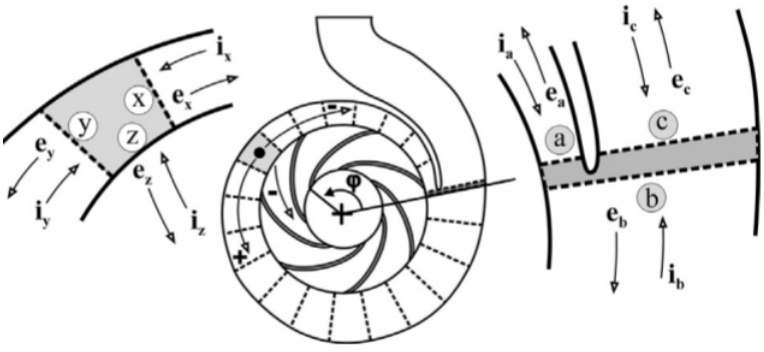

Figure 2.5: Divided acoustic cells for determination of the sound emission from an ideal source, Keller et al. [14].

$$\begin{bmatrix} e_x \\ e_y \\ e_z \end{bmatrix} = \begin{bmatrix} T_{xx} & T_{yx} & T_{zx} \\ T_{xy} & T_{yy} & T_{zy} \\ T_{xz} & T_{yz} & T_{zz} \end{bmatrix} \begin{bmatrix} i_x \\ i_y \\ i_z \end{bmatrix}$$

(2.1)

The model was validated quite well with experimental data obtained from a conventional centrifugal pump as seen in Figure 2.6. The observation from both Brownell et al. [13] and Morgenroth & Weaver [12] that the 100% nominal flow rate produced the smallest acoustic amplitude while nominal flow rates away from the designed value produced the highest acoustic amplitudes was confirmed in the work of Keller et al. [14] as shown in Figure 2.6. However, it was interesting to note that although the expected narrow region of the volute observed the maximum pressure fluctuation amplitude, it was not the only region along the span of the volute to act as a sound source. It is clear that seven peaks and valleys are present within the figure corresponding to the seven blades of the modelled centrifugal pump. This was proposed to be due to the reinforced or destructive combination of the acoustic emission and the hydraulic perturbations in the volute. The common link between the work of Morgenroth & Weaver [12], Brownell et al. [13] and Keller et al. [14] is that they had all considered the interaction between the pump-pipeline coupling and illustrated the potential amplification of the pressure pulsations induced by the blade passing frequency. They had highlighted the excessive levels of noise and vibration potentially occurring under these dangerous conditions and Morgenroth & Weaver [12] had proposed some design changes to mitigate the sound generated from the centrifugal pumps. However, an industrially feasible solution for suppressing the acoustic resonance in pipelines caused by centrifugal or reciprocating turbomachinery is still not clear. The motivation of this work is to develop a technique to mitigate such sources of pressure pulsations in pipelines for both on-resonance and off resonance conditions in piping systems, and therefore the following sections will highlight the fundamental findings in the literature regarding off-resonant and resonant conditions

in pipelines.

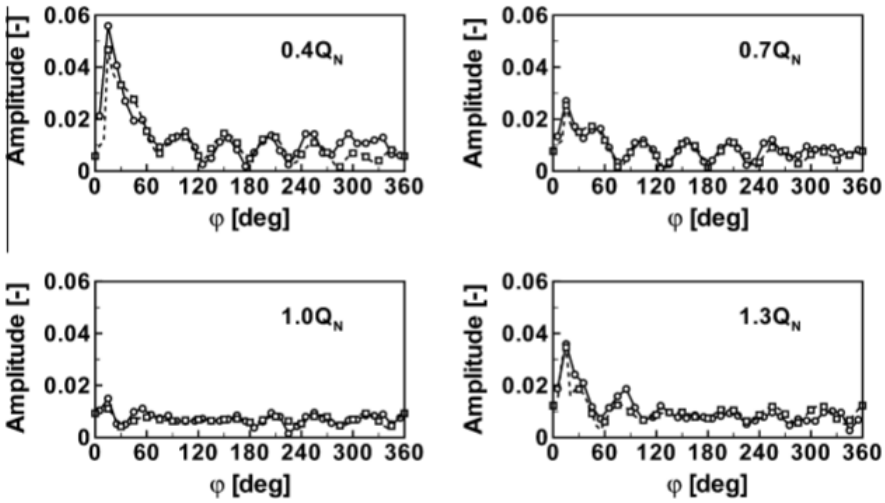

Figure 2.6: Amplitude of the pressure fluctation at the blade passing frequency along the volute for several nominal flow rates. Circles: Experimental Data, Squares: Prediction from Ideal Sources Model, Keller et al. [14].

2.2 Natural Damping of Acoustic Waves in Pipeline Systems

The initiation of acoustic resonance in pipelines is contingent on the coincidence between the pressure pulsation frequency and the natural frequency of the in-line piping system. Acoustic resonance is also dependent on the extent to which natural damping is present within the piping system. If the natural damping of the system is high, there may not be sufficient energy provided by the source to overcome the energy required to excite acoustic resonance. If the energy provided by the source is sufficiently large enough to overcome the natural damping, acoustic resonance will take place and the extent of natural damping present in the system will govern the value of the pressure amplitudes of the standing wave formed in the pipeline. One of the founding works which analytically

outline the visco-thermal attenuation of acoustic waves propagating in piping systems was by Kirchhoff [15]. Kirchhoff was able to analytically develop a model for the attenuation of acoustic waves in pipes as a function of the Prandtl number Pr, heat capacity ratio γ the shear number s and the wavenumber k as defined in Eqn. 2.2

$$\alpha_0 = k_0[\frac{1}{s\sqrt{2}}(1+\frac{\gamma-1}{\sqrt{Pr}}+\frac{1}{s^2}(1+\frac{\gamma-1}{\sqrt{Pr}}-\frac{\gamma(\gamma-1)}{2Pr})] \tag{2.2}$$

Although this was a valuable contribution to the field, there was a need to develop the concept further for applications with mean flow as Kirchhoff's model did not take this into account. In particular, the frequency-dependence of friction (Zielke [16]), the convection effects of the mean flow on the acoustic damping (Dokumaci [17]), and the effects caused by wall turbulence (Howe [18]). The model developed by Howe [18] is one of the most prominently used throughout the literature to date, as it is the most detailed (includes the formerly mentioned effects) and has been validated through experiments conducted by Peters et al. [19] and Anderson et al. [20]. Although the formerly mentioned works have contributed greatly to the literature, the damping was considered only for anti-resonant conditions. That is, traveling waves in piping systems. Therefore, the following section will focus on the amplification of pressure pulsations in pipelines through acoustic resonance.

2.3 Amplification of Pressure Pulsations in Pipelines through Acoustic Resonance

The amplification of pressure pulsations in pipelines is most prevalent when acoustic resonance occurs. The natural frequency of the piping system is primarily a function of the length of the pipeline, the end conditions present and the speed of sound in the medium. This natural frequency will govern the standing waveform present in the pipeline as shown in Figure 2.7. The end conditions will determine the constant acoustic

pressure boundary, for example an acoustic pressure maximum (known as an anti-node) will form at a closed end of a pipe while an acoustic pressure minimum (node) will form at an open end of a pipe. The coincidence between the source frequency and one of the natural frequencies may cause acoustic resonance, and thus the acoustic mode which is excited will be dependent on this factor. The acoustic mode will determine the number of wavelengths which will form inside the pipeline during the standing wave resonance. The equation which governs such behavior is shown in Eqn. 2.3 where n is the acoustic mode (positive non-zero integers) and L is the length of the open-open pipe. The frequency of the acoustic mode of interest can be found using Eqn. 2.4

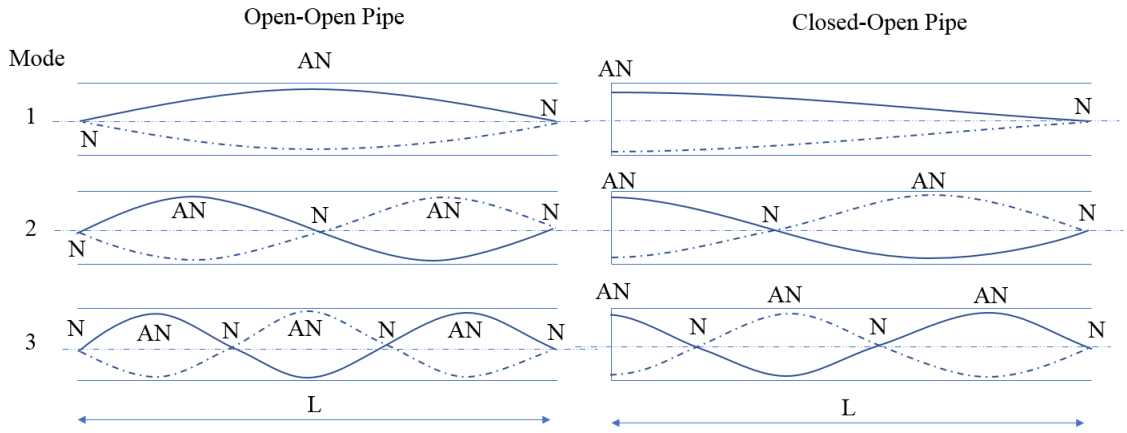

Figure 2.7: Acoustic pressure distribution of an open-open pipe and a closed-open pipe. Pressure anti-nodes denoted as AN and pressure nodes denoted as N.

$$L = \frac{n\lambda}{2} \tag{2.3}$$

$$f = \frac{c}{\lambda} \tag{2.4}$$

An example of the acoustic resonance in pipelines was studied in the work of Rzentkowski and Zbroja [21] where a controlled test-loop was designed to target a problem

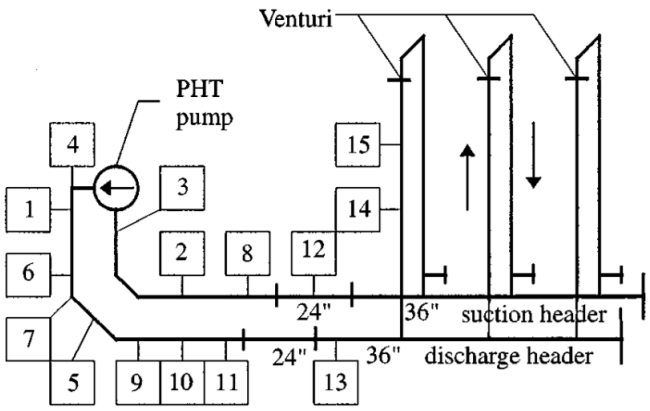

Figure 2.8: Experimental setup for the test-loop designed by Rzentkowski and Zbroja [21].

observed in a specific industrial pipeline. An 11,000 hp electric motor is used to drive a mixed-flow double volute pump which is used in the CANDU reactor. Several pressure measurements were obtained along the length of the piping system as shown in Figure 2.8 with the respective data of each monitor point outlined in Table 2.1. The centrifugal pump has a running speed of 30 Hz with five impeller blades.

Pump discharge side		Pump suction side	
Location	Distance (m)	Location	Distance (m)
4	0·864	12	7·314
1	2·278	8	5·514
6	2·978	2	4·815
7	4·641	3	2·260
5	5·201		
9	6·224		
10	6·924		
11	7·624		
13	12·179		
14	20·332		

Table 2.1: Pressure measurement parameters for the set-up outlined in Fig. 9 Rzentkowski and Zbroja [21].

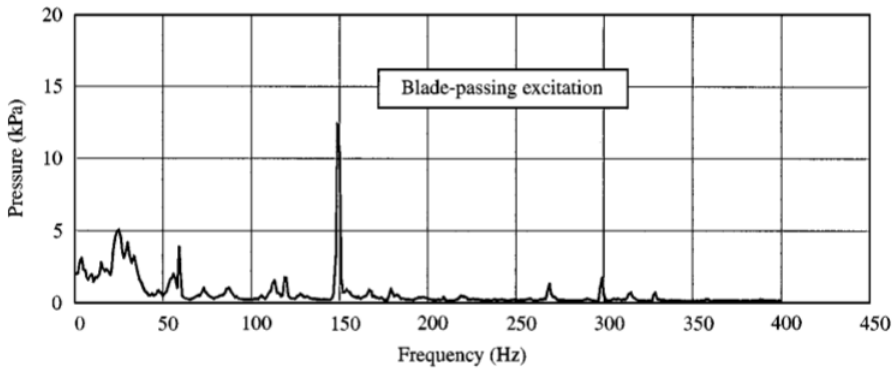

Figure 2.9: Pressure spectrum of the pump discharge T=265 degree Celsius Rzentkowski and Zbroja [21].

The acoustic response of a pressure transducer mounted 2.2 m away from the discharge port of the pump is seen in Figure 2.9. A clear peak is noticed at 30 Hz which is the rotational frequency of the pump. This noise is likely due to the high levels of turbulence at this frequency and the peak at 60 Hz due to the harmonics of the formerly mentioned value. A dominant peak is noticed at the 150 Hz blade passing frequency with a maximum amplitude of pressure. The corresponding harmonic of 300 Hz also shows a noticeable peak. The acoustic response of the pump as a sound source is of particular interest for this work as the noise generated is similar to pulse excitation (a discrete frequency). As opposed to broadband noise, pulse excitation can be targeted differently with respect to damping and noise attenuation techniques which will be discussed in later sections of the current work. The acoustic resonance observed in the experimental work of Rzentkowski and Zbroja [21] is most clearly observed in Figure 2.10. The pressure measured on both the discharge and suction sides of the pump is a clear function of temperature. The temperature was a control variable which was adjusted by changing the power level in the reactor. Not only did this change the temperature of the fluid, but also the flow rate (and blade passage frequency) as this is a requirement for cooling the reactor. As the temperature of the medium changes, the speed of sound will change. This relationship

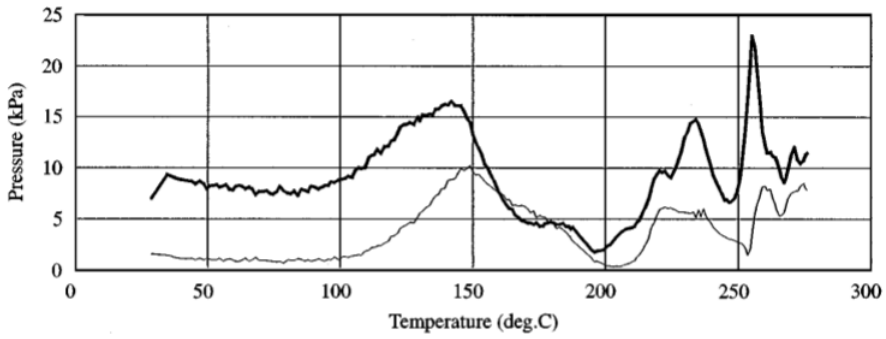

Figure 2.10: Pressure pulsations extracted at the blade passing frequency for several temperatures. Thick line: Discharge, Thin line: Suction Rzentkowski and Zbroja [21].

will ultimately change the wavelength of the standing wave formed within the pipeline and produces a source frequency sweep effect. At a temperature of 256 degrees Celsius a resonant peak is noticed where the dynamic pressure recorded reaches a maximum value of 23 kPa. The acoustic resonance in the pipeline is further observed in Figure 2.11 when viewing the pressure pulsations of the blade passing frequency as a function of the axial location along the pipeline. In comparison to Figure 2.7, the experiments observe a similar phenomenon, whereby the pressure amplitude is a function of the location along the pipeline, further indicating the effects of the acoustic resonance in the piping system. It is evident that location 1 and 9 are likely very close to a pressure anti-node of the piping system while locations 6,7 and 11 are close to a pressure node of the piping system. The exact locations are not outlined in this experiment due to large length of the pipeline and the physical difficulties imposed by this limitation however, the solid line represents the predicted mode shape of the system using a proposed two-port model developed for the investigated pump. The experiments agree quite well with the analytically predicted values which illustrate the one-dimensionality of the pressure field in this system during resonant conditions.

The work of Chatergoon and Li [22] continued the study conducted by Rzentkowski and Zbroja [21], however, with a focus on the amplitudes and frequency of acoustic res-

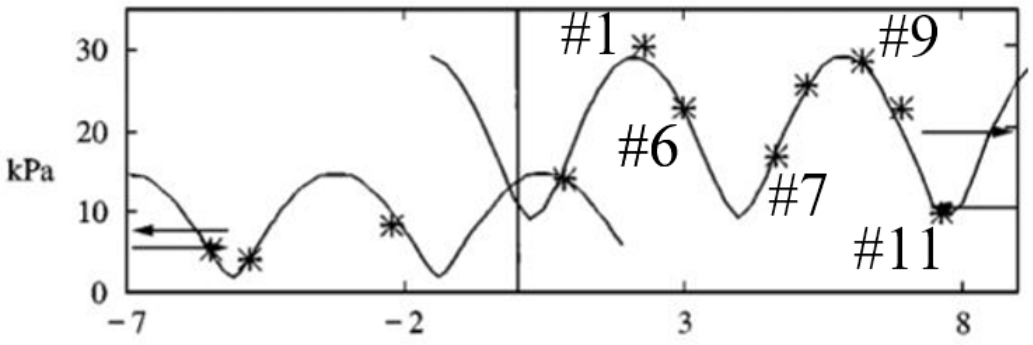

Figure 2.11: Pressure pulsations extracted at the blade passing frequency for several axial locations along the test-loop (265 degrees Celsius) Rzentkowski and Zbroja [21].

onance exhibited within the pipeline as opposed to characterizing the acoustic source of the pump. The objective of Chatergoon and Li was also concerned with the effect of mean flow in the piping system and of different end conditions (open and closed). The experiments were conducted in a water filled test-loop with a large steel tank acting as an open end condition (zero pressure outlet). Two lengths were considered of 7.03 m and 9.2 m in order to target the 150 Hz frequency for the closed and open end condition, respectively. The excitation source used in the work of Chatergoon and Li was a shaker and cylinder to produce pressure waves at varying frequencies. The flow rate was monitored with a turbine flow meter and pressure and temperature with a pressure gauge and thermocouple. The dynamic pressure measurements were conducted with pressure transducers located upstream and downstream of the test line. The work of Chatergoon and Li [22] highlighted that the presence of mean flow does have a significant effect on the amplitudes observed under resonant conditions. As seen in Figure 2.13, the amplitudes of resonance above the 150 Hz show a decreasing trend with the presence of mean flow, however the mechanism by which this trend was occurring was not addressed within this work. It is also evident that below the 150 Hz frequency, the resonant peaks showed similar pressure amplitudes. It was additionally noted that the width of the resonant

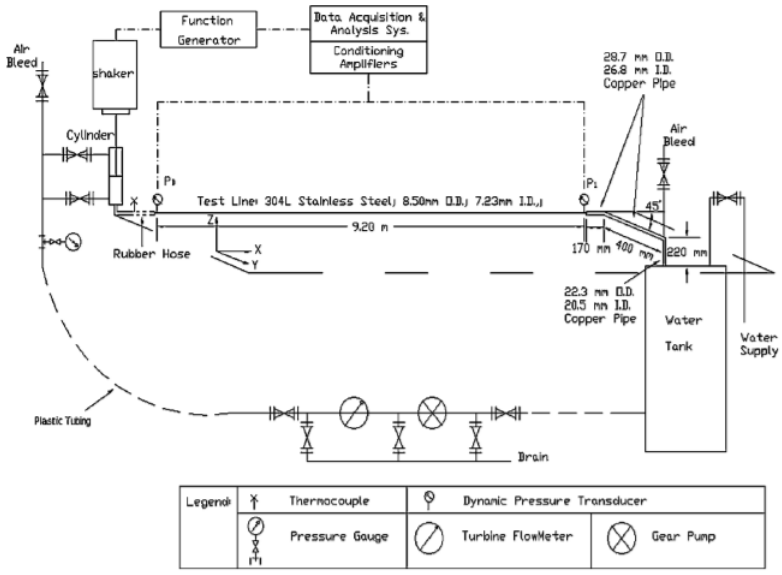

Figure 2.12: Open end test-loop experimental setup constructed for the work of Chatergoon and Li [22].

peaks was substantially reduced with the presence of mean flow.

The amplification of pressure pulsations due to acoustic resonance is of critical importance in engineering applications due to the potential vibrations and noise caused by such a phenomenon. Such engineering applications include the flow-excited acoustic resonance observed in heat exchanger tube bundles[2] as well as the flow over cavities found in HVAC, piping and aerospace applications[4]. For the application in piping systems, the amplified pressure pulsations put components in-line with the pipeline at risk of fretting and premature fatigue failure induced by fluctuating stresses[23].

A well known case of acoustic resonance in pipelines observed by Gabbani et al.[1] sparked the research of several studies seen in the literature to date. The pressure pulsations reported by Gabbani et al.[1] in a piping system of a nuclear generating system were seen to originate from the five-vane primary heat transport (PHT) pumps which generated pulsations at the blade passing frequency of 150 Hz. These pumps were the acoustic source for the research conducted by Rzentkowski and Zbroja [21] which was

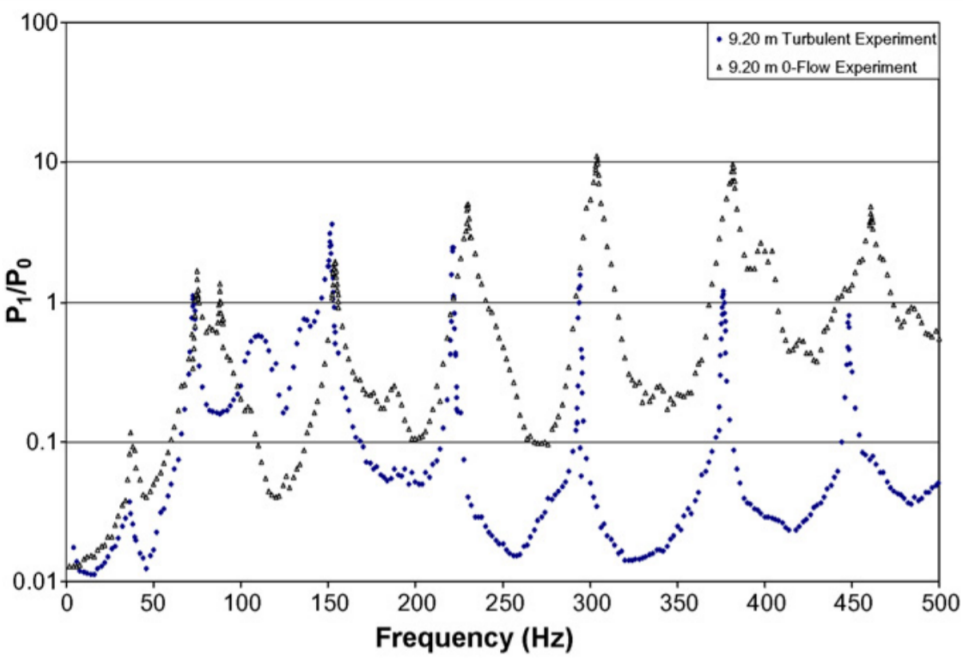

Figure 2.13: A comparison of the turbulent flow and no flow cases for the open end test loop, Chatergoon and Li [22].

formerly reviewed in section 2.3. As a result of the coincidence between the blade passing frequency and one of the natural frequencies of the system, the fuel channels became acoustically excited. This ultimately caused fuel bundle end plate failures due to the high amplitudes of fluctuating stresses. The solution to such problem was to shift the frequency of the source out of coincidence with the system by altering the number of blades on the PHT pump from 5 to 7. Although this may avoid the acoustic resonance phenomenon, pressure pulsations in some units are still of concern to the fatigue life and operation of the components within the system. The current work focuses on understanding the mechanism of attenuation and the preliminary guidelines for implementing a specific damping device into a piping system subjected to pressure pulsations. Therefore, the following section will address an overview of several different types of acoustic damping devices.

2.4 Acoustic Damping Devices

2.4.1 Active Devices

Active devices utilize an energy source during functionality and have a control loop which relies on real-time measured input signals. In the field of aeroacoustics, active noise control has been proven to attenuate flow-induced noise by modifying the fluid-structure-sound interaction mechanism. A noteworthy example of this active control was displayed by Huang and Weaver [24] whereby the shear layer oscillations past an axisymmetric cavity were controlled and acoustic resonance in the pipeline was eliminated. The active feedback controller would in essence, alter the acoustic particle velocity disturbance at the point of flow separation to attenuate the shear layer oscillations. Figure 2.14 illustrates the feedback loop utilized by Huang and Weaver [24] whereby a hotwire or microphone signal is obtained and processed through a bandpass filter and phase shifter. This input signal can be altered to either enhance or attenuate the shear layer oscillations, dependent on the phase shift applied. A power amplifier amplifies the signal to be excited through a loud speaker. A Fourier Analyzer is used to observe the signals and the phase controller adjusts accordingly until attenuation is achieved. Huang and Weaver [24] performed experiments for the first, second and third hydrodynamic mode however, a typical result from their experiments illustrating the third hydrodynamic mode is seen in Figure 2.15 whereby the no control, enhancement and actively controlled cases are displayed alongside the flow visualization. The active suppression case was concluded to work for a small range of feedback signal phase shifts such that the phase shift coincided with the maximum stability for the no-flow feedback loop-pipeline system. Zimmer et al. [25] were similarly able to apply the concept of active noise control using cancellation of waves in their study with a focus on the cancellation of traveling acoustic waves. Figure 2.16 illustrates the experimental set-up used by Zimmer et al. [25] whereby a similar feedback loop was employed to generate an out of phase signal to cancel the source exci-

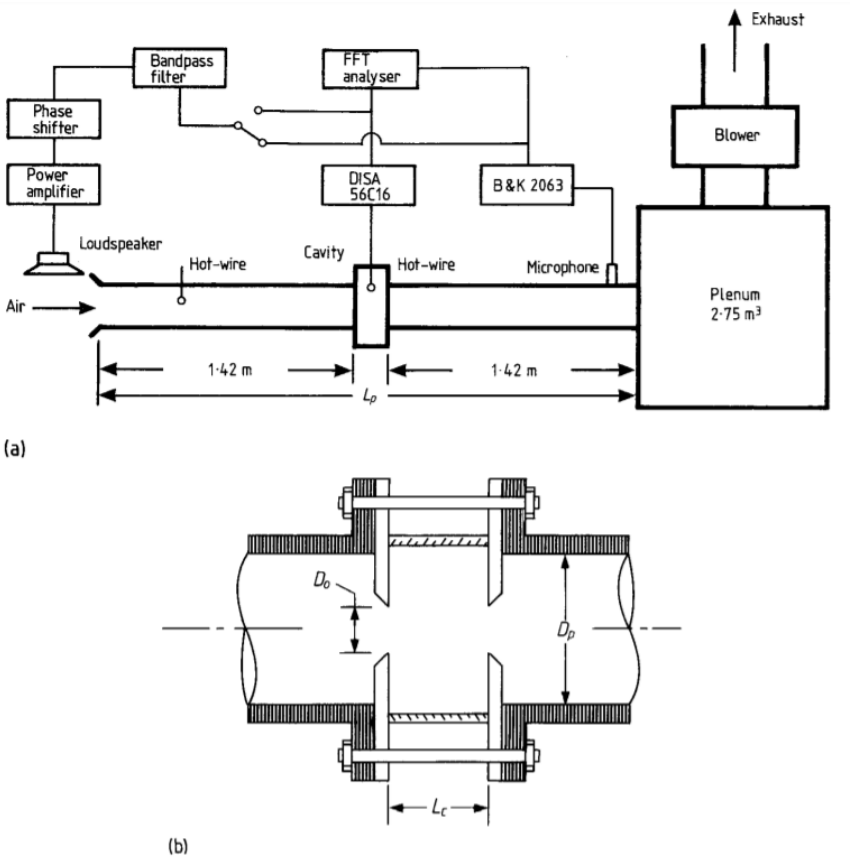

Figure 2.14: a) Schematic of pipe-cavity with instrumentation and feedback loop b)Cross section of the cavity; $D_p = 0.14$ m, $D_0 = 0.067$ m and $L_c = 0.075$ m, Huang and Weaver [24].

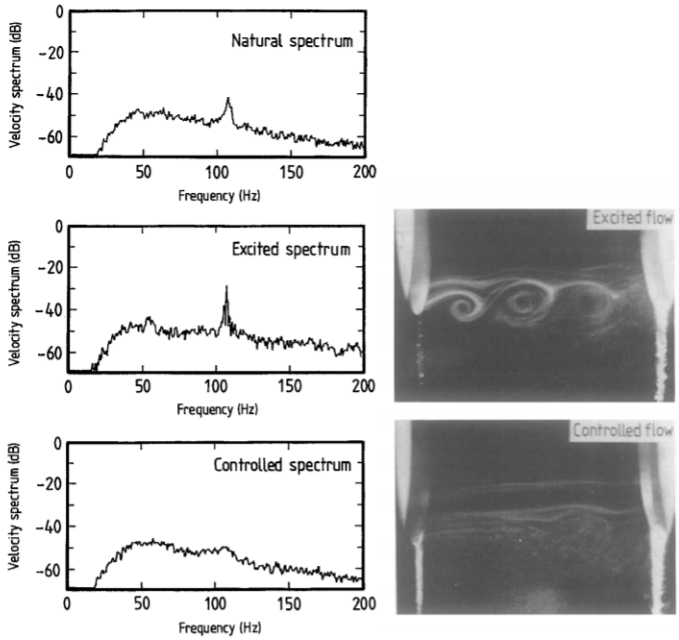

Figure 2.15: Hot-wire spectra compared with the shear layer visualization under the no control, enhancement and suppression conditions, Huang and Weaver [24].

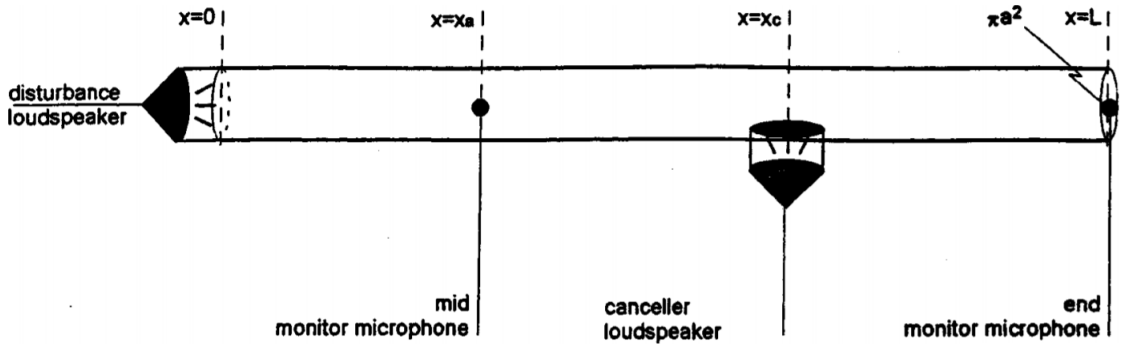

Figure 2.16: Experimental setup for the active noise control in a duct, Zimmer et al. [25].

tation speaker. The work of Zimmer et al. [25] was unique as they were not only able to experimentally employ this concept, but were also able to analytically model the coupled duct-loud speaker system to predict the cancellation effect of this methodology. The result of their developed model showed good agreement with the experiments conducted. The work of Ziada [26] also employed an active control mechanism similar to that of Huang and Weaver [24] however, the active control was employed using synthetic jets. The targeted flow structures included planar jets and shallow cavities. Attenuation of up to 30 dB was achieved during experiments.

The main benefit of active noise control is that a wide range of frequencies can be attenuated. It is also beneficial because the real time response allows for constant monitoring of the system which enables active changes throughout the operation of the system. However, the implementation of active systems is costly especially when considering applications with water where hydrophones and underwater speakers would be required. For a piping system, the active damping technique would also be quite intrusive to install and would require regular maintenance which may compromise the efficient operation of the piping system. For the aforementioned reasons, passive damping devices will be investigated for study throughout this work with the practical benefits of such technique outlined in the following section.

2.4.2 Passive Devices

Passive damping devices are those which do not require an energy source for operation and do not require any real-time input signals. Passive damping devices are of particular interest for the current work as they can be easily installed into an existing or new piping system, with certain designs inducing a minimal pressure drop penalty. Passive damping devices are also beneficial for applications where discrete tonal or pulse excitations (similar to that exhibited by the blade passing frequency) are present as the passive devices will typically attenuate a bandwidth of frequencies centered about a target frequency.

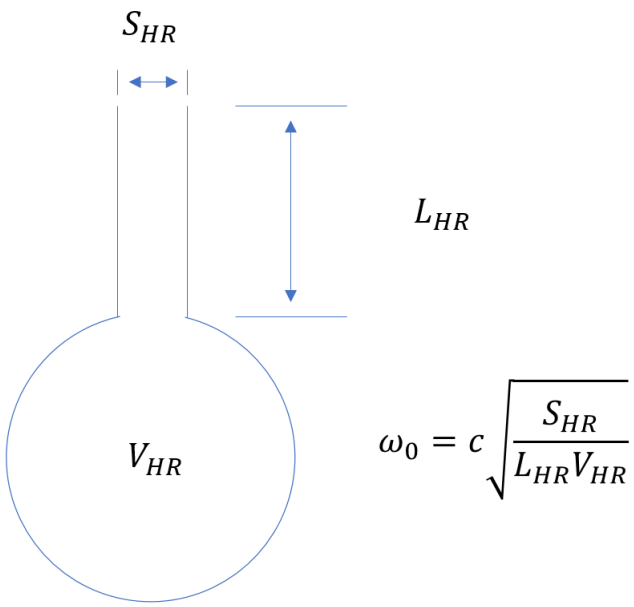

Figure 2.17: Schematic of a Helmholtz Resonator (HR) and its corresponding natural frequency of acoustic resonance.

These passive devices have been properly tuned to attenuate the noise present in a wide variety of applications including turbofan engine noise [27], gas turbine combustor instability [28], automotive fork muffler systems [29] and most importantly the blade passing frequency of radial fans [30] and centrifugal fans [31]. Two of the most commonly used devices in the current literature include the Helmholtz Resonator (HR) and the Quarter Wave Resonator (QWR). A schematic of the HR is shown in Figure 2.17.The mechanism of attenuation of a HR is most clearly understood by considering a mass-spring-damper oscillator. The mass of the system is considered as the fluid in the neck while the stiffness is presumed to be provided by the volume of fluid in the cavity. As the mass of the fluid in the neck compresses the fluid volume in the cavity, a resulting displacement and condensation would take place. The force required to maintain this displacement is what governs the stiffness of the HR and is a function of the density, speed of sound, cross sectional area of the neck and the volume of the cavity.

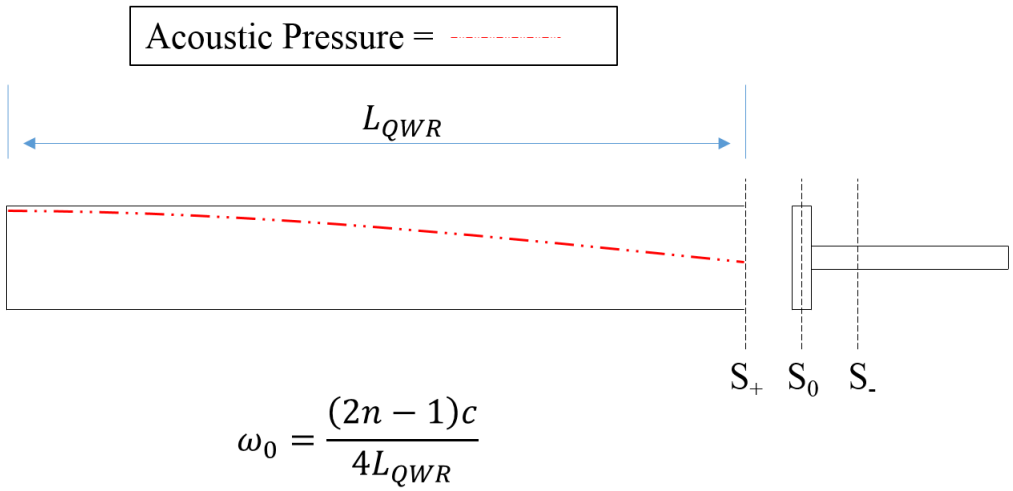

Figure 2.18: Schematic of a Quarter Wave Resonator (QWR) and its corresponding natural frequency of acoustic resonance.

A schematic of the QWR is shown in Figure 5.3 whereby a pipe of length L_{QWR} is closed at one end and open at the opposing end.

The HR and QWR have both received alot of attention in the literature to date and there has been several practical applications of both passive devices. A particularly noteworthy study was conducted by Sadek et al. [32] whereby preliminary simulations and experiments were performed in order to apply both the QWR and HR to suppress pressure pulsations observed in piping systems. It was concluded that the quarter wave resonator had a greater ability to suppress pressure pulsations in pipelines. It was also shown numerically that the location along the pipeline which the device is placed has a significant effect on the performance of the device.

Abdelmwgoud et al. [33] and Sachedina et al. [34] applied a similar experimental technique to investigate the suppression of acoustic pressure pulsations in pipelines using Helmholtz Resonators. The transmission loss of the HR was experimentally evaluated utilizing the transfer matrix technique. The two source location method was implemented to obtain the four transfer matrix coefficients which were subsequently used to calculate

the transmission loss of the damping device. The study revealed that the transmission loss was greatly increased with the increase in the HR cavity volume. The strategic implementation of multiple locations along a resonant piping system proved to enhance the performance of the HR device. The effects of mean flow velocity displayed an adverse effect on the attenuation of pressure pulsations in the resonant piping system.

2.5 The Herschel-Quincke Tube

The interest in the Herschel-Quincke Tube (HQ) for the current work is driven by the simplicity in the design of the device, a major practical benefit for manufacturing such a device for industry use. Considering that the current literature for passive acoustic damping devices is predominantly focused on HR and QWR damping devices, one of the motivations for selecting the HQ device for the current work is due to the potential of overlooking the use of HQ devices for attenuating pressure pulsations in piping systems. The HQ tube has not received the widespread attention which the HR and QWR devices have already drawn and therefore the current literature regarding the HQ device is quite scarce.

It was also noted that the investigation of multiple HQ devices was only considered in limited cases by Hallez [35] and Brady [36] such that the focus was placed on the effects of multiple devices on the attenuation of higher order modes. This was applied only to an anti-resonant system, where the HQ device was not coupled with the natural frequency of the system. The current work has selected to study the HQ device in order to identify the change in attenuation as a function of the number of HQ devices applied to a resonant piping system. In addition to this, it will also focus on relating the observed attenuation effects to the total equivalent fluid volume of the HQ device array, an important practical consideration for industrial application.

Additionally, The HQ device has not yet been applied to a resonant piping system

therefore, it is of interest here to apply the HQ device to a resonant system in order to clarify the mechanism of attenuation of the HQ device under these conditions.

2.5.1 Conventional Mechanisms of Attenuation

Up to the current date, HQ devices have not yet been experimentally applied to systems with a longitudinal standing wave phenomenon. Therefore, the mechanism of attenuation has been conventionally explained using a feed-forward mechanism. Figure 2.19 illustrates a schematic of the working principle of the HQ device under the traveling wave scenario. The incident acoustic wave is divided between two unequal path lengths such that the difference is a half of the wavelength of attenuation. This difference in path length between L_3 and L_2 is crucial when tuning the frequency of attenuation of an HQ device. Upon recombination of the two acoustic waves at the downstream junction, the magnitude and phase of each wave are opposing one another, thus causing the inhalation of the acoustic wave. This mechanism of attenuation is known as the type "1" mechanism.

The HQ tube also exhibits a second mechanism of attenuation due to the reflection of the acoustic wave at each of the junctions (where a change/discontinuity in cross-

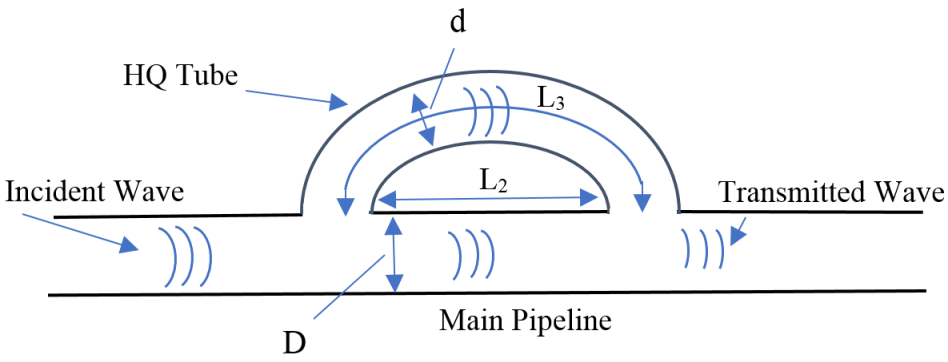

Figure 2.19: Schematic of a Herschel-Quincke Tube (HQ)

sectional area exists) and thus two additional frequencies of attenuation are present for the HQ device.

2.5.2 Analytical Modeling

The earliest known research regarding HQ tubes was conducted by J.F Herschel [37] who focused his initial research on the absorption of light by colored media. Herschel [37] determined that the difference in path lengths L_3 and L_2 of the two HQ device branches must satisfy the relation $(2m+1)(\frac{\lambda}{2})$ in order to obtain the cancellation of waves. This was the foundation of the operation mechanism of the HQ device and was later validated experimentally by the work of Quincke [38]. The first analytical model was proposed by Stewart [39] in 1928 who utilized plane wave analysis to quantify the transmission loss of the Herchel-Quincke Tubes. The $(2m+1)(\frac{\lambda}{2})$ frequencies of attenuation as well as an additional condition specifying frequencies of attenuation at $m\lambda$ were predicted by Stewart's analytical model and were verified alongside experiments which he conducted on a single HQ device. Figure 2.20 shows a good agreement between the experiments conducted and the theoretical predictions from the analytical model with discrepancies at some frequencies as outlined by Stewart which are due to neglecting viscothermal losses in the analytical model.

The analytical model developed by Stewart had some restrictions which included the requirement of equal pipe cross sections between the main and side branches of the HQ device. For industrial applications, this was a challenging constraint which lead to very little interest in the HQ device from industry and ultimately, a large gap in the time line of the literature for quite some time. The work was then continued by Selamet [40] in the late 1900's. Selamet [40] performed a theoretical, computational and experimental investigation of the HQ device to eliminate the restrictions set out by Stewart (the equal area duct requirement). The Theoretical model employed the principle of pressure equality (Eqn. 2.5 & 2.6) and conservation of volumetric flow (Eqn. 2.7 &

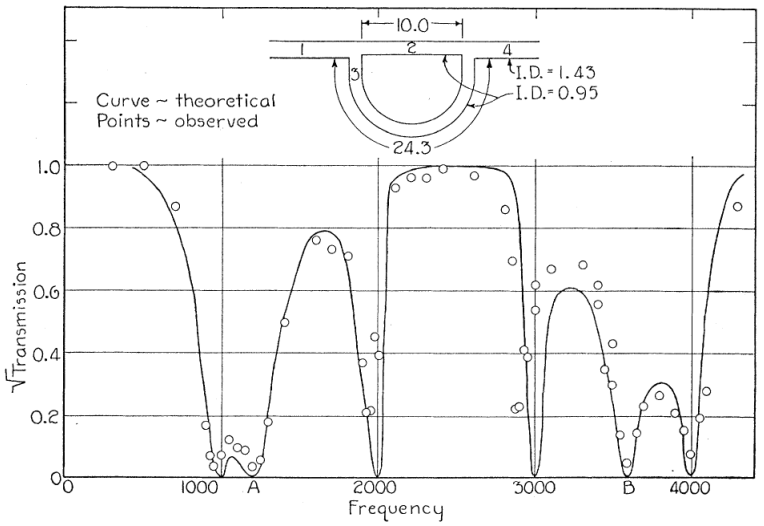

Figure 2.20: Experimental result and Analytical model comparison for the transmission of an HQ device, Stewart [39]

2.8) at the HQ junctions shown in Figure 2.21.

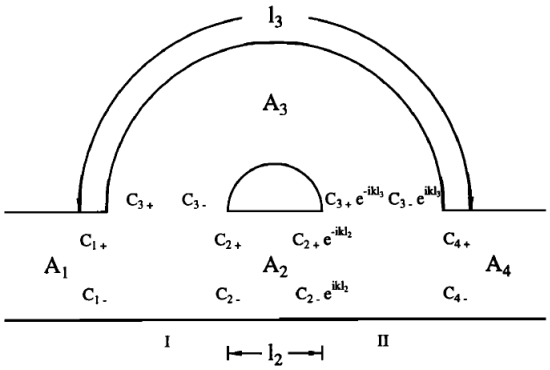

Figure 2.21: Schematic of an HQ device developed for the theoretical model created by Selamet [40]

$$C_{1+} + C_{1-} = C_{2+} + C_{2-} = C_{3+} + C_{3-} \tag{2.5}$$

$$C_{2+}e^{-ikl_2} + C_{2-}e^{ikl_2} = C_{3+}e^{-ikl_3} + C_{3-}e^{ikl_3} = C_{4+} + C_{4-} \tag{2.6}$$

$$A_1(C_{1+} - C_{1-}) = A_2(C_{2+} - C_{2-}) + A_3(C_{3+} - C_{3-}) \tag{2.7}$$

$$A_4(C_{4+} - C_{4-}) = A_2(C_{2+}e^{-ikl_2} - C_{2-}e^{ikl_2}) + A_3(C_{3+}e^{-ikl_3} - C_{3-}e^{ikl_3}) \tag{2.8}$$

The final expression for the theoretical model is shown in Eqn. 2.11 where the transmission loss coefficients α and ϕ are defined in Eqn. 2.9 & 2.10 respectively.

$$\alpha_j = \frac{e^{-ikl_j}}{1 - e^{-2ikl_j}} \tag{2.9}$$

$$\phi_j = \frac{1 + e^{-2ikl_j}}{1 - e^{-2ikl)j}} \tag{2.10}$$

$$TL_{HQ} = 10log_{10}\left|-(\frac{A_2}{A_1}\alpha_2 + \frac{A_3}{A_1}\alpha_3) + \frac{[1 + \frac{A_2}{A_1}\phi_2 + \frac{A_3}{A_1}\phi_3]^2}{4[\frac{A_2}{A_1}\alpha_2 + \frac{A_3}{A_1}\alpha_3]}\right|^2 \tag{2.11}$$

Both the theoretical and computational model developed by Selamet are accurate in predicting the frequencies of attenuation as well as the general trend of the the curve as shown in the experimental comparison in Figure 2.22. However, Selamet states that the theoretical transmission loss becomes infinite at the resonance frequencies due to the effects of dissipation which were not taken into consideration. This provided the current work with a good point of validation for the experimental results for the overall trend of the curve and the frequency of attenuation. The theoretical model developed by Selamet is also an excellent tool used when manufacturing a HQ device, to allow for viewing the general effects of adjusting the various geometric parameters of the device before construction.

Selamet also extended the previously mentioned analytical model to include the addition of a side branch expansion chamber [41] as well as for multiple n-duct configurations of HQ devices [42]. The formerly mentioned work by Selamet had an interesting focus whereby the analytical investigation of the transmission loss profile was conducted for multiple HQ devices each tuned for different frequencies in order to view the complex behavior of such a configuration. Very similar to the first analytical model proposed by Selamet [40], all of his works are good tools to predict the frequencies of attenuation and the overall transmission loss of different HQ device configurations, however as previously

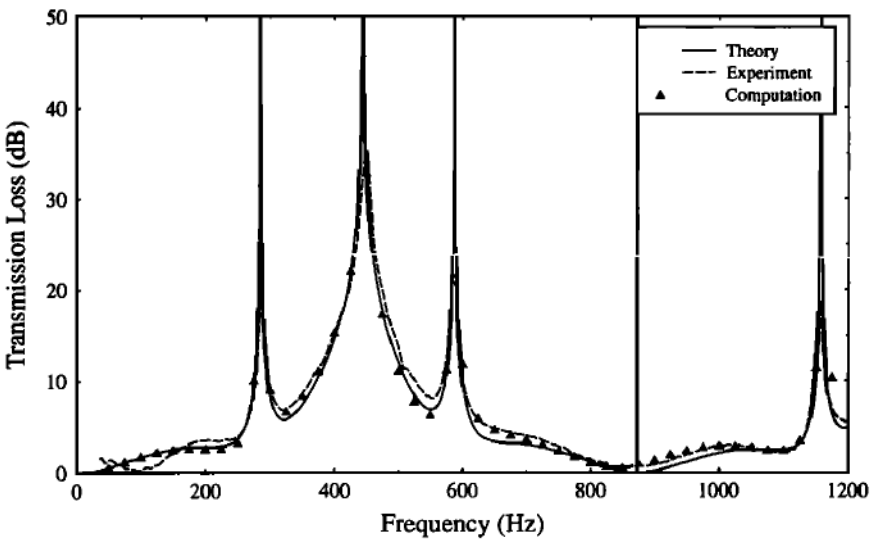

Figure 2.22: Theoretical, computational and experimental comparison of the work done by Selamet [40] (d_1=d_2=4.859 cm, d_3=4.674 cm, l_2=39.85 cm, l_3=78.45cm).

mentioned, the three analytical models do not account for any dissipation and so the values of transmission loss at the resonance frequencies are not captured.

The analytical modeling of the HQ device was further investigated in the literature regarding an interesting modification to the HQ device, an adaptive HQ device. The first analytical model was proposed by Griffin et al. [43] where a schematic of the adaptive HQ device concept is shown in Figure 2.23. When considering the appeal of the HQ device being that it provides multiple frequencies of attenuation as opposed to the HR or QWR devices, the benefit of an adaptive HQ device concept is that these frequencies of attenuation could be actively adjusted. The concept encompasses an additional element (such as a polyvinylidene fluoride (PVDF) membrane or a piston) inside of the HQ device. This additional element introduces another degree of freedom to the system, where the change in the mechanical properties of the piston can be achieved by a control signal in order to alter the frequencies of attenuation of the HQ device. The analytical model was further enhanced to include the piezoelectric properties of the PVDF membrane,

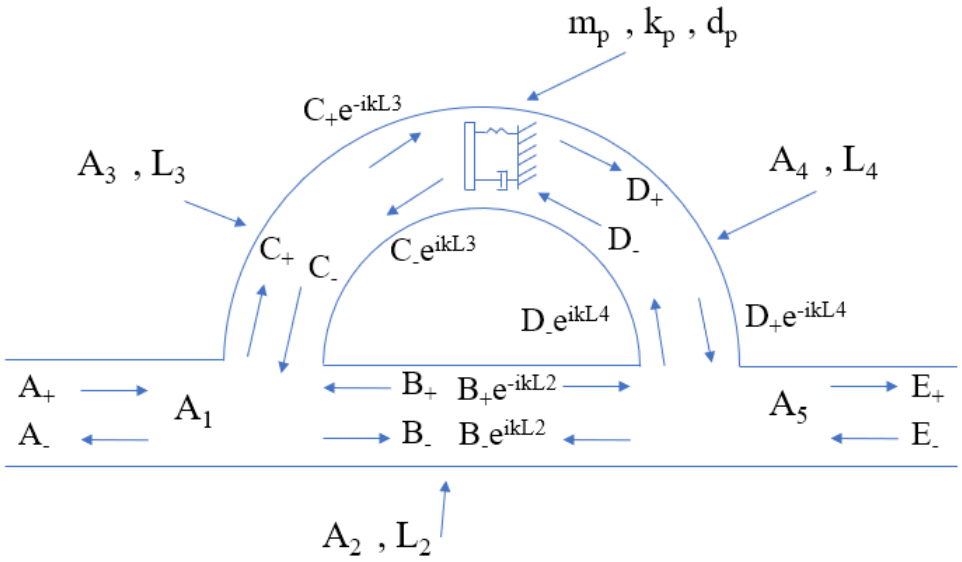

Figure 2.23: Schematic of an Adaptive HQ Tube [43]

such that for a given applied voltage across the membrane, the mechanical response (displacement) of the membrane was predicted and utilized to quantify the change in the transmission loss spectra of the adaptive HQ device. Figure 2.24 illustrates the changing transmission loss response as a result of varying the applied voltage to the PVDF membrane while keeping all other geometric parameters of the HQ device constant. It is clear that a varying frequency can be achieved for the Type I mechanism, an important discovery for applications to automotive or aircraft engines where the tonal noise varies with engine speed.

Although the work of Griffin et al. [43] was quite extensive and progressive to the literature regarding the HQ device, there were no experimental tests performed in order to validate the model proposed. The work of Alonso et al. [44] proposed a similar adaptive analytical model but added experimental results to validate the proposed model. Two different concepts were investigated throughout the work of Alonso et al. [44]: A ball placed within the HQ device as shown in Figure 2.25 (a) and a diaphragm device shown in Figure 2.25 (b). The ball device operates by moving the ball to different positions along

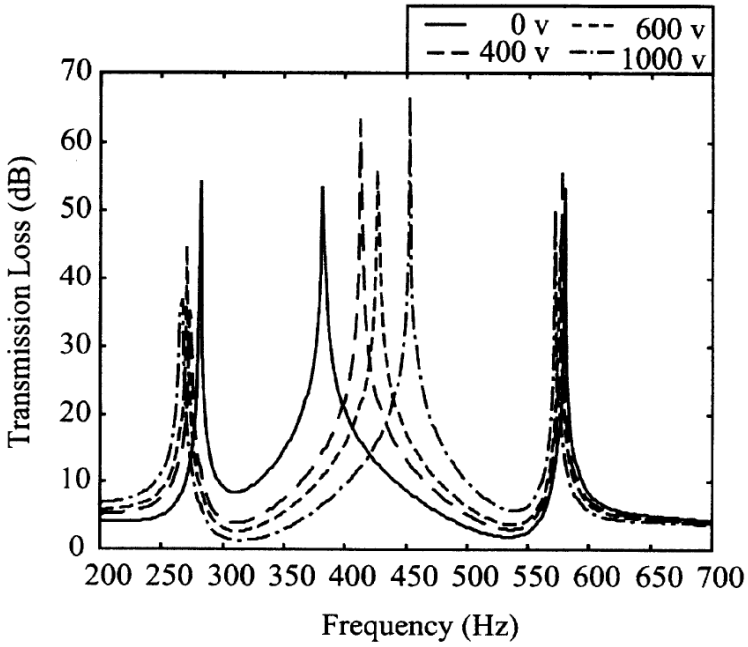

Figure 2.24: Transmission loss of the adaptive PVDF membrane HQ device for constant geometric parameters and changing values of applied voltage [43]

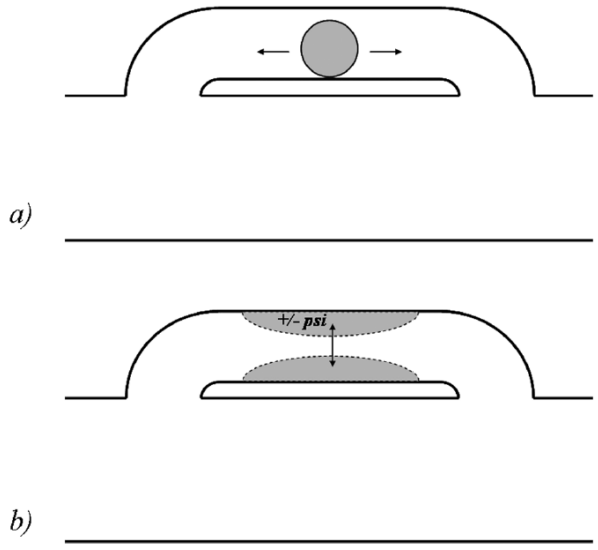

Figure 2.25: Schematic of adaptive HQ tubes using the a) ball and b) diaphragm devices [44]

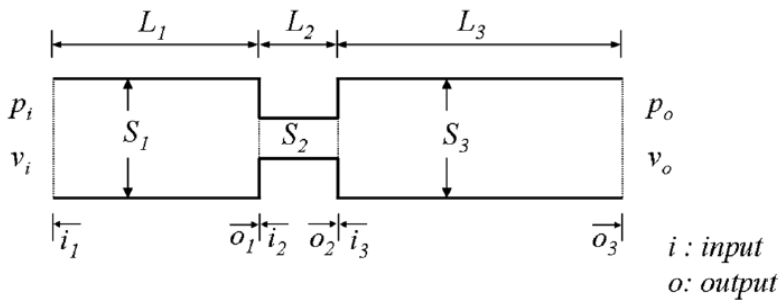

Figure 2.26: Model of a straight wave guide with a single constriction [44]

the HQ device in order to achieve different frequencies of attenuation. The ball placed within the device causes an effective area contraction at that location and is acoustically modeled using the transfer matrix method. A schematic of the ball device model is shown in Figure 2.26 whereby transfer matrices are developed for each of the three straight wave guide sections and are later integrated into a single transfer matrix. The diaphragm device is acoustically modeled in a similar manner however, the constriction is defined as a variable sector as shown in Figure 2.27 instead of that of a single constriction. The diaphragm is activated by applying varying pressure to the internal part of the diaphragm in order to alter its dimensions and change the acoustic response of the HQ device.

The analytical model was validated utilizing an acoustic impedance tube setup as shown in Figure 2.28. The two microphone wave decomposition method was used for two microphone pairs located on either end of the HQ device. This was done in order to determine the four acoustic impedance coefficients which were a good method of validation as seen in Figure 2.29 which displays the measured and predicted impedance coefficients for the diaphragm design. The ball HQ device also showed a similar agreement between the measured and theoretical result. The predicted resonance frequencies of the system was measured for several different configurations of both the ball device (Figure 2.30 Left) and the diaphragm device (Figure 2.30 Right). It is clear that both adaptive concepts are successful in altering the frequency of attenuation of the HQ device, further

validating the analytical work put forth by Griffin et al. [43].

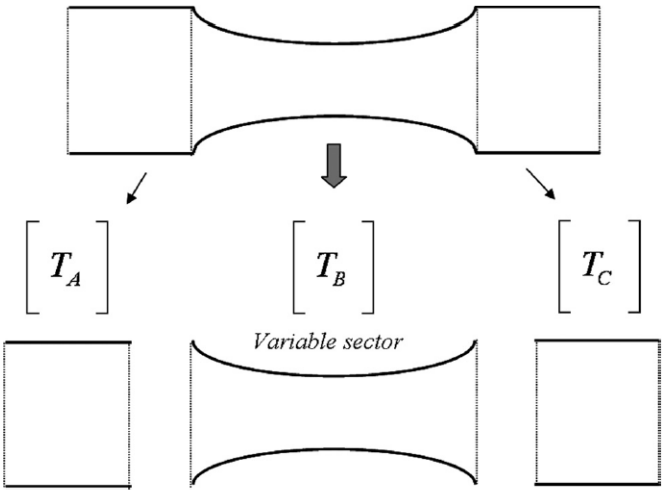

Figure 2.27: Model of a straight wave guide with a smooth variable constriction [44]

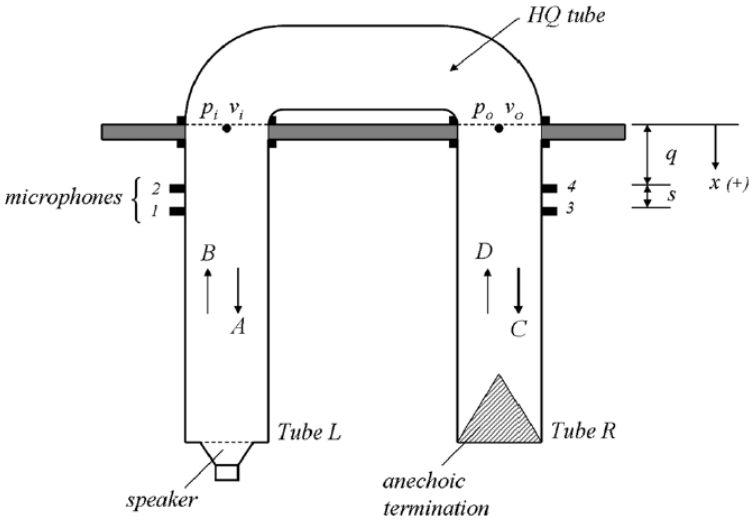

Figure 2.28: Schematic of the experimental apparatus [44]

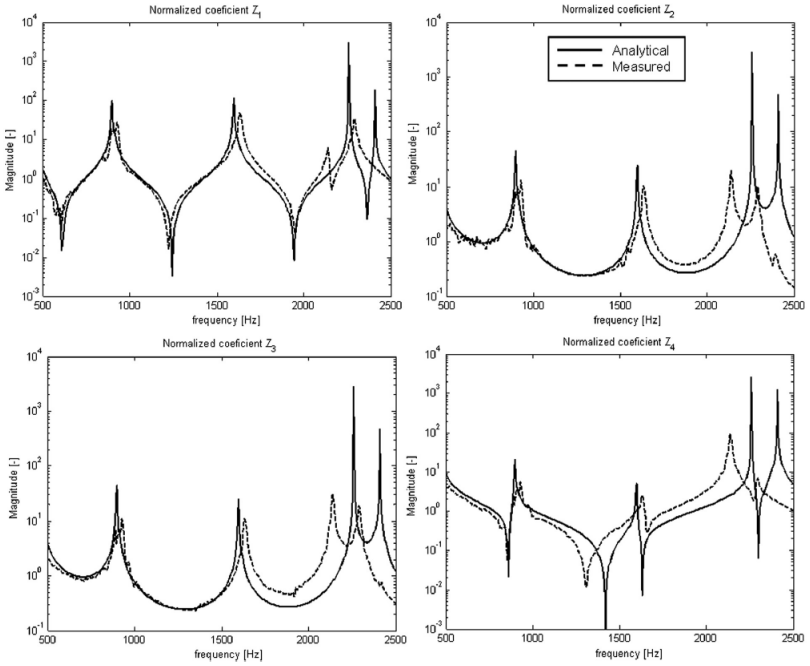

Figure 2.29: Impedance matrix coefficients for the diaphragm HQ tube. Applied pressure is 4.0 psi [44]

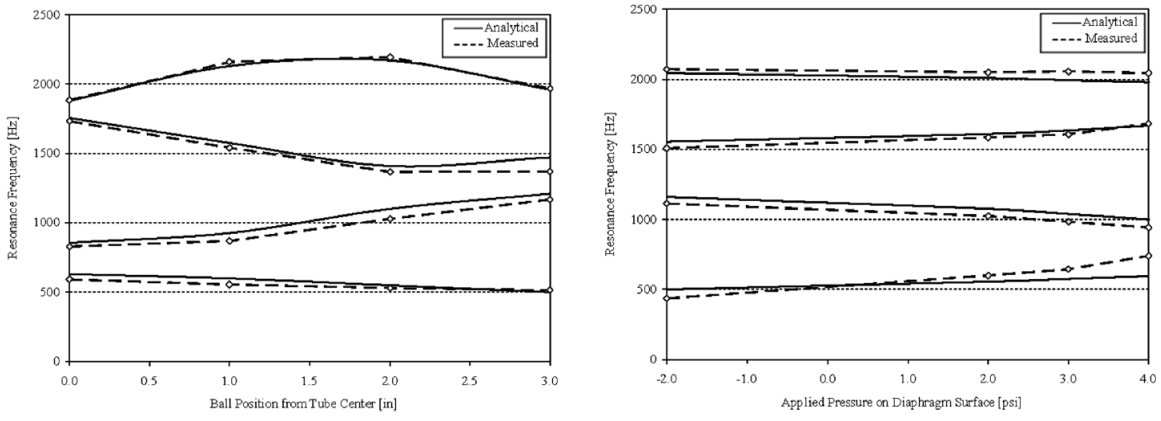

Figure 2.30: Frequency adaptation of resonance frequencies for ball-in HQ tube (left) and diaphragm HQ tube (right) [44]

2.5.3 Applications with Mean Flow

The application of HQ devices in piping systems suggests that the effect of mean flow on the acoustic performance of the device is crucial to investigate. The work of Torregrosa et al. [45] was the first to investigate such effects utilizing analytical modeling. The acoustic model was developed by creating a set of transfer matrices representing the two interfering branches. It consisted of the known expression of the transfer matrix defining a straight duct with flow [46]. The transmission loss was then evaluated from the formerly obtained transfer matrix. A simple incompressible and steady flow calculation was performed using the Darcy-Weisbach equation to determine the change in Mach number in each of the two branches of the HQ device. This allowed for the prediction of the acoustic field in a moving medium and in addition, the viscothermal losses and frictional effects were considered in this model.

The results presented for the analytical model formerly developed had shown some interesting trends with a sample of the results seen in Figure 2.31 which illustrates a contour plot of transmission loss with respect to frequency and changing diameter ratios. The diameter ratios studied in this work range from 0.5 to 2. The length ratio l_2/l_1 is fixed at a value of 2. It is noted that the main Type I resonance peak is shifted slightly away from unity. This shift was noted to be due to the unequal Mach numbers in each of the two branches. It is also noted that for smaller diameter ratios, the secondary peaks are greatly reduced for M =0.15. This effect was not explained further by the author, and it was not confirmed for lower Mach numbers or for diameter ratios less than 0.5.

It is also prevalent that a new resonance peak appears for the M =0.15 cases near $\frac{fl_1}{a_0}$ = 2 for $0.5 < D_2/D_1 < 1.5$. For the no flow cases, at this frequency the transmission loss is nearly zero. Again, this phenomenon was noted but not further explained.

The work of Torregrosa et al. [45] was quite interesting as it made some interesting discoveries on the effects of mean flow on the performance of the HQ device however, the analytical model was not well verified and had unanswered questions as to why these

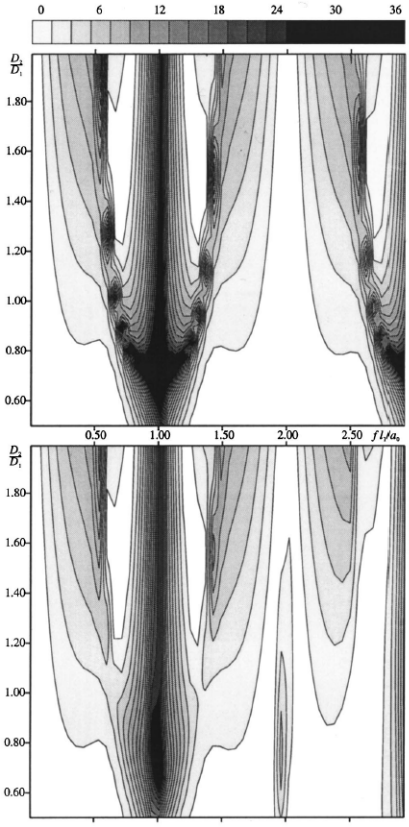

Figure 2.31: Transmission loss contours: $l_1 = 2l_2$. Top M=0; bottom M=0.15 [45]

trends were apparent.

Karlsson et al. [47] extended the work of Torregrosa et al. [45] by creating an analytical model utilizing the mobility matrix, able to accommodate multiple duct configurations. This analytical model is a closed form solution for the transmission loss of the HQ device taking into account mean flow as well as viscothermal and frictional losses. The aim of the work of Karlsson et al. [47] was to verify the trends observed by previous works and to understand and explain the attenuation conditions and their sensitivity to mean flow. The model was further enhanced and modified to include curved ducts, in order to determine the effects of a bended junction. The work of Karlsson includes experimental measurements of transmission loss utilizing the two microphone wave decomposition method in combination with the two port method. These experimental measurements

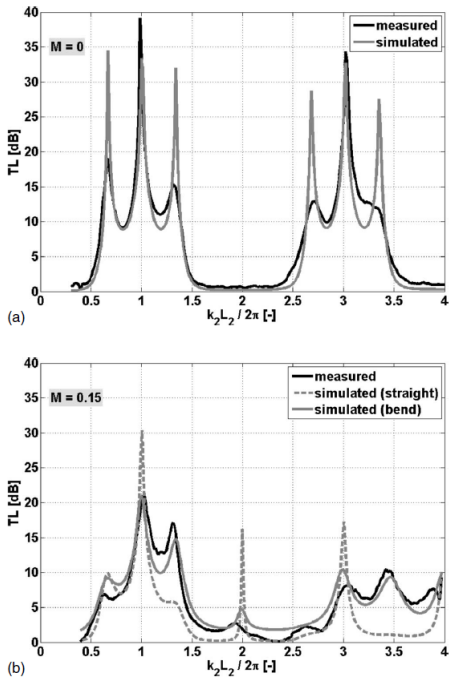

Figure 2.32: Simulated and measured transmission loss at a) M=0 and b) M=0.15 for an HQ device with d/D = 1 [47]

were a point of validation for the analytical model developed. Figure 2.32 a) and b) compares the measured transmission loss result and the analytical model result to one another for an HQ device with d/D = 1 and M=0 and M=0.15, respectively. Confirming the results of Torregrosa et al. [45], the Type I attenuation peak is shifted slightly, however the magnitude of damping of the type one peak was in fact validated in the work of Karlsson et al. [47]. The author further explains this reduction in transmission loss of the Type I attenuation peak for the bent pipe case by attributing it to the trends observed by Keefe and Benade [48] such that the shear losses within the bulk of the fluid are not always negligible when compared to the wall losses.

The sensitivity of the Type II condition to mean flow was also confirmed to be largely dependent on the difference in Mach number between the two branches, previously discovered by Torregrosa et al. [45]. In addition to this, the Type II condition was found to

be sensitive to imperfections at the junctions and was stated that the Type II condition specifies the interaction between branches, which explained the inaccurate prediction of the damping of the Type II condition by the analytical model.

Finally, the work of Karlsson et al. [47] was noteworthy as it analytically explained the additional attenuation maxima which was reported to occur with the presence of mean flow in the work of Torregrosa et al. [45]. Without the presence of mean flow, the Type I attenuation only occurs at odd multiples of half a wavelength difference, while the cases with flow exhibited attenuation at all integer multiples of the half wavelength. The analytical expression developed quantified this phenomenon and proved that certain frequency and Mach number combinations do exist where the even multiple of half a wavelength difference in path lengths do cause attenuation.

2.5.4 Higher Order Modes

The investigation of the application of HQ tubes to attenuate higher order modes was first carried out in a joint effort by Hallez [35] and Brady [36] where circumferential arrays of HQ tubes are applied to the inlet of a turbofan aircraft engine under mean flow conditions. This was the first attempt to analytically model the HQ device to scenarios other than plane waves which were considered in previous literature. An analytical technique to predict the acoustic effects of applying HQ devices to the circular inlet was developed which involved modeling the device-inlet junctions as piston sources to allow for the coupling between the acoustic field in the inlet with that of the acoustic field inside the HQ devices. Experimental measurements were conducted from two actual turbofan engines in order to validate the accuracy of the model, which was shown to agree quite well with the experimental data. This analytical model was utilized to understand the attenuation mechanisms of the higher order modes and it was shown that the attenuation of a particular mode was caused by the scattered contributions from various incident modes.

Based on these findings, several other HQ device configurations were considered such as a helix pattern along the inlet. A second configuration consisted of arrays which were not parallel to the inlet axis, given some angle of rotation. A final configuration was tested including a combination of both formerly mentioned structures.

It was evident that the helix configuration alone did not show an improved effect of the HQ system. The performance of the angled HQ tube array however, did improve the performance with no correlation between the angle of the HQ tube array and that of the propagation of the acoustic modes.

The work of James [49] was primarily aimed toward evaluating and validating the accuracy of the analytical model set forth by Hallez [35] through experimentation with different mode structures, changing the number of HQ tube arrays and tubes as well as the axial position along the turbofan jet engine. The objective of the experiments was also to confirm the insight into the noise control mechanisms of the higher order modes (mode reflection, circumferential scattering and radial scattering).

James [49] was able to carry out the formerly mentioned objectives and provided some interesting conclusions regarding their findings. The experiments conducted confirmed that both for a single incident mode and multiple incident modes, the analytical model showed good agreement of the level, shape and resonance frequencies. When testing the analytical model for different number of HQ tubes and different axial positions, the model was quite robust. The trend of increasing the number of HQ devices increased the resonant frequencies of the array as well as increasing the peak attenuation. The change in axial position of the HQ device array during multiple incident modes was seen to exhibit a variation in frequency and attenuation. The model was able to predict this variation accurately, however no physical explanation was provided for this result and was tested for the case of an anechoic termination only (i.e. non-resonant conditions). The model was seen to show poor agreement at the cut-off frequency of the acoustic modes due to the theoretical model neglecting the open end reflection contributions.

2.6 Summary and Research Needs

The literature to date has detailed a number of interesting and conclusive findings which have helped to progress the understanding of the HQ device. However, there exist several gaps in the literature with respect to the practical application in industry. The current work aims to provide an in depth investigation for both resonant and anti-resonant conditions, in order to identify the differences and similarities between both conditions, as they are both very crucial scenarios encountered in the piping industry. The resonant tests involve understanding the effect an HQ device has on the total natural response of the piping system. This will be particularly important in practical scenarios because the design of the HQ device can be changed to account for the change in the natural response of the system, to better attenuate the targeted frequencies of interest. The effects of device placement along the axis of the pipeline has not been studied for the resonant conditions. Therefore, the effects of placing an HQ device at different locations along the standing wave will be investigated. Insertion loss measurements will be utilized to characterize this effect, considering the previous literature has been concerned with anti-resonant conditions only and therefore has used primarily transmission loss to characterize the performance of the device.

In addition to this, the implementation of multiple devices will be investigated to determine the effects of dividing a single large HQ device into smaller HQ devices with a total equivalent area, as this has not been considered to date. A limited scope of diameter ratios has been experimentally considered for the HQ device (ranging from 0.5 to 1) and clarification is required to validate the normalization of the transmission loss with the relative diameter ratio. The current work will test this normalization parameter by using several different sized test sections to see if the diameter ratio truly scales with the pipeline size, an investigation not considered to date. The effect of mean flow has been considered for a limited scope of diameter ratios (0.5-1) and for high Mach numbers (above M=0.15) which are not practical for the specific industrial application

concerning the current work. Therefore, smaller diameter ratios (below 0.5) and lower Mach numbers (M< 0.1) will be considered throughout this study in order to determine if the trends previously observed in the literature apply to this particular scenario.

For the travelling wave piping system, the literature has investigated the effects of modal reflection, scattering and transmission loss for different axial locations. However, the change in magnitude of attenuation was not fully explained when studying the different HQ device placements along the axial location of the piping system. Moreover, the current work aims to clarify the trends exhibited regarding changing the axial location of the HQ device by also considering insertion loss measurements, as this may reveal some undiscovered effects previously overlooked through transmission loss measurements within the literature. This work will focus on frequencies below the cut-off frequency and will not consider the effects of higher order transverse modes as the frequency of interest is well below the cut-off frequency. The off resonance scenario will also be of interest in the current work when considering the trends of implementing HQ devices with varying relative diameter ratio d/D and will be compared to the resonant system experiments to see how the magnitude of attenuation changes. The off resonance scenario is quite practical as acoustic resonance is not often materialized in a piping system (considering the devastating effects) and so the performance of the HQ device with regards to the formerly mentioned test parameters is of crucial importance.

The conventional mechanism of attenuation of the HQ device is defined in the literature as a feed-forward mechanism, but no application has been made for a HQ device implemented into a longitudinal-resonant piping system. The conventional feed-forward mechanism becomes counter-intuitive when you consider a resonant system, where incident and reflected waves are uniquely combined to create locations of acoustic pressure maxima and minima along the pipeline axis. Some questions may arise for such a scenario including the function of both junctions of the HQ device and if they are both causing some sort of destructive interference. It is also questionable how the HQ device

interacts with the main pipeline at these junctions to sustain (or potentially reduce) resonance in the pipeline. The mechanism explaining how the acoustic energy transmitted downstream of the HQ device is attenuated within the pipeline remains unexplained. Is the primary mechanism of attenuation focused on reflecting acoustic energy back to the source, dissipated within the device or annihilated by the out-of phase recombination of waves at the junction (or junctions)? The current work aims to understand and clarify these questions by conducting a detailed investigation of the mechanism of attenuation of the HQ device under resonant conditions. To carry out these objectives, acoustic pressure measurements will be taken at several locations along the HQ device and the junctions of the main pipeline to better understand the nature of the acoustic field within the device and the interaction with the main pipeline. The HQ device will also be investigated by measuring the change in acoustic impedance induced by the implementation of the HQ device, to better understand the mechanism of attenuation. The reflection coefficient will also be measured for the HQ device to further clarify the formerly mentioned questions. Phase angle measurements will be computed to determine the relationship between various pressure signals including comparing different locations along the HQ device to one another. Theses measurements will also be conducted to understand the interaction taking place at the HQ device to main pipeline interface. Furthermore, computational aeroacoustic simulations will be performed using ANSYS Fluent to further solidify the experimental results and to provide insight into the acoustic particle velocity distribution within the HQ device. The domain of the simulations will mimic the experimental conditions as closely as possible to ensure proper validation efforts are conducted utilizing comparisons to the experimental measurements. This will achieve proper visualization of the mechanism of attenuation of the HQ device.

Chapter 3

Experimental Setup

This chapter will outline the experimental setup which was utilized to conduct a variety of experiments designed to carry out the objectives of this thesis. The design and manufacturing of the Herschel-Quincke tube is outlined within this section along with a detailed description of the measurement techniques employed to quantify the insertion loss, transmission loss, acoustic reflection coefficient, specific acoustic impedance ratio and acoustic pressure signal phase.

3.1 The Test Setup

The experimental test setup utilized here in this work is illustrated in the schematic shown in Figure 3.1. The open air loop is designed to accommodate flow velocities of up to a maximum of 20 m/s within a pipe of 101.5 mm (4 in.) in diameter. A centrifugal air-blower is used to drive the mean flow velocity and the flexibility in its configuration allows for testing the mean flow in both directions. A bell mouth intake or flow straightener is utilized (depending on the directionality of the flow) to reduce turbulence at the inlet. A flow control valve is utilized to control the flow rate through the test section and a fan flow meter is utilized to measure the flow speed. The fan flow meter was selectively mounted outside of the test section so that any acoustical effects induced by the flow

meter are minimized. Considering the absorptive muffler will induce some pressure drop across its geometry, the fan flow measurement is initially calibrated with a pitot tube mounted inside the test section in order to capture the change in velocity measurements. The pitot tube is removed from the test section when the experiments are conducted. The absorptive muffler is utilized to isolate the acoustical effects of the centrifugal air-blower and the flow control valve. The absorptive muffler was designed and tested to ensure that the boundary condition induced at the absorptive muffler is similar to that of an open end. This was completed so that the reflections present at the inlet and outlet sides of the test setup are sufficiently symmetric. The absorptive muffler also minimizes the acoustical effects of the flow control valve such that the boundary condition at the absorptive muffler remains constant as the flow control valve is adjusted to different positions. The test element is located between two clusters of microphones which have a spacing of 196.85 mm (7.75 in.) between each of the two microphones. This spacing was selected to achieve a cut-off frequency of 873 Hz while also maintaining a high degree of accuracy in the measurements. The microphones used throughout these experiments are 1/4 inch phase matched pressure microphones that are flush mounted on the inside wall of the piping test section. The microphones are mounted with brass NPT fittings and sealed with a gasket. The data acquisition card acquires the signal with a sampling frequency of 20 kHz and a total time per experiment of 90 seconds.

The excitation source is able to move to two different locations as shown in Figure 3.1 which is required for the two source location measurement method utilized to aquire the transmission loss spectra. This change in speaker location is also utilized during the measurement of insertion loss such that different directionality can be studied where the downstream and upstream incident acoustic propagating wave can be visualized in Figure 3.2 a and Figure 3.2 b, respectively.

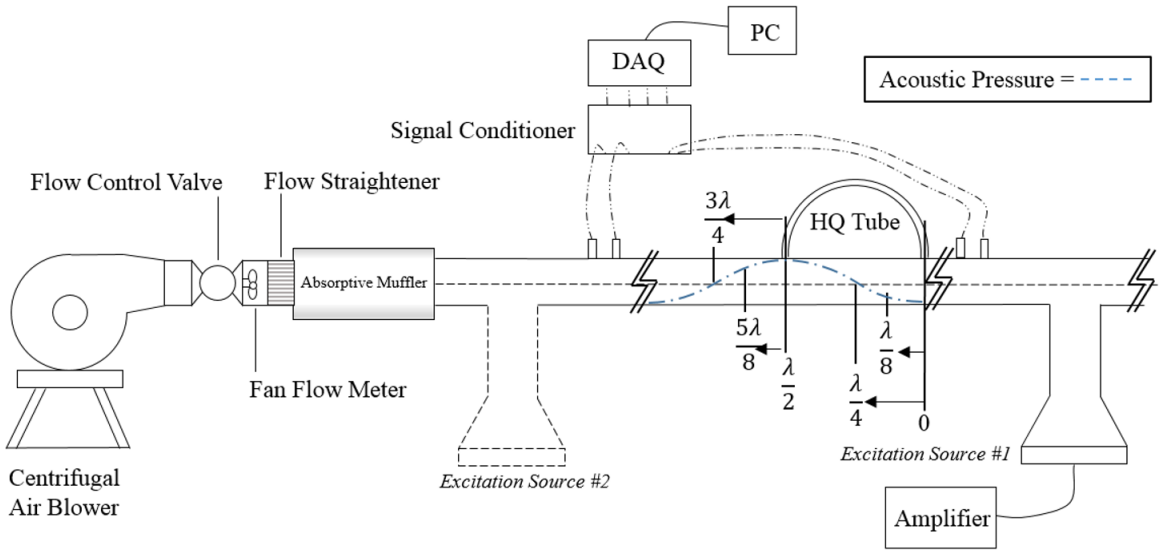

Figure 3.1: Schematic of the experimental set-up for the air loop pipeline system

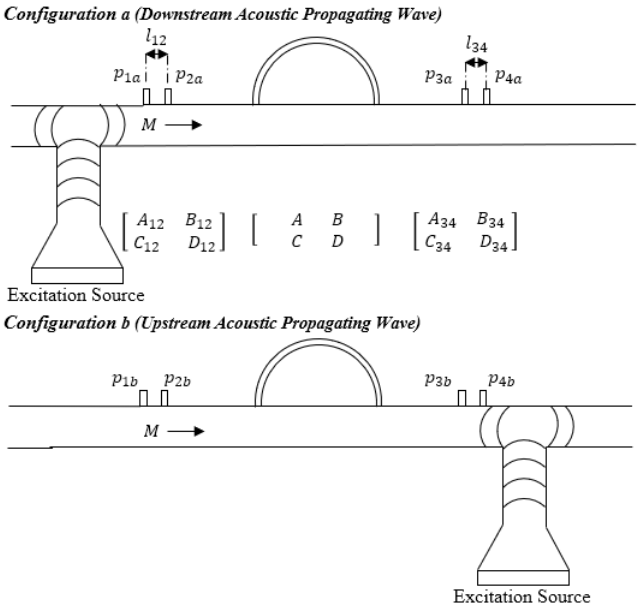

Figure 3.2: Schematic of the setup for the a) downstream and b) upstream incident acoustic wave configuration

3.2 Herschel-Quincke Tube Design and Manufacturing

The Herschel-Quincke tubes geometric parameters were selected so that the Type I attenuation condition targeted the 150 Hz frequency of interest. The design lengths were verified and validated utilizing the analytical model developed by Selamet [40] and a detailed comparison is shown in section 3.4 of this thesis. The diameters were selected to target a range of relative d/D ratios which were not previously covered in the literature (0.0833<d/D<0.5).

The Herschel-Quincke tubes which were utilized throughout this work were manufactured using standard Polyethylene (PE) piping or Polyvinylchloride (PVC) piping. PE piping was selected for cases where the bending radius was sufficiently large due to the fact that it is easily flexible. However, for cases where the radius of curvature was smaller, the PE piping when bent causes a deformation in the cross sectional area. For these cases, the thermoplastic properties of PVC piping was leveraged as it is much more rigid at room temperature. The PVC pipes were first filled with sand to prevent collapsing the cross sectional area upon bending. The pipes were then heat treated and a wood jig was utilized to bend the pipes to their required geometry as shown in Figure 3.3. Upon cooling, the sand was removed from the PVC pipes. This method allowed for a tight radii of curvature to be obtained while retaining the constant cross sectional area, rigidity and strength.

The HQ devices were attached to the pipeline using adapters which had NPT threading on one side, and a standard PVC slip connection on the other. This allowed for modularity in pipe diameter (using reducer bushings) and for ease of installation. The NPT adapter and/or reduced bushing added some length to the HQ device (ranging from 1.125-2 inches depending on which attachments were utilized) which was accommodated for during the manufacturing of the HQ tube in order to ensure the correct central fre-

Figure 3.3: Schematic of the moulding jig utilized during the manufacturing process of a PVC HQ device using thermoplastic heat treatment

quency of attenuation was targeted. The NPT threads although tapered, were sealed using thread seal tape.

3.3 Measurement Techniques

The experimental measurement techniques employed throughout this thesis are outlined within this section. A variety of parameters are experimentally obtained such as transmission loss, insertion loss, specific acoustic impedance ratio, acoustic reflection coefficient and acoustic pressure signal phase measurements. All measurement techniques use the aforementioned air loop seen in section 3.1, however some modifications were made for the different parameters measured whereby within each of the respective sections a schematic of the changes in the test section are illustrated. For each of these measurement param-

eters, 1/4" pressure microphones are utilized to obtain a fluctuating voltage signal. The microphones are calibrated with a piston phone to relate a change in voltage to a change in acoustic pressure. This pressure v.s time signal for each microphone is imported into MATLAB and processed to obtain the aforementioned acoustic parameters.

3.3.1 Transmission Loss

Transmission loss is a useful parameter typically used in industry to characterize the acoustic performance of a muffler or silencing device. The HQ tubes tested within the current work utilizes transmission loss because by definition, transmission loss characterizes the test element independent of the source and end terminations. This allows for isolating the damping device to eliminate the effects of the pipe end terminations and the source impedance.

There are three well known techniques to obtain the transmission loss spectra for a given test element: the decomposition method, the two-load method and the two-source method. Although the formerly two mentioned methods are noted to be the least cumbersome methods to employ, several works comment on the superiority of the two-source method. The work of Tao and Seybert [50] performed a comprehensive comparison between these three methods and also compared them to the results obtained from a boundary element method (BEM) computational solver. It was found that there are limitations to the decomposition method in the absence of an anechoic termination. An anechoic termination can not be used in the current work for the on-resonance experiments as the reflections are a crucial part to setting up a standing wave within the piping system. The four-pole parameters are also not able to be obtained using the decomposition method. The two load and two source methods were found to accurately measure the transmission loss without an anechoic termination. Although the transmission loss was accurately captured by the two-load method, the four-pole parameters were not as concise as those found by the two-source method. Including the aforementioned reason-

ing, the two-source location method was also selected due to the investigation performed by Munjal [51] where the two-source method was proven to be functionally more stable than the two-load method.

To carry out the two-source location method, two separate experimental cases are required for calculation of the four pole parameters. As seen in Figure 3.2, the excitation source is placed in the downstream location (a) and secondly in the upstream position (b). During each of the two configurations, the excitation source is a white noise signal with uniform power across the frequency spectra. A pair of microphones are placed on either end of the test section (two acoustically upstream and two acoustically downstream) as illustrated in Figure 3.2. Their axial locations along the pipeline and the microphone pair spacing remains constant throughout the procedure at a value previously specified in section 3.1 of this thesis: 196.85mm (7.75 in) in order to achieve a cut-off frequency of 873 Hz with sufficient accuracy in the measurements. The four microphones are phase matched and simultaneously capture the acoustic pressure response for their respective locations. This allows for the complete determination of the set of complex transfer functions for the acoustic pressure signals relative to one another (H_{12}, H_{23} and H_{43}) for each experimental configuration (a and b) utilizing Equation 3.1.

$$H_{ij} = \frac{p_i}{p_j} \tag{3.1}$$

The transfer matrix of the test element (located between the two microphone clusters) is calculated by manipulating the matrix multiplication of three transfer matrices:A transfer matrix representing a straight pipe between microphones one and two, a transfer matrix representing the test element, and a transfer matrix representing a straight pipe between microphones three and four, as illustrated in Figure 3.2. The four pole parameters of the transfer matrices of the straight pipe sections (for the a and b experimental

configurations) are calculated using the following expressions:

$$\begin{bmatrix} A_{ij} & B_{ij} \\ C_{ij} & D_{ij} \end{bmatrix} = e^{-M\beta_{ij}} \begin{bmatrix} cosh\beta_{ij} & Zsinh\beta_{ij} \\ \frac{sinh\beta_{ij}}{Z} & cosh\beta_{ij} \end{bmatrix} \ , \ \Delta_{ij} = e^{-2M\beta_{ij}} \tag{3.2}$$

$$\beta_{ij} = (ik_c + \alpha_c)l_{ij} \ , \ k_c = \frac{k}{1-M^2} \ , \ \alpha_c = \frac{\alpha}{1-M^2} \tag{3.3}$$

$$k = k_0 + \alpha \ , \ \alpha = \alpha_0 + \frac{MF}{2D} \ , \ Z = Z_0[1 - \frac{\alpha}{k_0} + \frac{i\alpha}{k_0}] \ , \ Z_0 = \frac{\rho c}{S} \tag{3.4}$$

By substitution and rearrangement of the above relations, the four pole parameters of the transfer matrix of the test element is determined utilizing Equation 3.5 - 3.9.

$$A = \frac{\Delta_{34}(H_{23,a}H_{43,b} - H_{23,b}H_{43,a}) + D_{34}(H_{23,b} - H_{23,a})}{\Delta_{34}(H_{43,b} - H_{43,a})} \tag{3.5}$$

$$B = \frac{B_{34}(H_{23,a} - H_{23,b})}{\Delta_{34}(H_{43,b} - H_{43,a})} \tag{3.6}$$

$$C = \frac{(H_{13,a} - A_{12}H_{23,a})(\Delta_{34}H_{43,b} - D_{34}) - (H_{13,b} - A_{12}H_{23,b})(\Delta_{34}H_{43,a} - D_{34})}{B_{12}\Delta_{34}(H_{43,b} - H_{43,a})} \tag{3.7}$$

$$D = \frac{B_{34}[(H_{13,a} - H_{13,b}) + A_{12}(H_{23,b} - H_{23,a})]}{B_{12}\Delta_{34}(H_{43,b} - H_{43,a})} \tag{3.8}$$

$$\Delta_{34} = A_{34}D_{34} - B_{34}C_{34} \tag{3.9}$$

Finally, Equation 3.10 defines the Transmission loss of the test element which is calculated utilizing the previously determined four pole parameters of the transfer matrix representing the test section.

$$TL = 20log(0.5\left|A + \frac{S}{\rho c}B + \frac{\rho c}{S}C + D\right|) \tag{3.10}$$

3.3.2 Insertion Loss

Although all of the work in the literature regarding HQ devices has focused primarily on measurements of Transmission loss, when considering a resonant system the effects of the boundary conditions and source are of critical importance. For this reason, Insertion loss was also selected for measurement because there is potentially an expectation that the transmission loss parameter may not capture some trends with respect to applying an HQ device in a resonant system.

The procedure to conduct Insertion loss measurements begins by exciting the pipeline with a 150 Hz Pulse signal with a duty cycle of 10% in order to mimic the acoustic excitation seen by a centrifugal pump. Insertion loss is calculated by first measuring the sound pressure level at a single location for a base case (in this work, a straight pipe section without a damping device is utilized) and subtracting the sound pressure level recorded at the same location, after a device is inserted into the given system. The insertion loss is calculated utilizing Equation 3.11. The insertion loss measurements are highly system dependent as to capture the trends related to a resonant system. To increase the reliability of the results, several microphone locations are simultaneously measured downstream of the device to ensure that the insertion loss measurements are not spatially dependent on the location downstream of the device.

$$IL = SPL_{Without\ damping\ device} - SPL_{With\ damping\ device} \tag{3.11}$$

3.3.3 Acoustic Reflection Coefficient, Specific Acoustic Impedance Ratio

In order to determine the acoustical effects induced by the attachment of an HQ device to a given system, as well as to understand the mechanism of attenuation of the HQ device, the acoustic reflection coefficient and specific acoustic impedance ratio are determined.

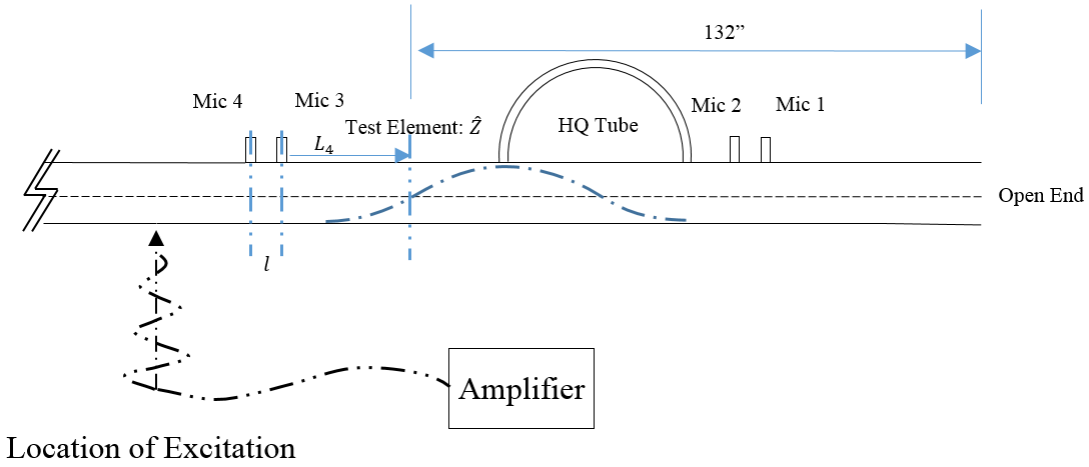

Figure 3.4: Schematic of the two microphone wave decomposition set-up utilize to determine the acoustic reflection coefficient and specific acoustic impedance ratio

The ASTM 1050 standard was utilized to carry out the aforementioned measurements and focus on the two microphone wave decomposition method[52]. The analysis procedure can be understood through the schematic shown in Figure 3.4 such that a white noise signal is excited within the piping system.

The reflection coefficient and specific acoustic impedance ratio are first measured for a straight pipe as a case for comparison and additionally for an open end case for validation. Microphones 3 and 4 record the acoustic pressure signal so that the transfer function between these two signals can be obtained through Equation 3.1. Through fixing the spacing between the microphones and recording the distance from the nearest microphone to the test element, the acoustic reflection coefficient and specific acoustic impedance/admittance ratio can be calculated using Equation 3.12 - 3.14.

$$R = \frac{H_{ij} - e^{-ikl}}{e^{ikl} - H} e^{i2k(L_4+l)} \tag{3.12}$$

$$\frac{z}{\rho c} = \frac{1+R}{1-R} \tag{3.13}$$

$$y\rho c = \frac{\rho c}{|z|} \tag{3.14}$$

After determining the aforementioned parameters for the straight pipe case, the HQ device is then attached to the system so that the acoustic reflection coefficient and specific acoustic impedance ratio can be calculated. The changes in the reflection coefficient and the specific acoustic impedance ratio are then compared for both the straight pipe case and the case with the added HQ device for investigation.

3.3.4 Acoustic Pressure Signal Phase Measurements

To further clarify the mechanism of attenuation of the HQ device under resonant conditions, acoustic pressure signal phase measurements were conducted for several strategic points along the axial location of the HQ device and within the main pipeline as shown in Figure 3.5. A square wave pulse signal at the targeted frequency of 150 Hz is utilized during this experiment to initiate a strong acoustic resonance within the piping system. To determine if a travelling wave or standing wave phenomenon is present within the device, the microphones were placed at locations where the first, second and third acoustic mode could be observed if present. To ensure accurate measurements of the phasing between the acoustic pressure signals, the microphones were phase matched using the phase correction methodology outlined in the ASTM 1050 standard [52]. The post processing of the gathered data consisted primarily of constructing the acoustic wave form, acoustic pressure-frequency spectra and obtaining the phase angle between different pressure signals. The pressure-frequency spectra is routinely obtained using MATLAB software, employing Hann windowing and ensemble averaging while the acoustic pressure signal phase measurements were computed utilizing the four quadrant inverse tangent of the complex transfer function relating the two pressure signals of interest.

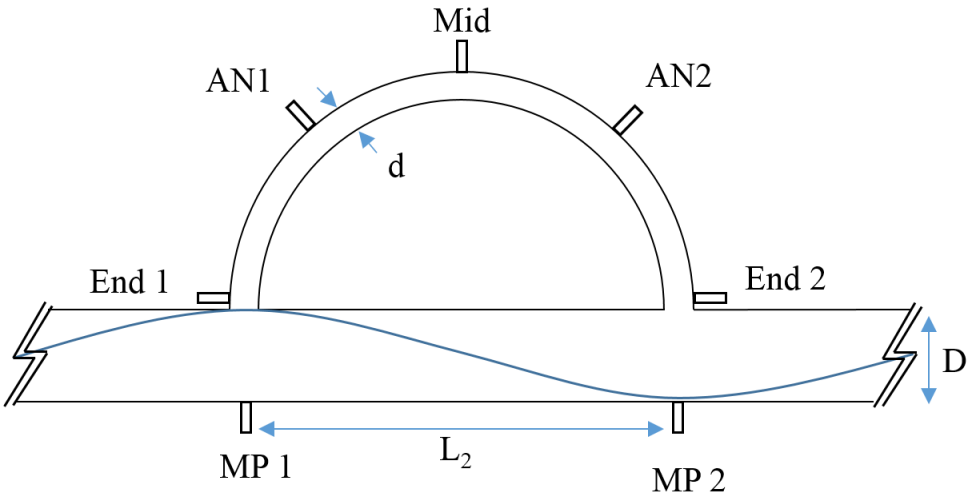

Figure 3.5: Schematic of the acoustic pressure signal phase measurements conducted within the HQ device and main piping system

3.4 Experimental Validation

Although the two source location method used to obtain the transmission loss was developed by Munjal [51] and previously validated by other studies, it was important for the current work to baseline the implementation of such a method into the current work along with the validity of the experimental set-up consisting mainly of the piping system, excitation source, pressure microphones, signal conditioner and DAQ device. To carry out such validation a reactive muffler was constructed with a cross sectional area ratio h=0.13 and a chamber length of L_1=609.6 mm . This allowed for the measured transmission loss to be compared with the known analytical formula obtained through the classical transfer matrix method as illustrated in Equation 3.15 [53], [54].

$$TL_{Reactive\ Muffler} = 10log[1 + 0.25(h - \frac{1}{h})^2 sin^2(kL_1)] \tag{3.15}$$

Figure 3.6 compares the measured and theoretical predictions for the transmission loss of the constructed reactive muffler. There exists a good agreement overall, with discrepancy arising above the cut-off frequency corresponding to the microphone spacing

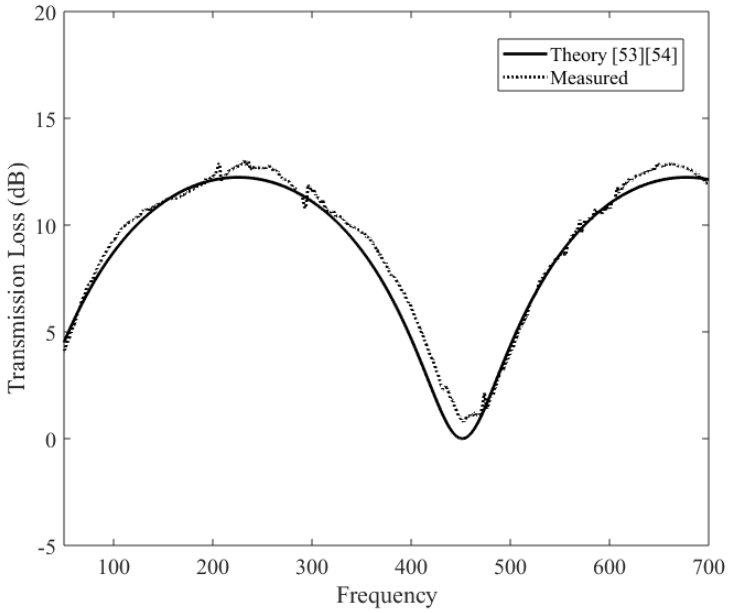

Figure 3.6: Measured and theoretical[53], [54] comparison of the transmission loss of a reactive muffler: h=0.13 ,L_1=609.6 mm

(approx. 873 Hz) while the typical measurement range of interest for this work is from 60 Hz-450 Hz.

An additional point of validation was conducted as shown in Figure 3.7 to also confirm the proper construction and implementation of the HQ device before proceeding with any experiments by comparing an HQ device of diameter ratio d/D=0.25 to that of the analytical model found in Eqn. 2.11 developed by Selamet [40].

When considering that the limitation on the theoretical model developed by Selamet [40] is the omission of the effects of dissipation, the magnitude of the peaks of the transmission loss at the resonant frequency can not be compared with that of the experiment. However, the results agree well with one another with respect to the prediction of the frequencies of attenuation for both the Type I and Type II mechanisms as well as the general trend with regards to the surrounding frequencies.

The two microphone wave decomposition method was also validated where for this

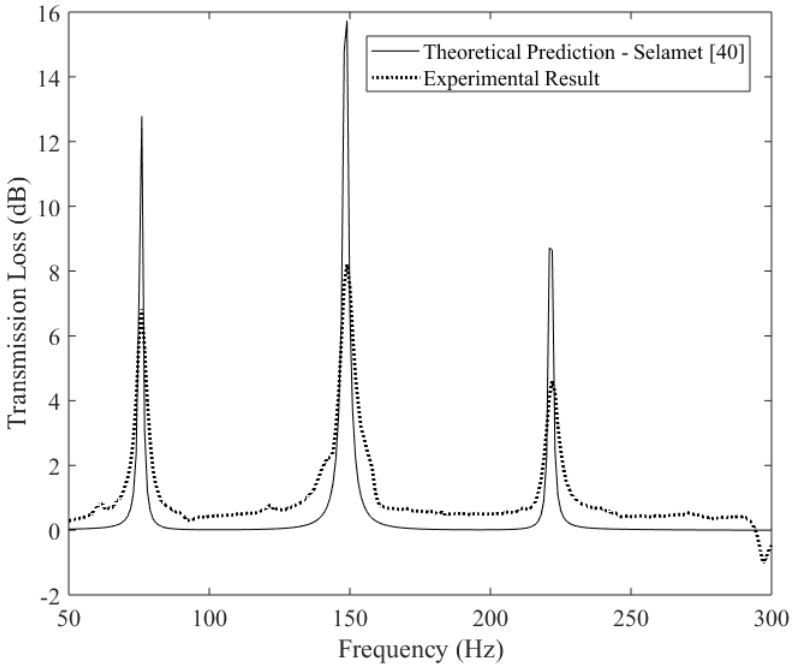

Figure 3.7: Measured and theoretical[40] comparison of the transmission loss of a HQ tube with d/D=0.25

comparison, the theoretical specific acoustic admittance ratio of an open unflanged circular pipe developed by Levine and Schwinger [55] was compared to that of the experimentally obtained results. a good overall agreement was obtained as shown in Figure 3.8 with discrepancy arising at the cutoff frequency of the microphone spacing selected (approaching 873 Hz).

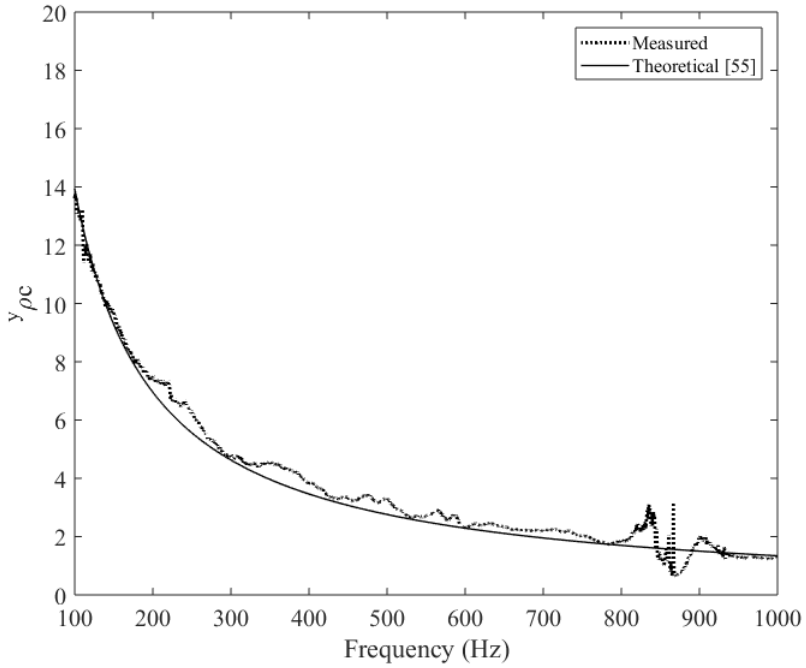

Figure 3.8: Measured and theoretical[55] comparison of the specific acoustic admittance ratio of an open unflanged circular pipe

Chapter 4

Passive Damping of a Resonant Piping System

In this chapter, the effects of an HQ device applied to a resonant piping system is studied with a variety of parameters including the relative diameter ratio between the HQ device and the piping system, the effects of placing an HQ device at different points along the axis of the pipeline, the effect of adding multiple HQ devices and finally the effects of mean flow and directionality on the performance of the HQ device. The experiments were strategically designed to answer the research needs outlined in Chapter 2.6. For all of the resonant piping system tests, the pipeline length was tuned so that the 5^{th} acoustic mode corresponds to the 150 Hz frequency of interest. The 5^{th} acoustic mode was selected due to the fact that the fundamental mode is very small in length, which is not sufficient to successfully implement an HQ device. In addition to this, the requirement of multiple locations of acoustic pressure nodes and antinodes along the standing wave formed in the test section is achieved with the higher order mode which was selected.

4.1 Relative Diameter Ratio (d/D)

Although the use of the diameter ratio between the HQ device and main piping system has been well used in the literature, there has been no work which characterizes if this parameter truly scales linearly with the transmission loss. One of the focuses of this work is to vary the diameter ratio as well as the test section diameter to see if the transmission loss of the Type I mechanism scales linearly. This is an important aspect for the practical implementation of HQ devices into piping systems as it will provide insight into the feasibility of scaling the HQ device to a larger piping system. Diameter ratios ranging from 0.083 - 0.5 were selected as this lower range below d/D=0.5 has not yet been investigated to date. The increase in the relative diameter ratio changes the acoustic impedance ratio between the two branches and thus affects the performance of the device. Considering a one dimensional acoustic wave propagating in a circular pipe, the acoustic impedance is equal to the specific acoustic impedance divided by the cross sectional area of the pipe. Thus, increasing the area will decrease the acoustic impedance causing a change in attenuation achieved by the HQ device. This mechanism is explained in further detail in section 6.2 of this work. It is evident that the change in diameter ratio does not affect the frequency of the Type I peaks as this is purely a function of the length ratio. However, the diameter ratio is seen to have an effect on the central frequency of the Type II attenuation peaks agreeing with previous findings in the literature [47] [45]. The transmission loss was recorded for several different diameter ratios (with varying test section diameters) as shown in Figure 4.1. In agreement with the literature, the increase of the relative diameter ratio causes an increase in the transmission loss, as well as a widened bandwidth around the Type I and II peaks. The magnitude of the Type I peaks in the transmission loss curves located at 150 Hz were extracted and plotted as a function of the relative diameter ratio as illustrated in Figure 4.2. It is now evident that the transmission loss clearly normalizes linearly with the relative

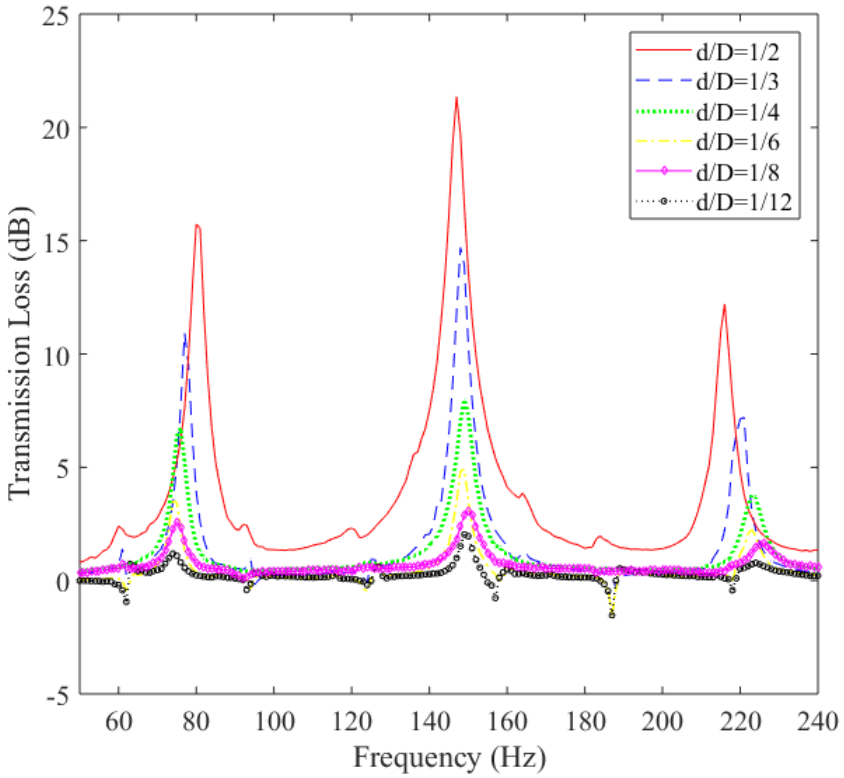

Figure 4.1: Transmission loss measured for several HQ devices with varying diameter ratio

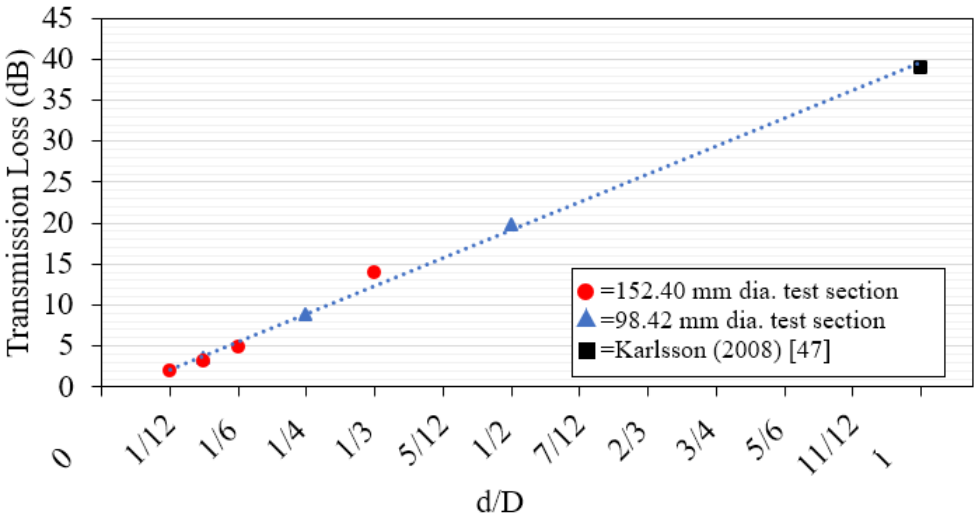

Figure 4.2: Extracted transmission loss peaks at the 150 Hz Type I peak normalized by relative diameter ratio

diameter ratio, even when the test section diameter changes from 98 mm to 152 mm. Two cases are plotted for the 98 mm and 152mm test sections for the data points with d/D=1/8 and lie on top of one another. The case of Karlsson [47] with d=D=85 mm is also supportive of this aforementioned trend. The agreement with the work of Karlsson [47] also illustrates the universality of transmission loss measurements, considering that their work was not subject to a resonant piping system. The independence of the end conditions and source impedance allow for this clear comparison. This practical finding strengthens the potential for implementation of an HQ device to larger piping systems in industry while showing that even a single small relative diameter ratio device can yield significant transmission loss under resonant conditions.

The effect of an HQ device on the total acoustic response of the piping system has not yet been addressed in the literature to date. The total acoustic response of the piping system was measured by means of a pressure microphone mounted at a pressure antinode of the piping system. As illustrated in Figure 4.3 the total acoustic response of the piping system was captured for HQ devices with various relative diameter ratios.

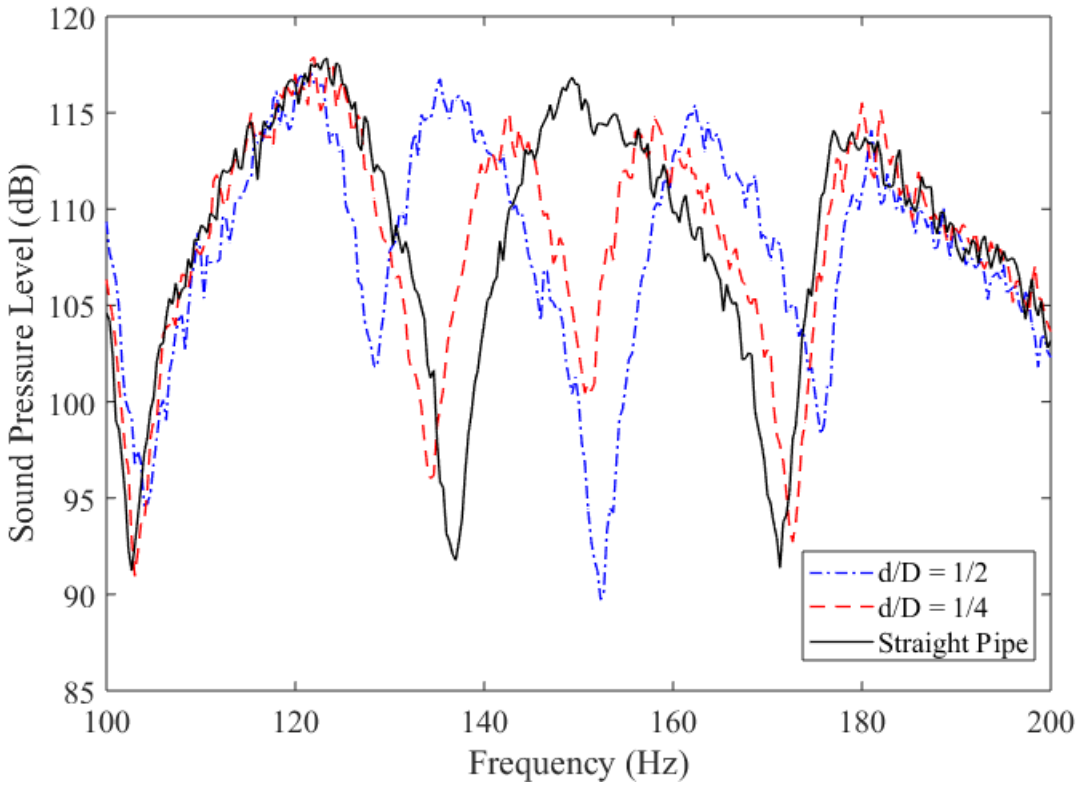

Figure 4.3: Natural acoustic response measured at a pressure antinode within the main piping system without and with HQ devices of varying relative diameter ratio

For low diameter ratios, the effects are seen to be quite small which allows for surety in the results for diameter ratios below 0.5. When considering insertion loss measurements in the future sections, it is important to verify the aforementioned point considering that the insertion loss is highly system dependant. A significant shift in the frequency of the total acoustic response of the system may provide falsely elevated values of attenuation attributed to the decoupling of the piping system to the source (resulting in a reduction of the intensity of the acoustic resonance within the piping system). It is evident that with the addition of an HQ device, there is a sharp decrease in the sound pressure level at the targeted frequency of 150 Hz, as intended to dampen the acoustic resonance. However, as the relative diameter ratio of the HQ device approaches 0.5, a shift in the adjacent

d/D	$f_{5,\,Shift}$ Measured (Hz)		$f_{5,\,Shift}$ Predicted (Hz)		Percent Error (%)	
	1st Aux. Peak	2nd Aux. Peak	1st Aux. Peak	2nd Aux. Peak	1st Aux. Peak	2nd Aux. Peak
0.25	142.7	158	146.46	153.5	2.6	2.8
0.5	135.3	162.3	136.67	163.33	1.0	0.6

Table 4.1: Measured and analytically predicted shift in the 150 Hz resonant frequency of the total acoustic response of the piping system. HQ devices with d/D=0.25, 0.5

resonant and anti-resonant peaks is noted. This shift in the total acoustic response near the Type I attenuation frequency of the HQ device concludes that only diameter ratios less than 0.5 can be studied throughout this work when considering insertion loss measurements in order to maintain the integrity of the results. In addition to the shift in frequency noted for the adjacent resonant and anti resonant peaks in the total acoustic response of the system, the effective antinode which is introduced at the central 150 Hz frequency also shows a slight deviation with the change in the relative diameter ratio of the HQ device.

The shift in the total acoustic response of the system is proposed to be due to the change in the fluid volume ratio between the HQ device and the main piping system, along with the added damping effects which are induced by the HQ device. The change in the fluid volume ratio between the HQ device and the main piping system causes a shift in the adjacent resonant and antiresonant frequencies of the total acoustic response of the system. An effective length can be utilized to account for the change in the aforementioned fluid volume ratio. The change in the fluid volume ratio between the HQ device and the main piping system is characterized analytically in this work using an effective length stated in Equation 4.1 where it represents the added length of the main pipe which has an equivalent fluid volume to that of the HQ device. Therefore, the effective length is added to the main pipeline length in order to predict the shift in the adjacent resonant frequencies. Equation 4.2 represents the shift of the 1^{st} auxiliary resonant peak while Equation 4.3 represents the shift in the 2^{nd} auxiliary resonant peak

with the change in frequency defined through Equation 4.4.

$$L_{Eff.} = \frac{d^2}{D^2} L_3 \tag{4.1}$$

$$f_{5,\,Shift\,(Left)} = \frac{5c}{2(L + L_{Eff.})} \tag{4.2}$$

$$f_{5,\,Shift\,(Right)} = \frac{5c}{2(L - L_{Eff.})} \tag{4.3}$$

$$\Delta f_5 = \| |f_5 - f_{5,\,Shift\,(Left)}| \| \tag{4.4}$$

Table 4.1 shows the comparison of the measured and predicted shifted auxiliary resonant peaks of the natural acoustic response of the piping system which are induced by attaching several sized HQ devices. With a percentage error less than 3%, the effective length analogy closely predicts the shift in the total acoustic response of the system as a result of changing the fluid volume ratio between the HQ device and the main pipeline. It is also of interest to compare this behaviour to that of a mechanical vibration absorber for discrete systems as there are striking similarities between the two. For a mechanical vibration absorber in a discrete system, the mass ratio between the absorber and the main system will govern the shift in the total response of the system [56]. Similarly, if we consider one of the shifted frequency equations 4.2, the denominator contains a $L + L_{Eff.}$ term, meaning that a shift in the adjacent resonant frequencies will take place *only* when $L_{Eff.}$ becomes of similar magnitude to L. This implies that the fluid volume of the HQ device relative to the main pipeline fluid volume also governs the shift in the natural acoustic response of the total system for the adjacent resonant peaks. This observed behaviour is further supported by the results found in Chapter 6, particularly the observed acoustic response of the HQ device.

It is also observed in Figure 4.3 that the central antiresonant peak introduced at the 150 Hz frequency is shifted slightly away from this targeted value as the diameter

ratio increases. When considering a damped mechanical vibration absorber applied to discrete systems, a change in the damping ratio is responsible for a shift in the location of the targeted frequency of the central antiresonant peak. The damping ratio of the mechanical vibration absorber also governs the change in the magnitude of the adjacent resonant peaks such that the 1^{st} auxiliary resonant peak is different in magnitude then that of the 2^{nd} auxiliary resonant peak [56].

Analogously, the visco-thermal losses of the HQ device are a function of the diameter of the HQ device, as well as the total length of the device. The change in visco-thermal losses along the HQ device are seen to exhibit very similar trends to that of a damped mechanical vibration absorber, whereby the antiresonant peak at the 150 Hz target is slightly shifted, along with a change in magnitude between the adjacent 1^{st} and 2^{nd} auxiliary resonant peaks. This knowledge can help to optimally tune a HQ device so that the shift in the targeted frequency caused by the changing damping ratio can be preemptively compensated for.

Number of HQ Devices	$f_{5,\,Shift}$ Measured (Hz)		$f_{5,\,Shift}$ Predicted (Hz)		Percent Error (%)	
	1st Aux. Peak	2nd Aux. Peak	1st Aux. Peak	2nd Aux. Peak	1st Aux. Peak	2nd Aux. Peak
1	144.3	155.7	148.4	151.6	2.86	2.73
2	142.3	157.0	146.9	153.2	3.20	2.51
3	141.0	158.3	145.3	154.7	3.05	2.43
4	140.0	160.0	143.8	156.2	2.71	2.43

Table 4.2: Measured and analytically predicted shift in the 150 Hz resonant frequency of the total acoustic response of the piping system for multiple HQ devices

To further validate this analytical concept, the added effective length analogy was applied to the scenario where multiple devices are attached to a resonant piping system. Figure 4.4 shows the change in the natural acoustic response of the system before and after several HQ devices are added. A very similar trend is observed when drawing comparison to Figure 4.3. For this scenario, the change in the fluid volume ratio from the multiple HQ devices was accounted for by increasing the total length L_3 in Equation

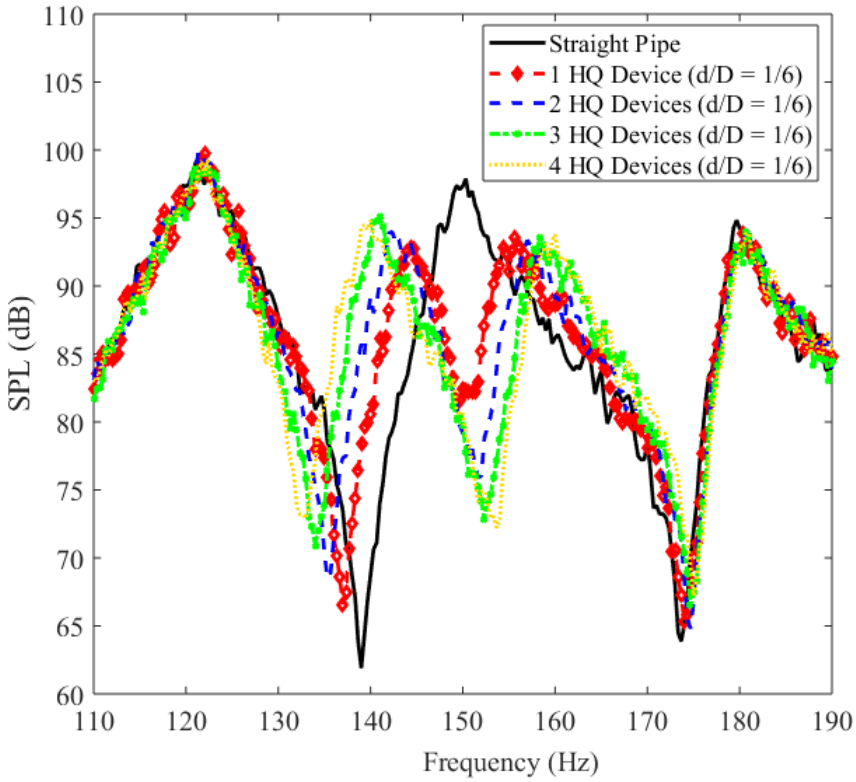

Figure 4.4: Natural acoustic response measured at a pressure antinode within the main piping system without and with multiple HQ devices

4.1 in order to compensate for the added HQ devices to the system (all of which having d/D=1/6). Table 4.2 shows a good agreement between the measured and predicted values for the shifted auxiliary resonant frequencies, further supporting this analytical analogy. The trends related to the added damping of the HQ device (a function of changing the diameter ratio and the total length of the HQ device) are observed in Figure 4.4 such that the shift in the central anti-resonant frequency is present along with varying magnitudes of the 1^{st} and 2^{nd} auxiliary resonant peaks.

4.2 Axial Location of an HQ Device

To successfully implement an HQ device into a resonant piping system, selecting the correct device location along the axial direction of the piping system is a necessity. The attenuation effects of placing an HQ device at different points along the standing wave formed in the main piping system has not been considered to date. The current work will investigate the change in transmission loss and insertion loss as an HQ device is moved to different locations along a quarter wavelength of the standing wave while maintaining a constant length ratio of $\frac{L_3}{L_2}$=2. The notation used to describe such positions can be seen in Figure 3.1 where both ends of the HQ device have a spacing of $\frac{\lambda}{2}$ along the piping system. This configuration allows for the acoustic pressure in the main piping system for each end of the HQ device to be equal in magnitude but opposite in phase. The measured transmission loss for several device placements along the standing wave in the piping system is shown in Figure 4.5. An interesting trend is observed such that the transmission loss was almost identical for all of the axial locations tested. This trend is likely due to the nature of the transmission loss parameter such that it is independent of the end terminations and source impedance. A parameter which is independent of the end terminations would imply that the measurements for a resonant system with reflections at the boundaries would be equivalent to that measured for anechoic end terminations without any reflections or resonance. The literature to date has not performed any insertion loss measurements regarding HQ devices for the aforementioned reasoning as it does not allow for the comparison to other research works considering that insertion loss is system dependent. This is also due to the fact that no measurements of an HQ device have been performed for a resonant system and so it was not necessary to measure insertion loss.

However, to capture the effects of changing axial location, insertion loss is measured as illustrated in Figure 4.6. It is now clear to see that the attenuation provided by the HQ device is significantly affected by the location which it is placed along the standing

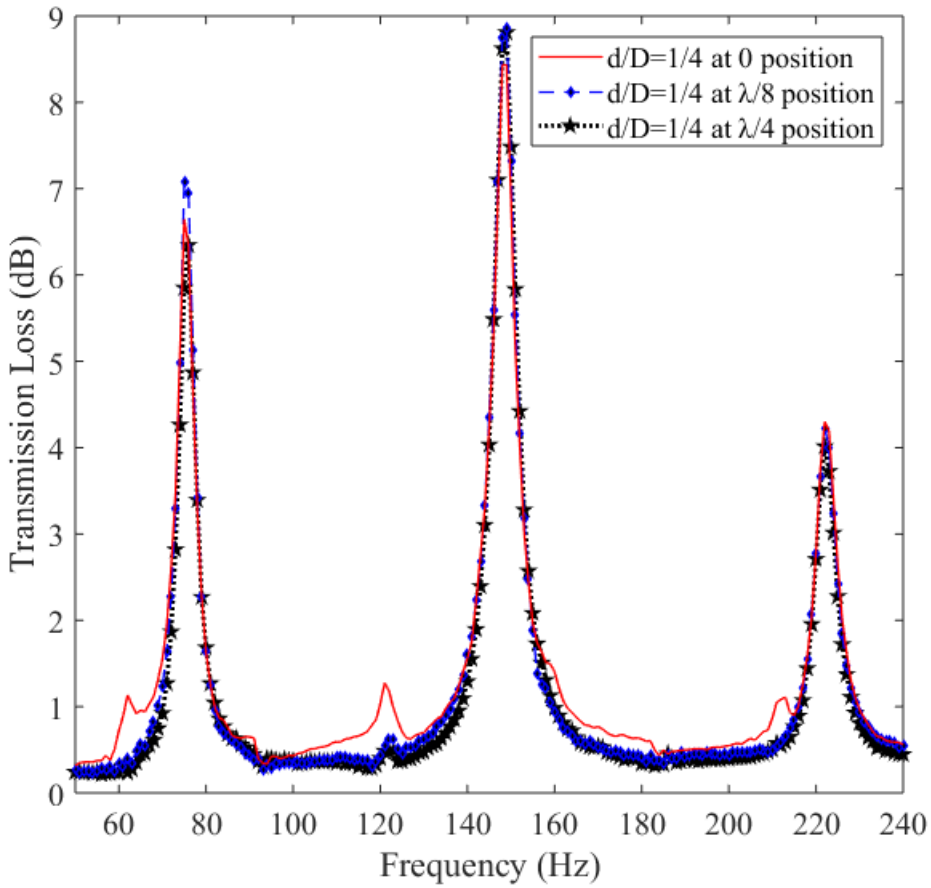

Figure 4.5: Transmission loss measured for various HQ device locations along the axial direction of the main piping system

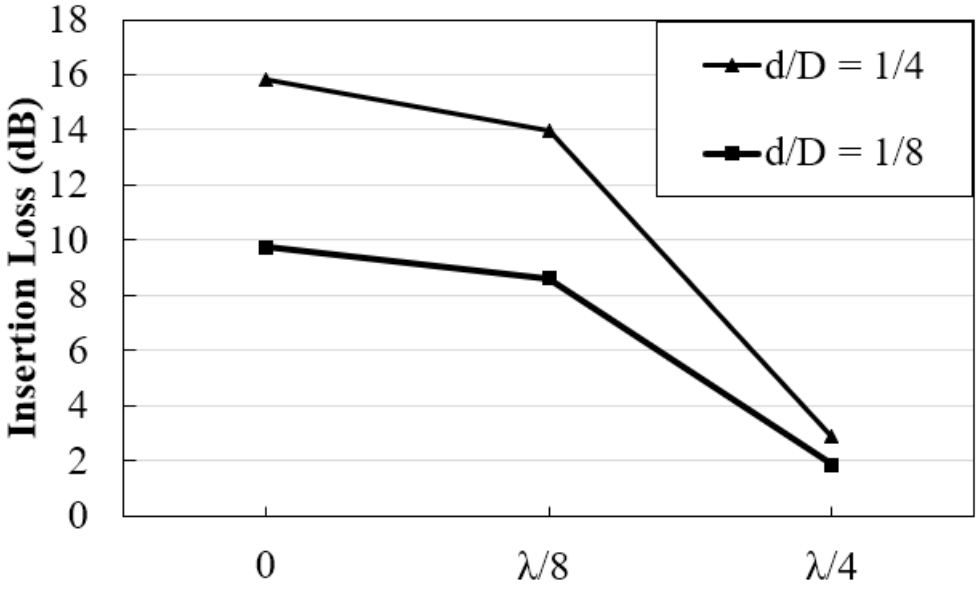

Figure 4.6: Insertion loss measured for various HQ device locations along the axial direction of the main piping system

wave. The acoustic pressure antinode is seen to have the best performance while the performance decreases toward the acoustic pressure node. Considering that this trend takes on a sinusoidal contour, it is clear that the attenuation is very much governed by the magnitude of acoustic pressure present at the ends of the HQ device. At the acoustic pressure node, no fluctuation in acoustic pressure is present and the HQ device can not be excited as intensely as when it is placed at an acoustic pressure antinode. This pattern was noted to be cyclical such that sweeping the location of the HQ device toward a different acoustic pressure antinode within the system would yield a similar result.

For industrial application, device placement along the axis of the pipeline is crucial for a resonant system. This is evident when comparing the different relative diameter cases such that a small but well-placed device (zero location) will yield more attenuation then a larger poorly-placed device ($\frac{\lambda}{4}$ location). This is useful if space is limited or a larger sized HQ device is not feasible.

4.3 Implementation of Multiple HQ Devices

For scenarios where large values of attenuation are desired, multiple damping devices may be of interest. However, to date it is unclear if a single large device can be split into multiple smaller devices and still maintain effectiveness. This information is useful for industry use as a single larger HQ device may be costly or hard to implement into piping systems. The current work considers the measurement of transmission loss and insertion loss for multiple HQ devices placed at a single acoustic pressure antinode in the main piping system. Figure 4.7 shows the effect of multiple HQ devices on the transmission loss. It is evident to have a similar effect to that of increasing the relative diameter ratio considering that the overall magnitude of transmission loss increases with the number of devices as well as the width of the transmission loss peaks becomes larger. It can be thought of that the increase in the number of devices will increase the total equivalent cross sectional area of the HQ devices, ultimately having an effect on the total acoustic impedance.

When viewing the change in insertion loss with respect to the number of HQ devices in Figure 4.8, we can see that the trend is relatively linear. More importantly, the horizontal dashed line passes through the data points of a single HQ device with $d/D = 0.25$ and the equivalent total fluid volume case of four HQ devices with d/D= 0.125. Interestingly, the two cases yield nearly identical values for insertion loss which shows a very promising potential for use in industry. An outlier is seen to take place when comparing a single HQ device of $d/D = 0.5$ to four HQ devices with $d/D = 0.25$. This dissimilarity of results is due to the phenomenon explained in section 4.1, Figure 4.3. The single HQ device of d/D=0.5 caused a significant shift in the total acoustic response of the piping system due to its fluid volume being of considerable size when compared to the main piping system. The system dependent insertion loss parameter thus captured this change, and so the discrepancy of the $d/D = 0.5$ HQ when compared to 4 HQ devices with $d/D = 0.25$ is not surprising.

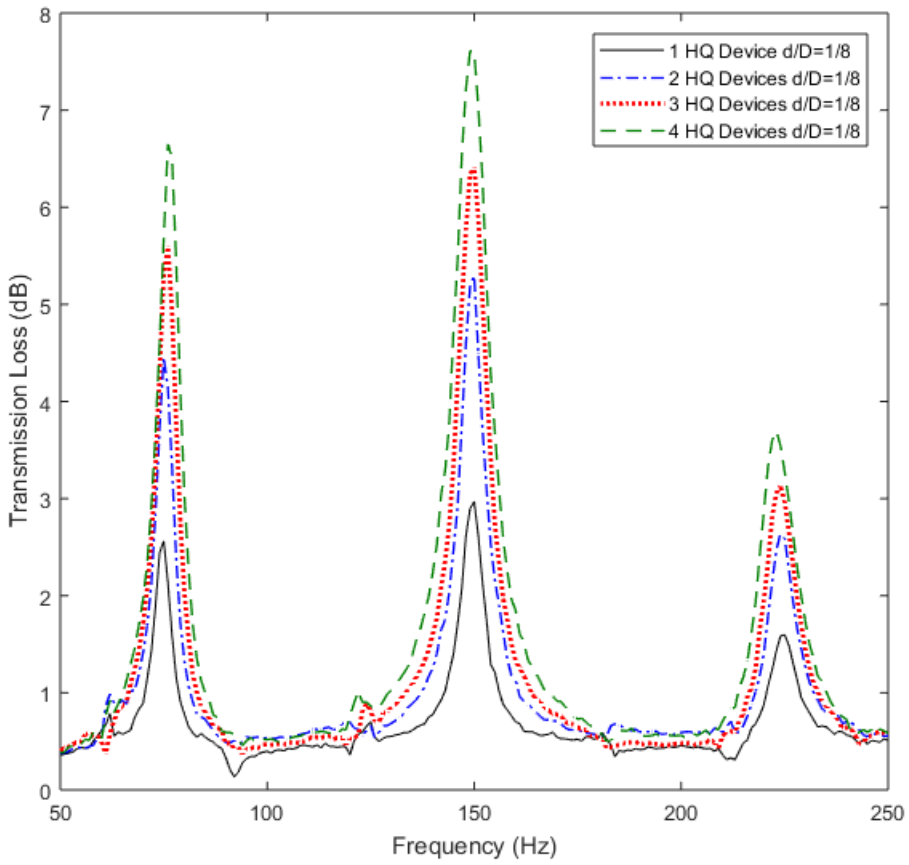

Figure 4.7: Comparison of multiple HQ devices attached to an acoustic pressure antinode on the measured transmission loss

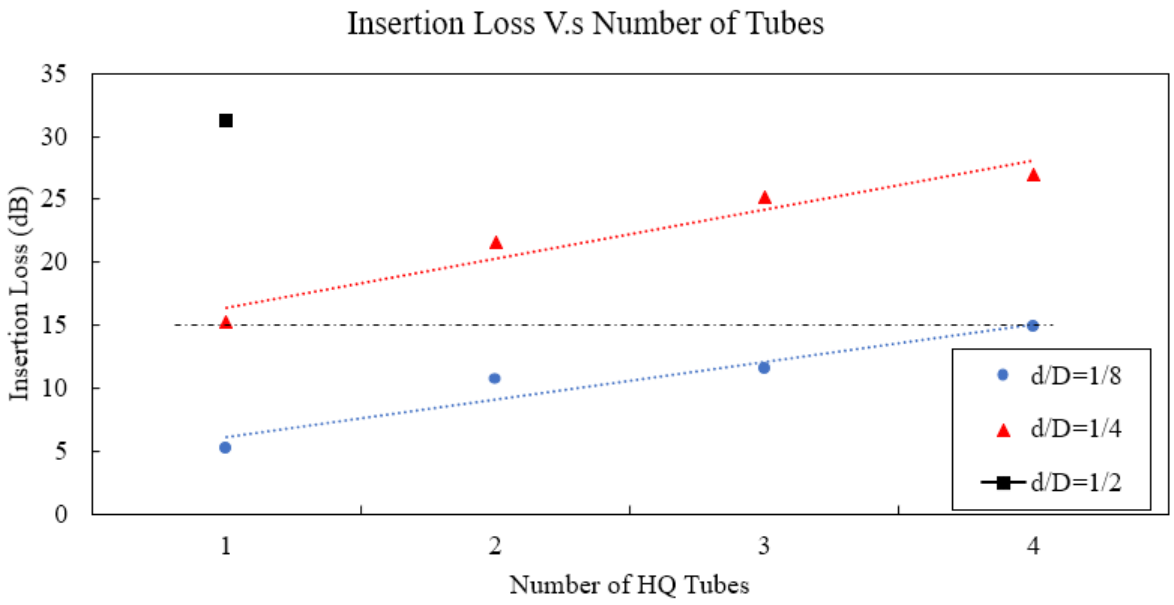

Figure 4.8: Measured insertion loss for multiple HQ devices attached to a single acoustic pressure antinode

To determine the feasibility of placing multiple HQ devices at different axial locations along the piping system, two HQ devices were placed either at a single pressure antinode, or dispersed at two different pressure antinodes as illustrated in Figure 4.9. The resultant effect of the aforementioned configuration on the insertion loss is seen in Figure 4.10 such that the devices can be dispersed or concentrated at the same point in the standing wave and still achieve nearly the same attenuation, a practical benefit where space is limited in a given piping system and the targeted wavelength of interest is known.

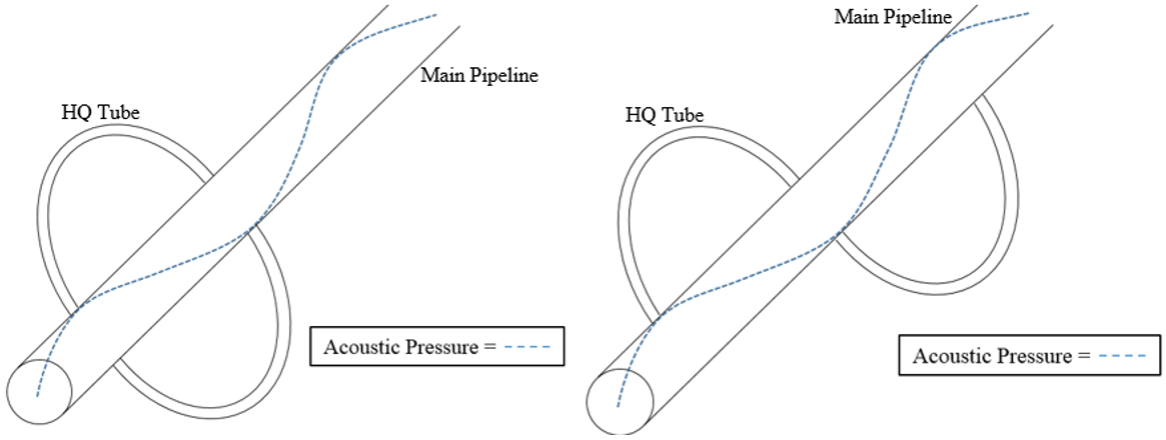

Figure 4.9: Schematic of two HQ devices of $d/D = 0.25$ attached to either a single acoustic pressure antinode (left) or different acoustic pressure antinodes (right)

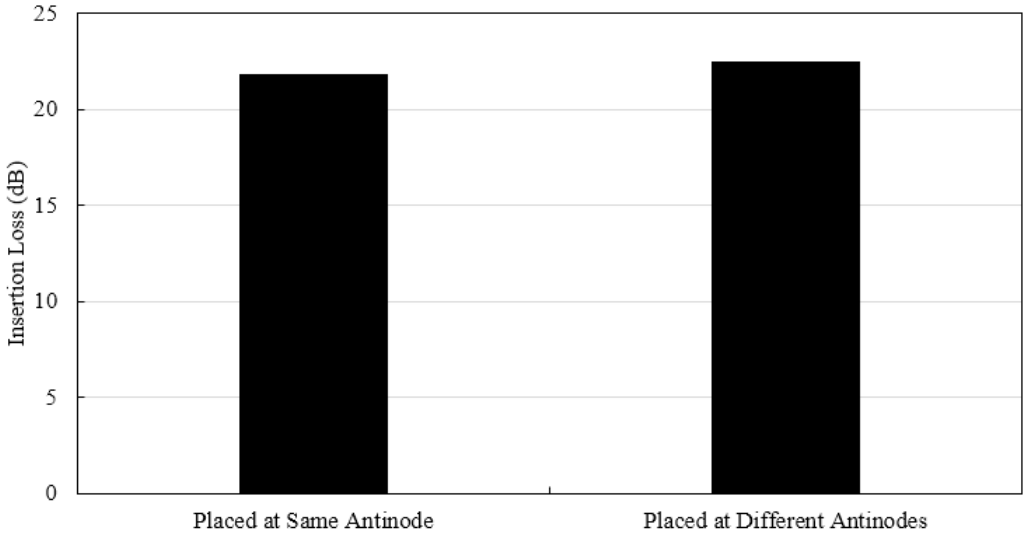

Figure 4.10: Measured insertion loss for two HQ devices of $d/D = 0.25$ attached to either a single acoustic pressure antinode or different acoustic pressure antinodes

4.4 Mean Flow and Directionality Effects

To consider the effects of mean flow velocity and its directionality relative to the incident acoustic propagating wave, flow velocities between 0-20 m/s (M=0-0.058) were selected not only to cover a range of industrially feasible values for a specific application, but also

to explore a range of Mach numbers below 0.15 as the literature to date has only studied cases with the mean flow greater than 0.15 Mach. The work of Karlsson [47] had shown that the presence of mean flow had decreased the transmission loss peak for the type I and II mechanisms, with a primary focus on the type I mechanism as it was observed to be much more sensitive to the presence of mean flow. For a Mach number of 0.15 almost 20 dB in decreased transmission loss was observed [47]. The current work shown in Figure 4.11 illustrates an agreement with the trends found in the literature. However, the mean flow effect on the type I transmission loss peak is much less pronounced for the lower mean flow velocity range which was studied with a decrease in TL of less than 3 dB for the largest mean flow of M=0.058.

There also exists a clear shift in the type I frequency of attenuation, such that an apparent increase in the frequency of attenuation of the HQ device is present. The work of Karlsson [47] attributes this shift in frequency to the unequal Mach number between the main pipe and the HQ device. The length of each of the two aforementioned branches governs the pressure drop induced by each branch (in addition to the junction geometry) which results in different mean flow velocities in each of the branches. Ultimately, this has an effect on the phase of the acoustic wave which is recombining at the downstream junction and thus a shift in the frequency of attenuation.

The junctions of the HQ device and main piping system may also induce some effect on the transmission loss in addition to that which was observed due to the uneven Mach number between the two branches. The effect of the shear layer separation over the mouth of the HQ device connection is expected to produce some contribution to the acoustic field as it impinges on the downstream wall of the junction. The directionality of the incident acoustic source produced in the experiment relative to direction of the mean flow becomes of interest, as the relative direction of the shear layer separation could play a role in affecting the attenuation of the HQ device. Figures 4.12 - 4.13 illustrate the change in insertion loss for both the downstream and upstream incident acoustic

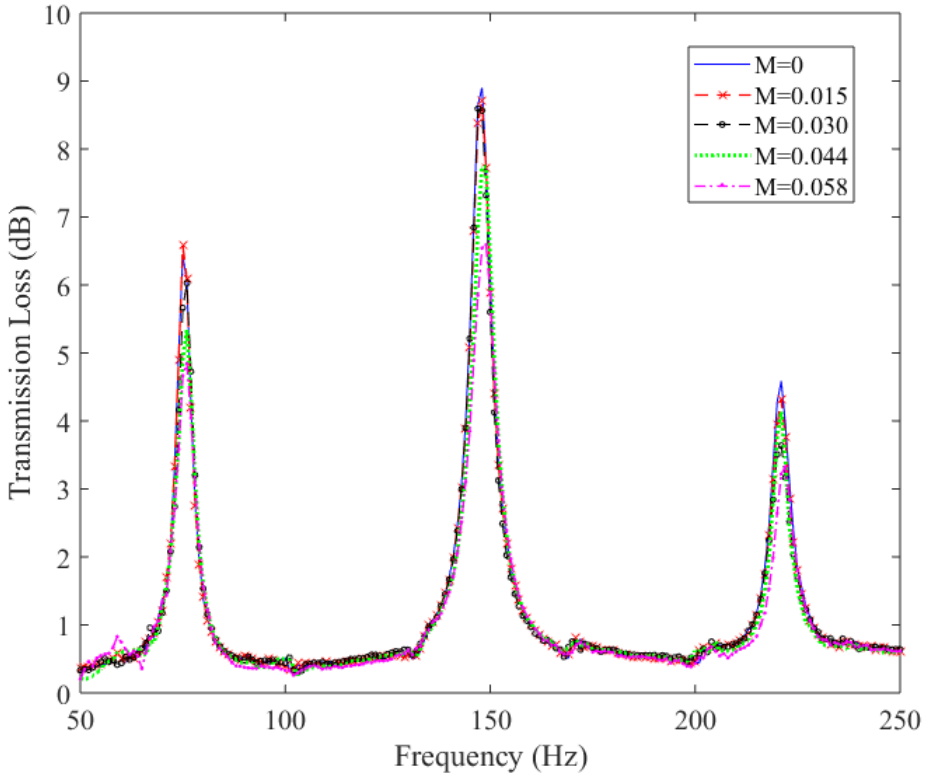

Figure 4.11: Comparison of mean flow with the measured transmission loss for an HQ device of d/D=0.25

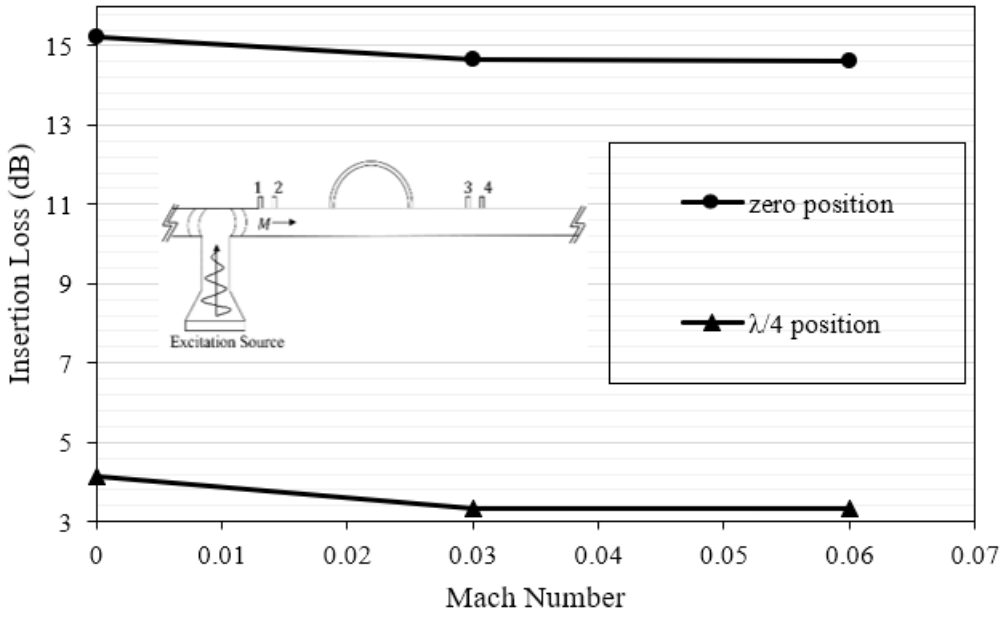

Figure 4.12: Mean flow effect on the transmission loss measured for a downstream incident acoustic propagating wave, HQ device of d/D=0.25

waves, respectively. It is observed that a downstream incident acoustic wave is seen to decrease the performance of the HQ device while the upstream incident acoustic wave shows improved attenuation. For the case of a downstream incident acoustic wave, the apparent sound speed is increased relative to an observer, while the upstream incident acoustic wave would case an apparent decrease in sound speed. The visco-thermal losses under turbulent mean flow conditions described by the analytical model developed by Howe [18] support the observed experimental trend, such that the visco-thermal losses are positively correlated to the frequency and negatively correlated to the speed of sound.

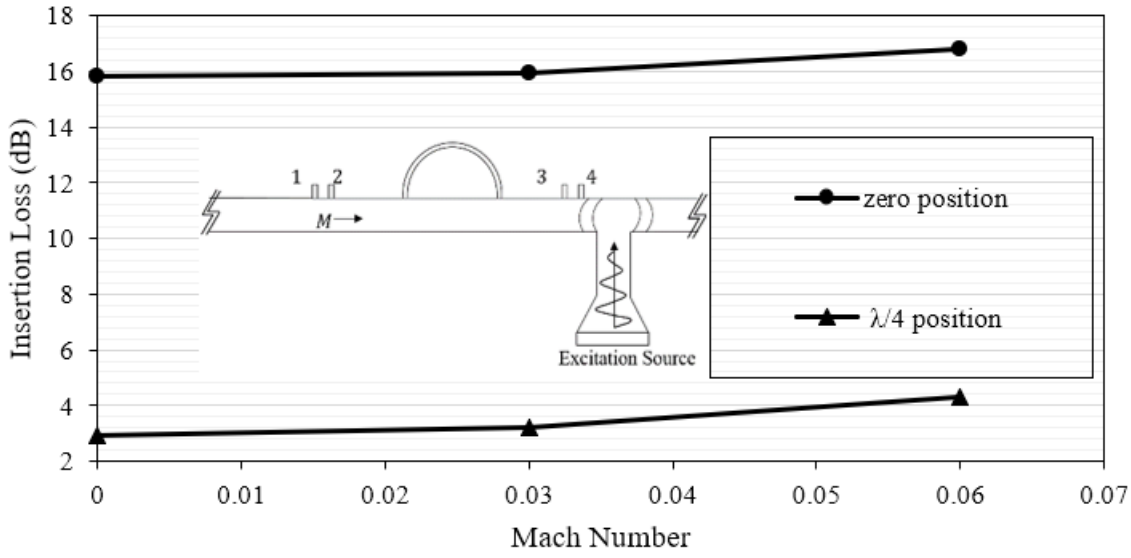

Figure 4.13: Mean flow effect on the transmission loss measured for an upstream incident acoustic propagating wave, HQ device of d/D=0.25

4.5 Summary and Conclusions

An extensive experimental study was conducted for HQ devices applied to a resonant piping system. Several piping system and damping device parameters were studied in order to understand their effects on the attenuation performance of the HQ device. The relative diameter ratio of the HQ device to the main piping system was seen to significantly impact the type I transmission loss attenuation peak magnitude, along with a shift in the type II transmission loss peak frequency. The relative diameter ratio was investigated for a range which was not yet experimentally tested in the literature and it was found in the current work that it provides a very good normalization for transmission loss, even for larger piping systems. The HQ device fluid volume relative to the piping system was also seen to control the shift in the total acoustic response of the system, a similar behaviour to that observed by a discrete system mechanical vibration absorber. This change in the mass ratio between the HQ device and the main pipeline was considered by proposing an analytical formula which outlined the effective length addition

to the main piping system as a result of changing the device diameter ratio and/or the number of HQ devices implemented. The HQ device placement along the axial direction of the piping system was seen to have a significant effect on the acoustic performance of the device such that the acoustic pressure antinode yielded the maximum attenuation while the acoustic pressure node showed poor acoustic attenuation. The division of a single large HQ device into several smaller HQ devices with an equivalent total fluid volume yielded nearly identical insertion loss values proving that a large device can be divided into smaller devices and still achieve very similar values of attenuation. It was also shown that dispersing multiple devices at different points along the piping system (at the same relative point along the standing wave) yielded nearly the same attenuation as placing multiple devices at the same axial location along the piping system, allowing for convenience and flexibility for application in industry. Finally, the effect of the presence of mean flow was investigated for a lower mean flow velocity range targeted for a specific application. It was found that although there was an agreement with the trends found in the literature, the mean flow effect on the attenuation of the HQ device was much less pronounced for this reduced range of flow velocities. The effect of the directionality of the mean flow relative to the incident acoustic source direction showed some effect on the attenuation of the HQ device such that the downstream incident wave decreased the attenuation while an increase in attenuation was observed for an upstream propagating acoustic wave. The contribution of the shear layer separation and impingement on the downstream wall of the HQ/main pipeline junction relative to the incident acoustic wave direction was discussed along with the changing apparent sound speed resulting in the cases of the downstream and upstream acoustic propagating wave.

Chapter 5

Attenuation Mechanism During Resonant Conditions

To clarify the mechanism of attenuation of the HQ device under resonant conditions, the acoustic response of the HQ device will be measured for several locations along the axial direction of the HQ device. Measurements will also be taken within the main pipeline at the junctions in order to determine the acoustic interaction between the main system and the HQ device. The imaginary impedance of the piping system will also be investigated in order to determine what change in impedance is induced by adding an HQ device to the piping system. The acoustic reflection coefficient will be studied for an HQ device to see what portion of the acoustic energy is reflected back to the source. Finally, Computational Aeroacoustic (CAA) Simulations will be conducted in order to further solidify the mechanism observed throughout these experiments. The simulations will also allow for a visualization of the acoustic particle velocity within the HQ device.

5.1 Acoustic Response of an HQ Device Under Resonant Conditions

To further the understanding of the mechanism of the HQ device, measurements within this chapter will take place under resonant conditions of the main pipeline. A 150 Hz pulse signal is utilized to excite a strong acoustic resonance in the piping system. The HQ device is placed at the location which was seen to be the most effective, located at the acoustic pressure antinode in the main pipeline. As illustrated in the schematic of Figure 5.1, several pressure microphones were strategically mounted along the axial direction of the HQ devices. The amplitude of the measured acoustic pressure is seen to vary significantly with the microphone location along the device. The AN1 and AN2 positions yield almost 3000 Pa peak-to-peak while the fluctuations occurring at the Mid location are less than 75 Pa. This heavy dependency of microphone location on the acoustic pressure shows that a standing wave is being formed within the HQ device, with the second acoustic mode of an open-open pipe being formed. This is seen when considering that the acoustic pressure antinodes AN1 and AN2 are located at $\frac{\lambda}{4}$ distance away from the ends of the HQ device and had a measured phase angle of 179.5 degrees. The acoustic pressure node is also located at the centre of HQ device length. At the ends of the HQ device, it is recorded that a non-zero acoustic pressure is noted with multiple different frequency components present. Intuitively, this poses a contradiction as to how an open-end condition can be satisfied at each end of the HQ device and so further explanation and measurement will take place to clarify this in the next consecutive paragraphs. One explanation for this non-zero value of pressure is that the microphone location at the ends of the HQ device as seen in Figure 5.1 is slightly offset from the actually end of the device. This is due to the physical requirement of an NPT fitting to properly connect the HQ device to the main piping system and so an 11% offset is present. The presence of multiple frequencies in the waveform measured for both the end

positions of the HQ device is due to the close proximity of the transition point between the main pipeline and the HQ device. These higher order frequencies are likely to be the contributions of harmonics from the main piping system.

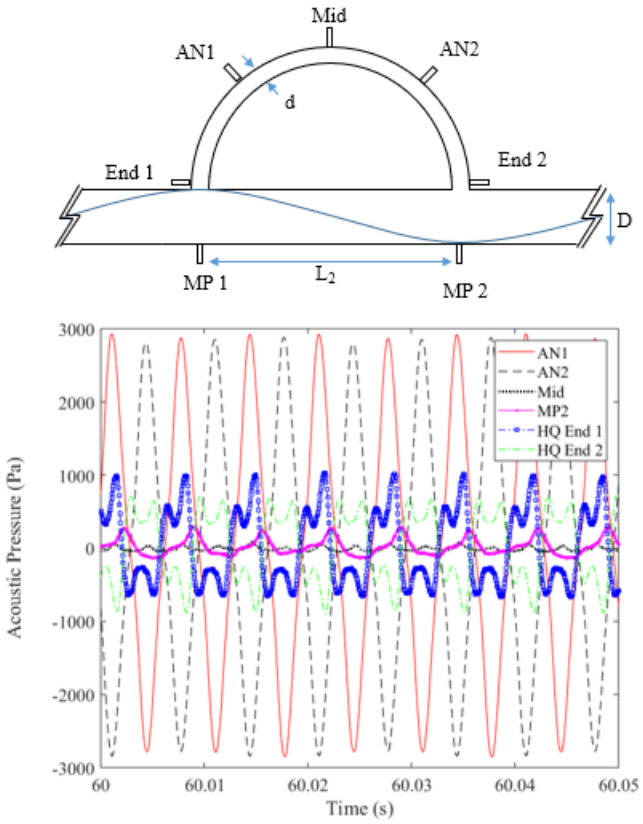

Figure 5.1: Acoustic response measured within an HQ device subjected to a resonant piping system excited by a 150 Hz pulse signal

It is also interesting to note the comparison between the MP2 wave form and the AN1 or AN2 waveforms such that the acoustic pressure is significantly higher within the HQ device than it is within the main piping system. This can be explained by the resonant nature of the HQ device such that the mechanism of attenuation is very similar to that of a side branch resonator. Acoustic energy is required to excite the standing wave within the HQ device and so this energy is extracted from the main piping system and trapped within the HQ device. This mechanism of attenuation is further supported when

considering the excitation of higher order longitudinal modes of the HQ device as shown in Figure 5.2 which compares the transmission loss measured for several different lengths of HQ devices. This change in length (L_3) causes the acoustic mode which is excited to vary from the second mode where $\frac{L_3}{\lambda} = 1$ up to the fourth acoustic mode where $\frac{L_3}{\lambda} = 2$. This result shows a decreased attenuation achieved by the HQ device with the increase in the length and the acoustic mode which is excited. The effectiveness of the HQ device is maximized when the energy transfer from the main piping system to the HQ device is subjected to minimal losses as this would allow for more energy to be transferred to and trapped within the HQ device. With the increase in length of the HQ device and the order of the acoustic mode which is excited, there are two additional losses being added which hinder the performance of the HQ device: visco-thermal losses and the added acoustic damping for higher order modes. Kirchhoff [15] defined the viscothermal losses as positively correlated with the length of the waveguide while the added damping caused by the increase in the acoustic mode has been previously observed by Caughey and O'Kelly [57]. These two sources of acoustic energy losses are the main reasons for how the observed trend of decreased performance of a longer HQ device is materialized. The elevated values of the acoustic pressure within the HQ device in comparison to the main piping system is also a product of the much larger length of the main piping system in comparison to that of the HQ device. It is much easier to excite the second acoustic mode of the HQ device then that of the 5^{th} acoustic mode of the main piping system, and so the strength of acoustic resonance achieved is much greater within the HQ device.

In order to clarify the previously mentioned open end condition contradiction such that the acoustic pressure measured at the ends of the HQ device was a non-zero value, acoustic pressure signal phase measurements were conducted. In particular, the phase angle between the HQ END 1 and MP1 signals was measured along with the phase angle between the HQ END 2 and MP2 acoustic pressure signals. This junction between the HQ device and main pipeline showed an interesting result such that the phase angle

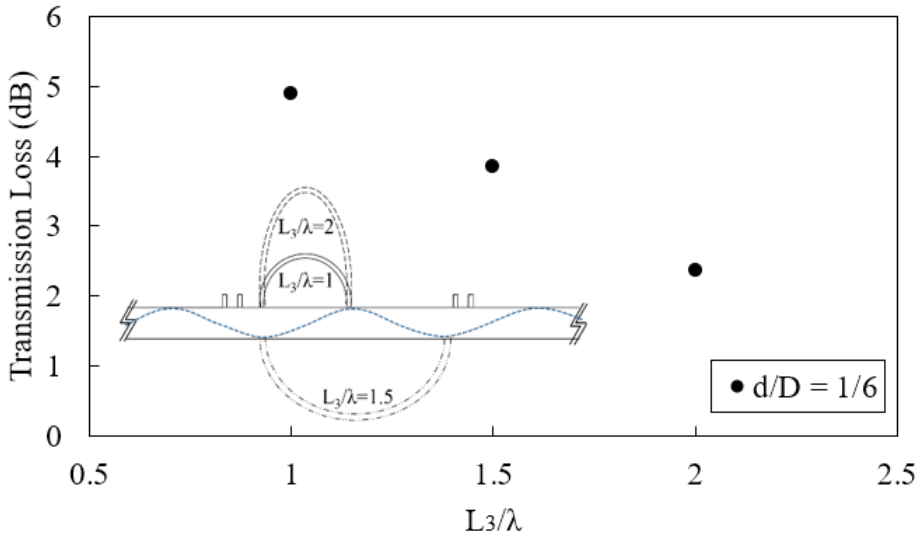

Figure 5.2: Transmission loss vs Length of the HQ device normalized by the targeted wavelength of attenuation. The second, third and fourth acoustic mode excited within the HQ device is studied.

measured between the HQ END 1 and the MP1 acoustic pressure signals was 99.5 degrees and 101 degrees between the HQ END 2 and the MP2 signals. These angles are noted to be quite close to 90 degrees, but with an approximate 10 degree offset. This offset in the phase angle is due to the previously mentioned microphone location at the ends of the HQ device and its 11% shift away from the actual end of the device. With this information discovered, it can be explained how the open end condition is satisfied at each of the ends of the HQ device when we consider the operating mechanism of a Quarter Wave Resonator (QWR) [58] and its schematic seen in Figure 5.3 used to explain such mechanism of attenuation. When a periodic source acts at the mouth of the quarter wave resonator, a compression of the air column inside of the QWR is created when the source moves from the S_0 position to the S_+ position. This wave will travel along the tube, reflect off of the closed surface and return back to the open end of the QWR. However, the timing of such reflection is crucial such that the reflected wave must arrive back at the opening just as the source is moving from the S_0 position toward the S_- position. This

timing is a requirement so that conservation of acoustic pressure and volume velocity is achieved and so that a closed end condition is avoided. The timing between the source and the acoustic pressure within the QWR at the open end of the device can also be understood in terms of the phase angle between these two aforementioned locations. Just as the compression wave reaches the open end of the QWR, it is seen as a maximum acoustic pressure, while the source is at its S_0 position, which for the case of this piston is the maximum velocity (minimum pressure). This corresponds to a phase angle between these two locations of 90 degrees which is also the measured value between the HQ device opening and the main pipeline at the junction. The mechanism of attenuation of the HQ device under resonant conditions is seen to be very similar to that of a QWR with the differences being the two open end conditions of the HQ device and the length which corresponds to a half of a wavelength of the frequency of interest.

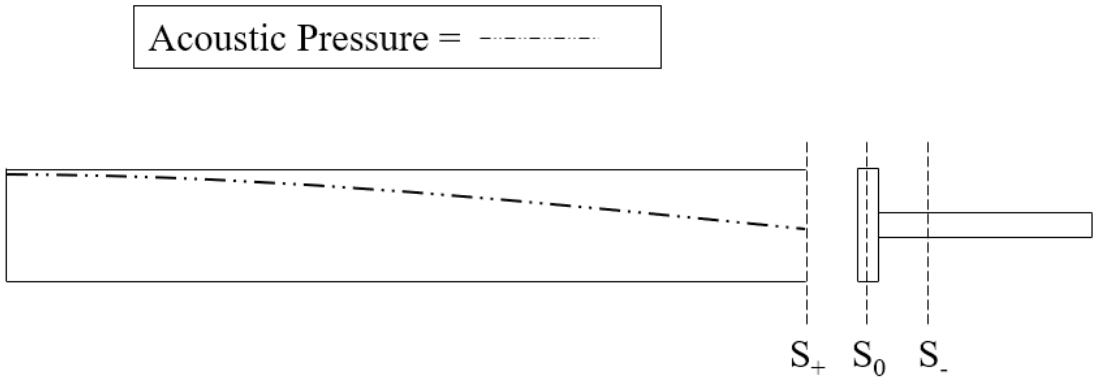

Figure 5.3: Schematic of the operating mechanism of a Quarter Wave Resonator (QWR)

The final requirement to ensure that the second acoustic mode of an open-open pipe is satisfied within the HQ device is the relative phasing of the particle velocity at the ends of the HQ device. To satisfy the second acoustic mode of an open-open pipe, the particle velocity at the ends must be 180 degrees out of phase. To ensure this condition was satisfied, the acoustic pressure signals of the MP1 and MP2 locations were measured during the implementation of the HQ device into the resonant piping system and the

phase angle between these two aforementioned pressure signals was measured to be 179.6 deg. This phasing of acoustic pressure indicates that there is a compression taking place in the main piping system at one of the MP locations, while the other will have a rarefaction taking place. This would imply that the particle velocity would be directed into the HQ device at one end and outwards from the device at the other end. Section 5.3.2 will further explore this condition with the use of Computational Aeroacoustic Simulations.

5.2 Change in Specific Acoustic Impedance Ratio and the Acoustic Reflection Coefficient

The mechanism of attenuation of the HQ device can be further solidified if the specific acoustic impedance ratio and reflection coefficient are investigated. The specific acoustic impedance ratio may also support the normalization of transmission loss with the relative diameter ratio as exhibited in Chapter 4.1 considering that the specific impedance ratio is inversely proportional to the cross-sectional area. The mechanism of attenuation was seen to be quite similar to that of a side branch resonator and therefore the dissipation mechanism is similar whereby radiative losses are present at the openings of the HQ device and absorptive visco-thermal losses will take place at the walls of the HQ device [58]. As seen in Figure 5.4, the imaginary impedance was measured for a straight pipe section subjected to a white noise excitation signal. Additionally, HQ devices of various relative diameter ratios were added to the piping system to understand the change in the specific acoustic impedance ratio as a result of adding an HQ device to a piping system. For a straight pipe module subjected to resonance, the absorption mechanism is a function of the applied force amplitude, cross sectional area, viscothermal attenuation constant, and the density and speed of sound of the fluid medium [59]. The absorptive effects are characterized by a small introduction of resistance in the real component of the specific acoustic impedance as well as to alter the reactance at the anti-resonant peaks so

that it is not infinite in magnitude, but is bounded and changes rapidly from a positive to negative value. The introduction of an HQ device observes this same behaviour such that an effective anti-resonant peak is introduced at the targeted attenuation frequency of 150 Hz. This supports the previously observed added mass effect outlined in Chapter 4.1. It is also noted that regions away from the targeted frequency of 150 Hz are not significantly affected because the HQ device does not target those frequencies and thus no change in impedance is recorded. It is clear however, that the Type II attenuation mechanism does induce some absorptive effects for the large diameter ratio device d/D=0.5 such that a bounded discontinuity in the imaginary specific acoustic impedance ratio is noticed at the 80 Hz and 216 Hz frequencies. The bounded discontinuity of the targeted 150 Hz frequency becomes much larger as the relative diameter ratio increases. This supports the previous findings in this work such that the acoustic volume velocity is changing relative to the cross-sectional area which results in a change in the specific acoustic impedance, increasing the measured attenuation for HQ devices with larger relative diameter ratios.

Although it is clear that a large portion of the acoustic energy is not transmitted past the HQ device due to the high values of measured transmission loss, it is not entirely clear at this point if the attenuation of the HQ device is primarily due to the trapping of acoustic energy. The possibility of the HQ device reflecting energy back to the source must be investigated to discover if these high values of transmission loss are due to the HQ device reflecting acoustic energy. The acoustic reflection coefficient was measured for an HQ device as well as a QWR of equal d/D ratio in order to see what proportion of acoustic energy is reflected back to the source with the setup shown in Figure 3.4. Figure 5.5 illustrates that both the HQ device and QWR have very low values of acoustic reflection at the targeted frequency of attenuation. The measurements were taken in a piping system which has an end termination with an open end. This is the explanation as to why all other frequencies show a higher value of reflection very similar to that

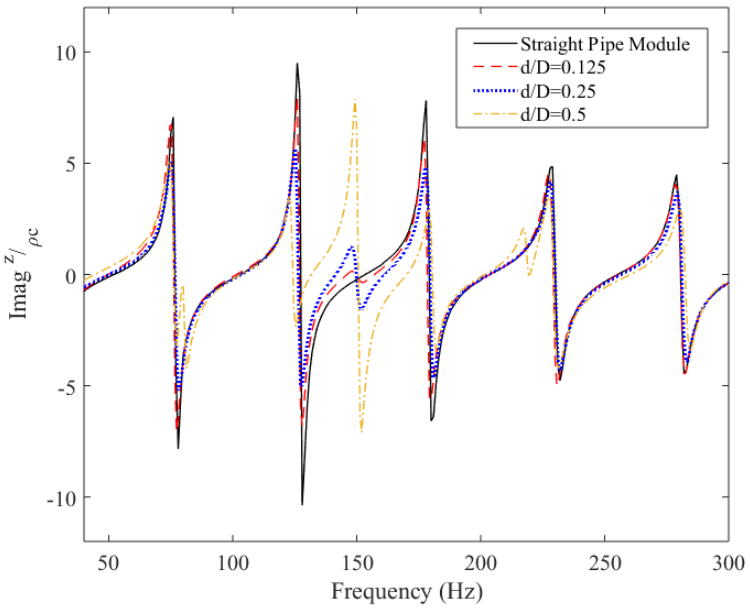

Figure 5.4: Imaginary component of the specific acoustic impedance ratio for a straight pipe module and subsequently for the addition of HQ devices with several relative diameter ratios

achieved from an open end for validation. It is clear that the reflection coefficient at these other frequencies is slightly less than that of an open end as this discrepancy is due to the added length of the piping system which is past the point of the test element. This length has some visco-thermal attenuation and thus lower reflection is achieved. The HQ device also has two additional peaks at the 80 and 215 Hz frequencies corresponding to the Type II attenuation peaks. The HQ and QWR devices have very low reflection back to the source and also very low transmission of acoustic energy past the point of the device. It follows that the acoustic energy which is attenuated from the downstream observer is thus trapped within these reactive damping devices.

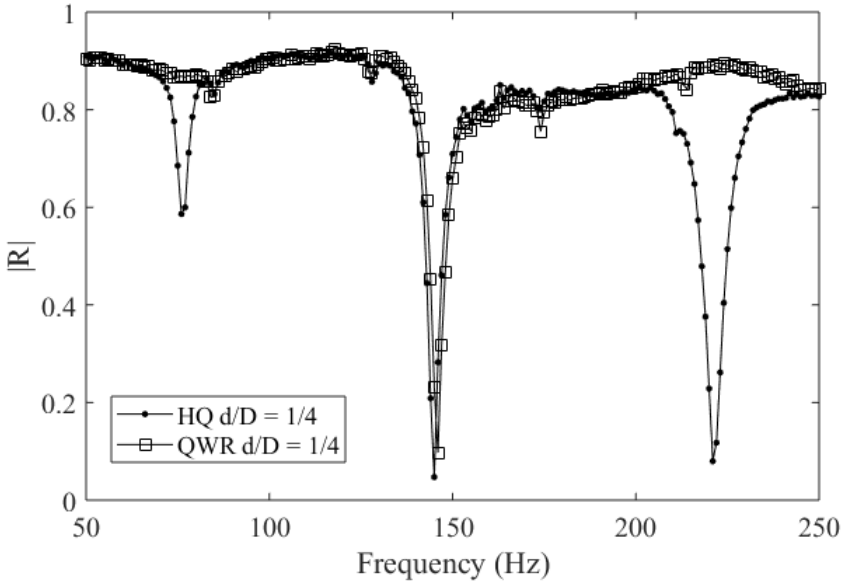

Figure 5.5: Measured acoustic reflection coefficient for an incident acoustic wave subjected to both an HQ device and QWR

5.3 Computational Aeroacoustic (CAA) Simulations

The mechanism of attenuation of an HQ device under resonant conditions is further investigated by means of Computational Aeroacoustic (CAA) simulations. CAA simulation operates on the underlying principle that the acoustic field can be captured within the compressible unsteady Navier-Stokes equation and so a turbulent model with a sufficient time step and mesh size can capture the acoustic field simultaneously with the flow field. The simulation setup, imposed boundary conditions and mesh description will be outlined first. Experimental validation of both a straight pipe experiment under resonance as well as the addition of an HQ device will be conducted in order to verify the findings found in Chapter 5.1. The visualization of the acoustic pressure and particle velocity will be of particular focus in order to visualize the standing wave formed inside the HQ device as well as to verify that the boundary conditions are satisfied at the HQ device ends to set up the second acoustic mode of an open-open pipe.

5.3.1 Simulation Setup, Mesh and Validation

The domain of the simulation was setup in ANSYS Fluent such that the total length of the piping system in the experiment was utilized with the added open-end correction for each of the two ends of the piping system implemented [59]. The dimensions of the speaker connection in the experiment were maintained throughout the simulation and monitor points were selected within the main piping system domain such that they correspond to the experimental location of the pressure microphones 1-4. The setup of the simulation domain can be observed in Figure 5.6 whereby a pressure inlet condition of 0 Pa was setup along with a pressure outlet of 0 Pa for a zero mean flow case. This condition was specified for the static pressure in order to ensure an open-end is achieved. The walls of the piping system were considered as a no-slip wall boundary. The acoustic excitation was created by a velocity inlet boundary located on the speaker surface. The profile

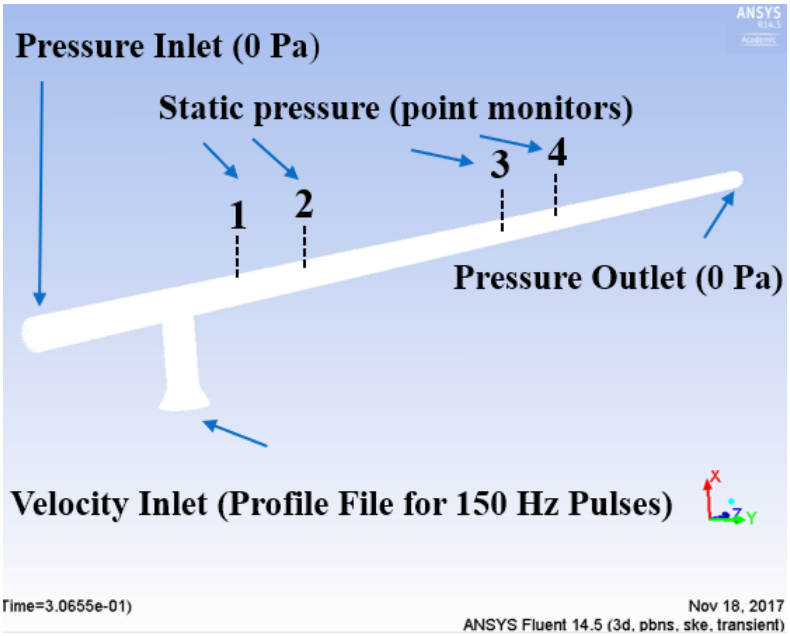

Figure 5.6: Simulation domain and imposed boundary conditions for the CAA simulation conducted in ANSYS Fluent

file was generated using a MATLAB code which generates the velocity value for each time step according to the developed Equation 5.1 which creates a 150 Hz pulse signal with duty cycle of 10%, equivalent to that used in the experiments. In this equation, H' represents the Heaviside function and D is the duty cycle. The value of 1.53 represents the value of the root-mean-square (rms) acoustic particle velocity obtained from experimental measurement of the acoustic pressure at the speaker during the experiment. The velocity profile of the 150 Hz pulse function can be seen in Figure 5.7.

$$v_{speaker}(t) = 1.53\sqrt{2}H'[cos(\omega t - 2\pi\frac{D}{2}) - cos(2\pi\frac{D}{2})] \tag{5.1}$$

The mesh created for the CAA simulation was primarily structured with hexagonal elements as shown in Figure 5.8. Considering that the CAA simulation computes the acoustic field simultaneously with the flow field, the mesh size was selected such that the points-per-wavelength criteria was satisfied for the 150 Hz frequency of interest:

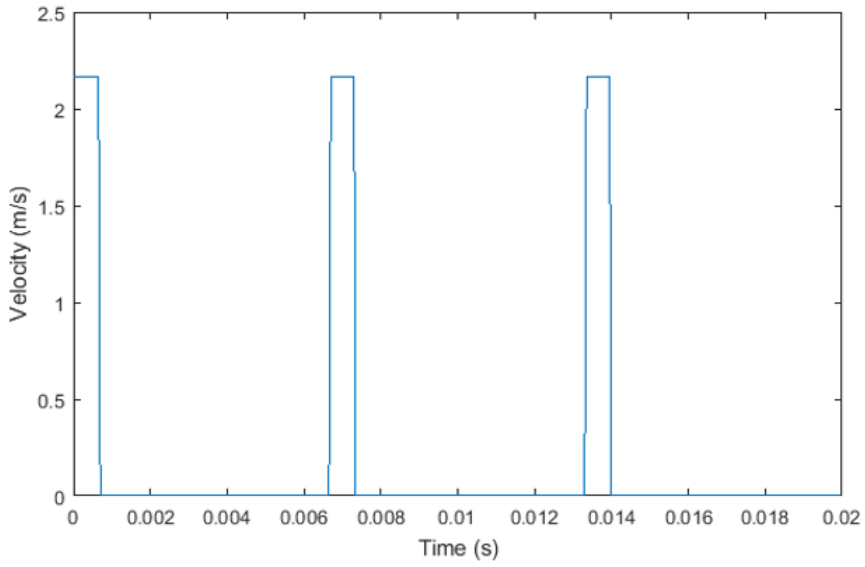

Figure 5.7: Velocity inlet profile generated by Equation 5.1 to be implemented at the velocity inlet boundary condition located at the speaker diaphragm.

$$PPW = \frac{c}{f\Delta x} > 30 \tag{5.2}$$

This criteria is crucial in order to ensure that a sufficient number of points are computed along a given wavelength of interest. This lead to a selection of a fine element size of $\Delta x = 17.15$ mm.

The time step for a typical CFD simulation is determined by the Courant number where the maximum flow velocity is used in conjunction with the smallest element size to calculate the minimum required time step. However, for CAA simulations the speed of sound in the fluid medium is the constraining parameter as the fluctuations in acoustic pressure will not be captured if the Courant number does not account for this parameter. The time step was selected using the Acoustic Courant-Fridrick-Lewy (CFL) number defined below:

$$CFL = \frac{c\Delta t}{\Delta x} < 1 \tag{5.3}$$

The time step selected to satisfy this critera was $5 \cdot 10^{-5} s$

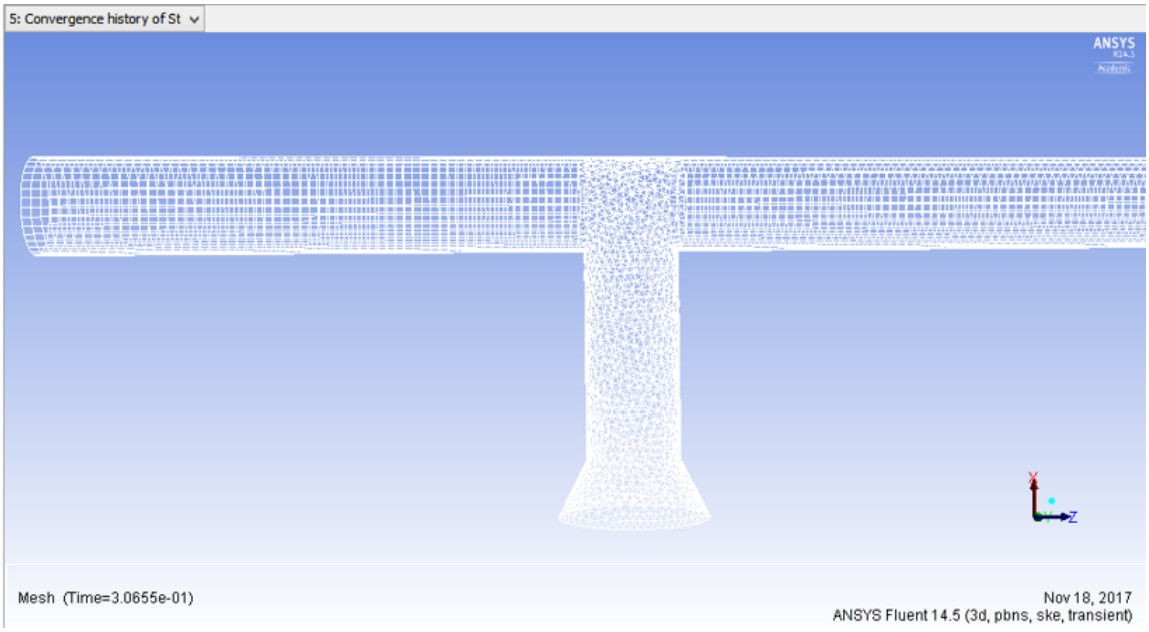

Figure 5.8: 3D Structured/Unstructured Mesh used for ANSYS Fluent Simulation (interior elements not shown

Although the results shown are for the no-flow case to highlight the acoustics of the HQ device, a SST - $K-\omega$ model was selected due to the fact that the periodic time of fluctuations of the acoustics is very small leading to very fast fluctuations in acoustic pressure and particle velocity. These rapid changes in velocity and pressure were not well captured using a laminar model. The $K-\epsilon$ model was also utilized however, it was found that the dissipation of the SST - $K-\omega$ model was better captured in comparison to the experiments.

Figure 5.9 is a comparison of the base case validation of the resonance of a straight pipe section for the simulated and experimentally determined acoustic pressure spectra for the location of Microphone 1. The simulated results are in very good agreement with that measured from the experiments. However, it is evident that the higher order harmonics such as 300 Hz and 450 Hz were not well captured. A summary of the additional

experimental measurements of microphone locations 2-4 are listed in Table 5.1 with their respective comparisons to the simulated values.

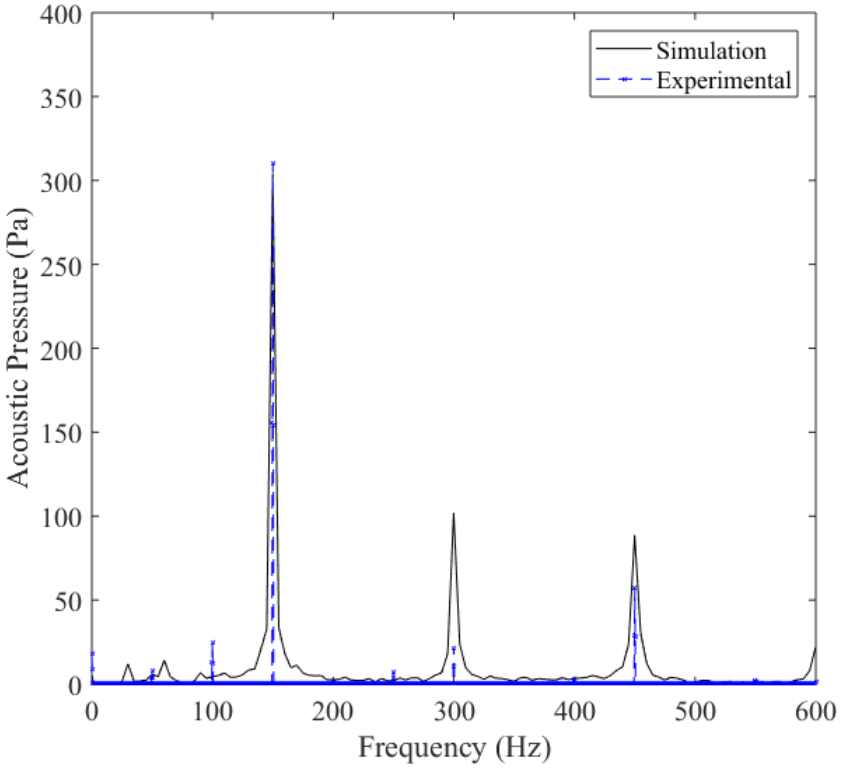

Figure 5.9: Experimental and Simulated comparison of the acoustic pressure spectra measured at Microphone 1 location. Excitation source for both the simulation and experiment was set to a 150 Hz pulse signal

Although the acoustic pressure signal from the four microphone locations was a good source of validation, it is required to look at the acoustic pressure and particle velocity distribution before proceeding with simulating the HQ device, in order to ensure that the proper coupling between the natural frequency of the piping system and the imposed acoustic source is achieved. A standing wave should be formed within the pipe such that the 5^{th} acoustic mode of an open-open pipe is present, equivalent to that achieved in the experiments. Figure 5.10 illustrates the acoustic pressure distribution along the pipeline

	Experimental (Pa)	Simulation (Pa)	Error (%)
Microphone 1	310.0	304.4	1.80
Microphone 2	416.9	397.4	4.68
Microphone 3	386.5	367.6	4.89
Microphone 2	243.8	236.6	2.95

Table 5.1: Measured and simulated comparison of the acoustic pressure signal measured at various microphone locations outlined in the experimental set-up

length for several different time instances along the 150 Hz cycle. Considering that the acoustic propagating wave is expected to capture the one-dimensional longitudinal waves, the pressure should remain constant at all points within the cross-section of the pipe at a given axial location and so a single data point is shown for each axial location along the pipeline axis. At $\phi = 0°$, we can see that there are 5 acoustic pressure antinodes present indicating that the 5^{th} acoustic mode of the pipeline has been excited. As ϕ progresses toward 180°, it is noted that the acoustic pressure is equal in magnitude and opposite in phase. The pressure antinodes maintain the same location along the pipeline and so we can confirm that a standing waveform has been initiated. It is also confirmed that the open end condition is maintained such that the acoustic pressure is forced to zero at the ends of the pipeline and is consistent at this value.

The acoustic pressure and acoustic particle velocity contours are illustrated in Figure 5.11 where by the standing waveform is further solidified. At the $\phi = 0°$ point in the cycle, the acoustic pressure reaches its maximum value and 5 pressure antinodes are present and evenly spaced along the axis of the piping system. Where the acoustic pressure reduces to zero, we see that the acoustic particle velocity becomes maximum. The ends of the pipeline are seen to be an acoustic pressure minimum and simultaneously the acoustic particle velocity is a maximum. The one-dimensional behaviour is also confirmed when

viewing the acoustic pressure along the wall of the pipeline and its uniformity. The no-slip wall condition is seen in the acoustic particle velocity contour such that the particle velocity is 0 at the walls.

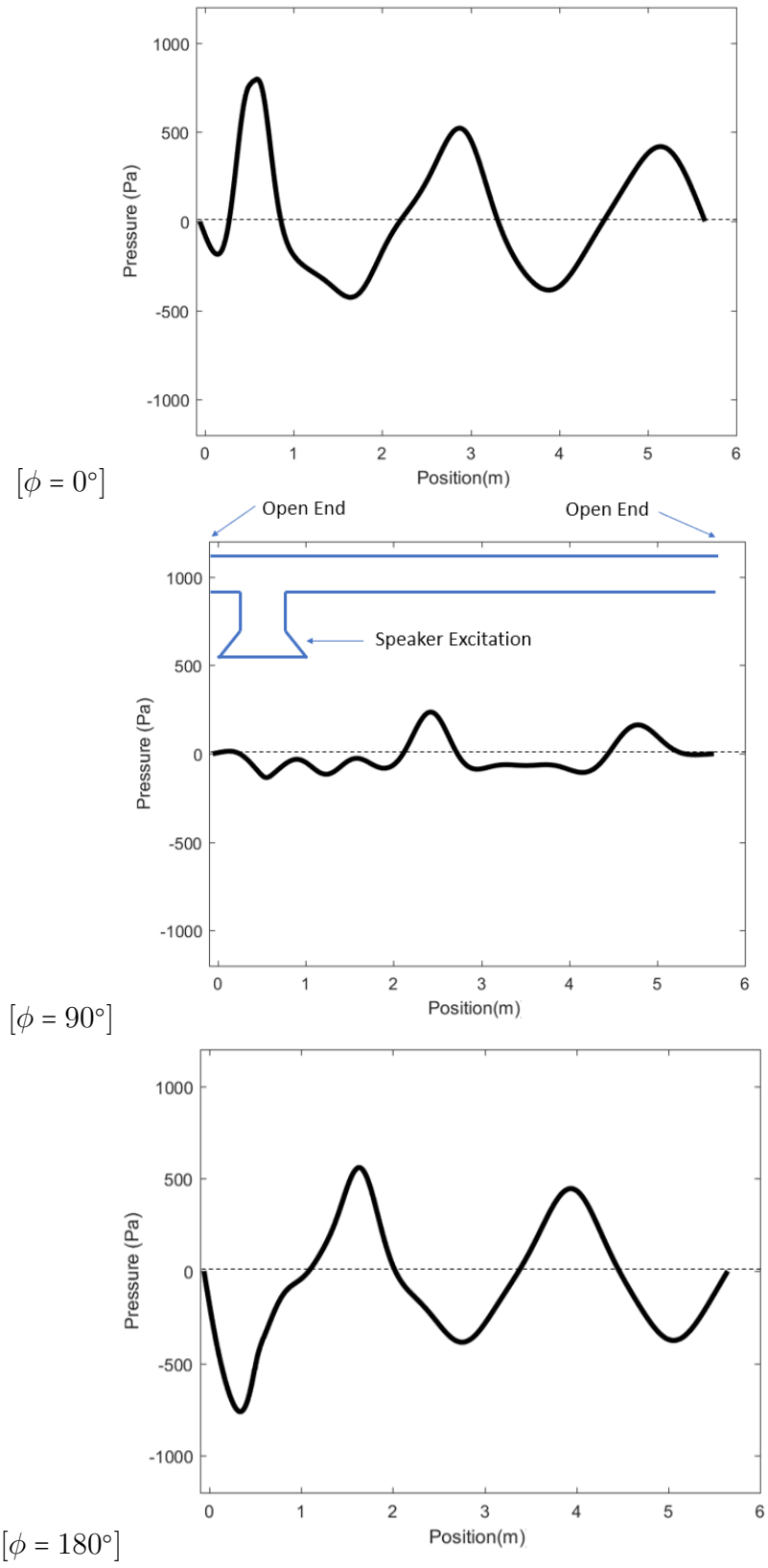

Figure 5.10: Simulated comparison of the acoustic pressure distribution along the pipeline at different points along the 150 Hz cycle. Excitation source was set to a 150 Hz pulse signal

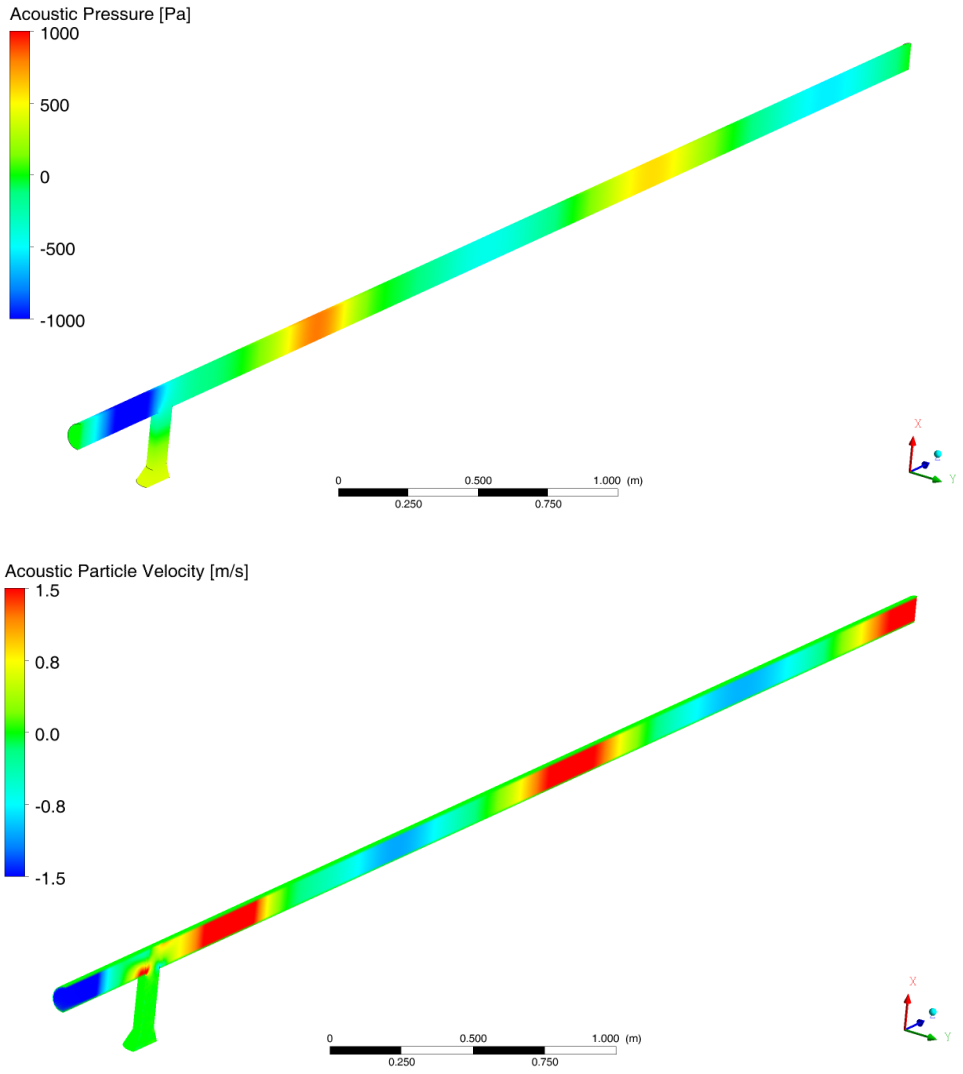

Figure 5.11: Simulated comparison of the Top: acoustic pressure, ϕ = 0° and Bottom: acoustic particle velocity distribution, ϕ = 0° along the pipeline. Excitation source was set to a 150 Hz pulse signal

5.3.2 HQ Device Simulation Results

The CAA simulation domain was extended to include an HQ device located at the optimal axial location along the piping system (acoustic pressure antinode) in order to study the mechanism of attenuation of the HQ device under resonant conditions. To validate the addition in the mesh which was generated to simulate the HQ device, several static pressure monitors were placed along the length of the HQ device at the positions previously measured in Chapter 5.1. Figure 5.12 shows a comparison of the time signals obtained from measurements within the HQ device to that of the time signal obtained from the simulations. The overall behaviour and magnitude is captured well with discrepancies noted in the HQ END 1 and HQ END 2 signals. For these signals, the additional frequency components are not as distinct as the experiment. This is due to the points per wavelength criteria which was focused on the 150 Hz targeted frequency. The acoustic pressure spectra was obtained for several of the measured locations and compared to the simulation. An example of such comparison is seen in Figure 5.13 where the acoustic pressure spectra of the AN2 position is compared for both the experiment and the simulation with a percentage error of less than 15%.

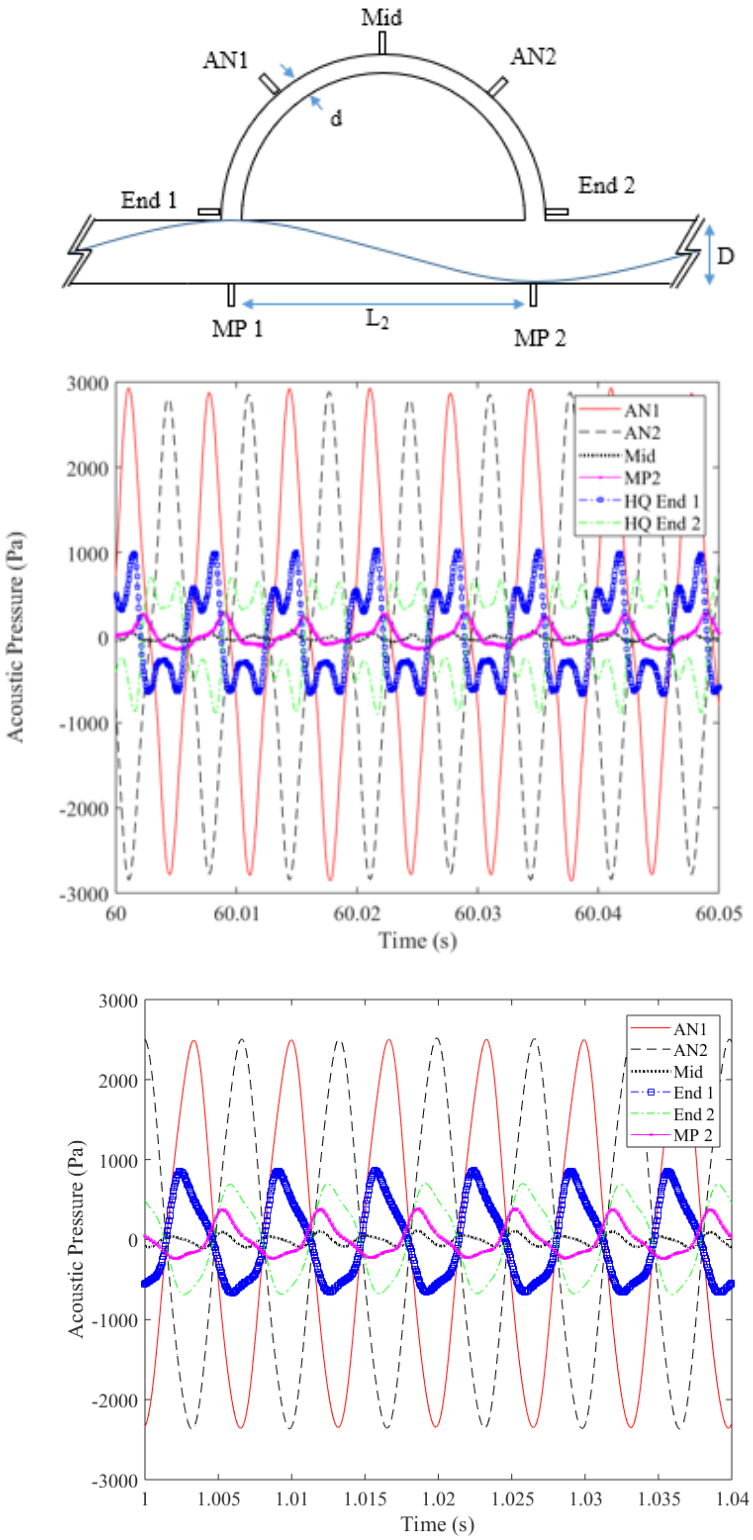

Figure 5.12: Top: Experimental and Bottom: Simulated comparison of the time signals for several locations along the HQ device

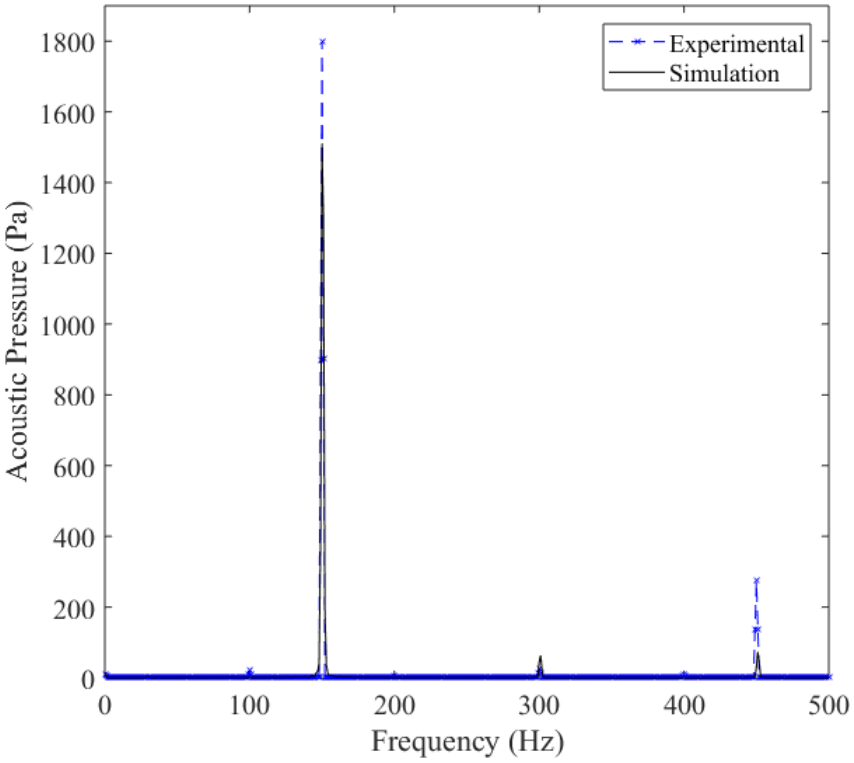

Figure 5.13: Experimental and Simulated comparison of the acoustic pressure spectra measured at the AN2 location within the HQ device. Excitation source for both the simulation and experiment was set to a 150 Hz pulse signal

The acoustic pressure contours of the HQ device are viewed for several different points along the 150 Hz cycle as illustrated in Figure 5.14. The overall behaviour confirms that observed in the experiment whereby the second acoustic mode of an open-open pipe is formed within the device. Two acoustic pressure antinodes are present with opposite phasing and equal magnitude and an acoustic pressure node is located at the centre of the HQ device. The phasing of each of the acoustic pressure antinodes changes when comparing $\phi = 0°$ to $\phi = 180°$.

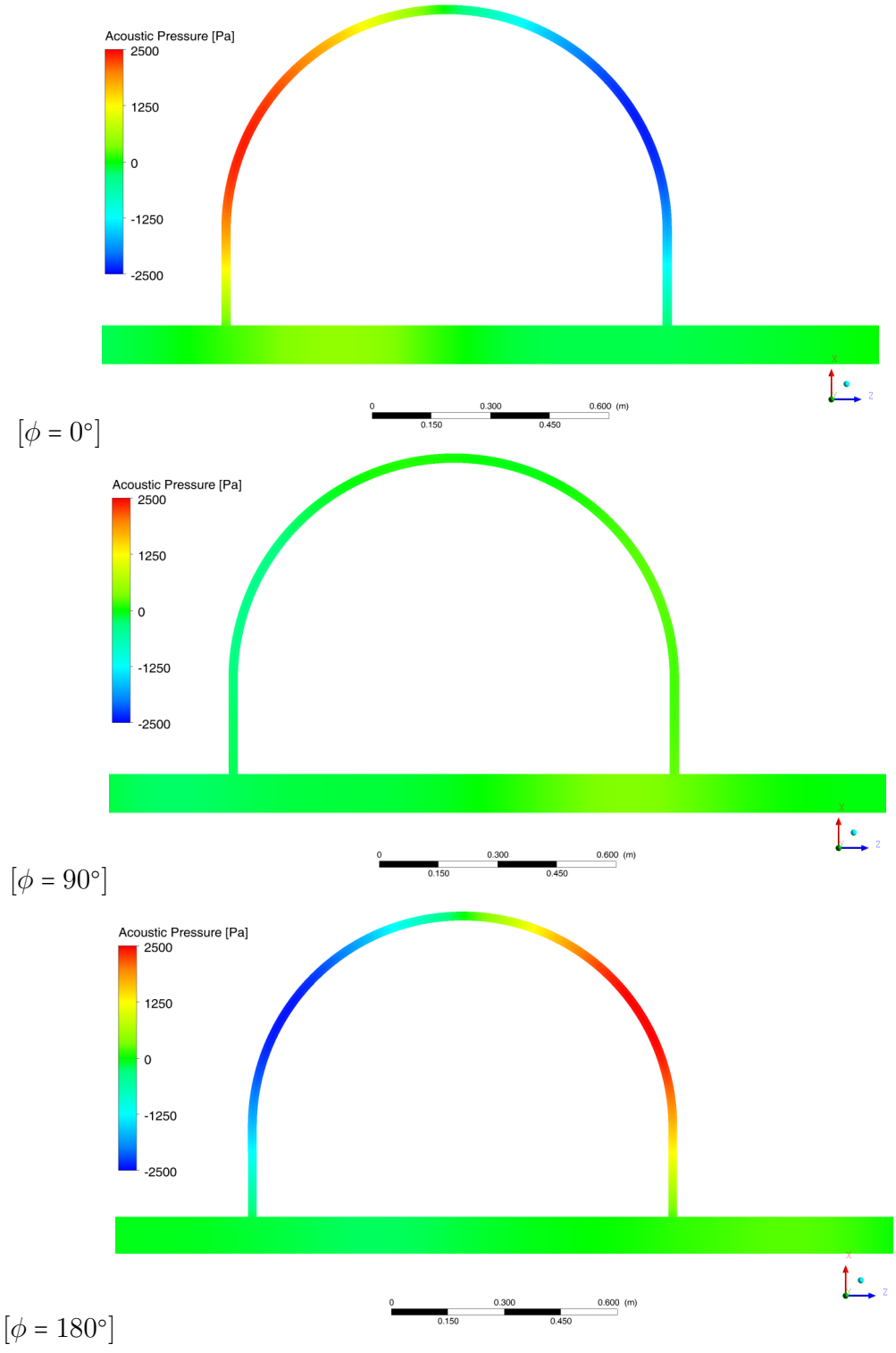

Figure 5.14: Simulated comparison of the acoustic pressure contours along the HQ device for different time instances along the 150 Hz cycle.

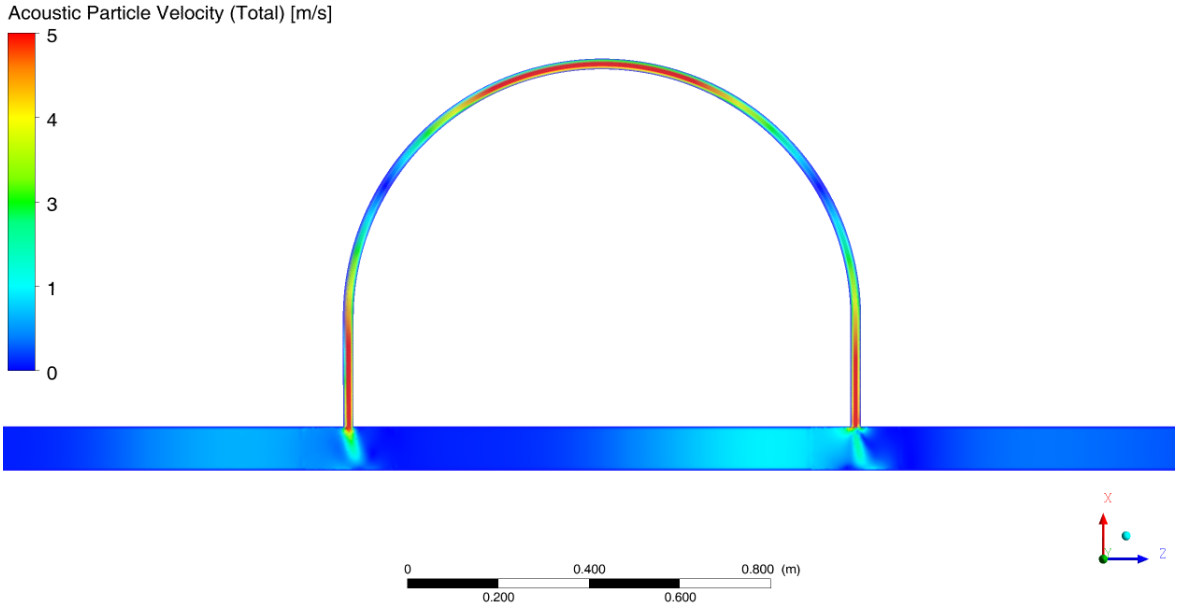

Figure 5.15: Simulated acoustic particle total velocity contour within the HQ device. $\phi = 0°$

The acoustic particle velocity contours are viewed using two different values: The total acoustic particle velocity and the acoustic particle u-velocity. The total acoustic particle velocity seen in Figure 5.15 is plotted at the $\phi = 0°$ time instance. Here we can see that the acoustic particle velocity is maximum where the acoustic pressure is at a minimum. The ends of the HQ device are acoustic particle velocity antinodes, showing that the acoustic open-end condition (zero acoustic pressure) is naturally achieved. This result is particularly interesting because the CAA simulation was not given this open-ended boundary condition, but the coupling between the HQ device and the resonant piping system was naturally engaged such that the phasing between the open end of the HQ device and the main piping system is 90 degrees. When viewing the particle velocity at the ends of the device in terms of the u-component as shown in Figure 5.16, we can see that the ends of the HQ device have particle velocities which are 180 degrees out of phase and their phasing alternates throughout the duration of the 150 Hz cycle. This

reinforces the condition required for the second acoustic mode of an open-open pipe to be formed within the HQ device.

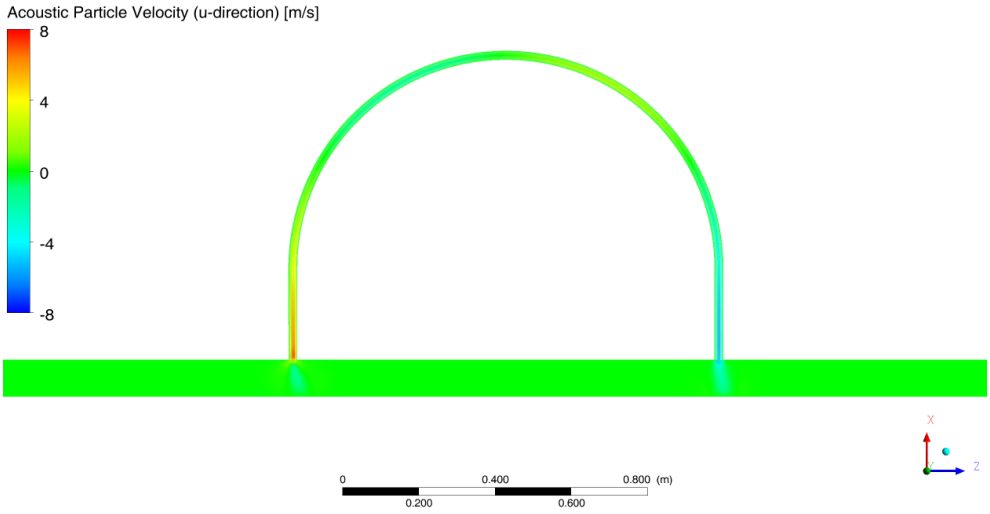

$[\phi = 0°]$

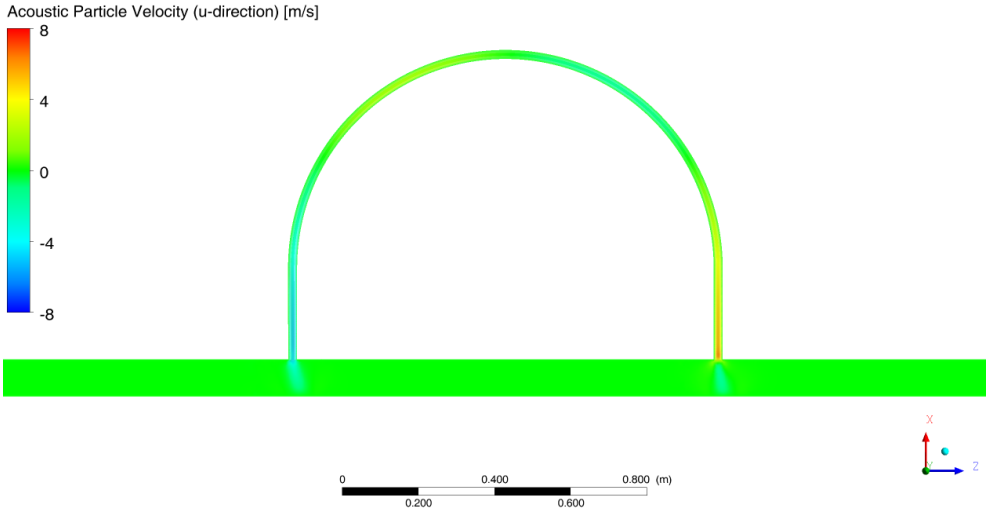

$[\phi = 180°]$

Figure 5.16: Simulated comparison of the acoustic particle u-velocity contours along the HQ device at different points along the 150 Hz cycle.

5.4 Summary and Conclusions

In this chapter, the mechanism of the HQ device under resonant conditions was investigated both experimentally and numerically. The experiments consisted of attaching the HQ device to a resonant piping system and observing its acoustic response with pressure microphones mounted at several locations along the axial direction of the HQ device. It was clearly noted that the acoustic pressure distribution is strongly dependant on the location of the microphone with two acoustic pressure antinodes located at $L_3/4$ distance away from each of the ends of the HQ device while an acoustic pressure node was located at the centre of the length of the HQ device. The second acoustic mode of an open-open pipe was formed within the device with the mechanism of attenuation being very similar to that of a side branch resonator such that acoustic energy is extracted from the main piping system and is trapped within the HQ device. The increased length of the HQ device resulted in increasing the acoustic mode which was excited in the device and an added contribution of damping was introduced to excite the higher order modes. This caused the attenuation of the HQ device to decrease, along with the increased visco-thermal attenuation losses caused by the increase in HQ device length. The complex phase angle was measured between several acoustic pressure signals in order to verify the second acoustic mode of an open-open pipe was formed within the HQ device. The open end condition was verified by measuring a phase angle between the end of the HQ device and the main piping system to be 90 degrees. This phasing is seen to be a crucial factor in ensuring the timing of the reflected waves from each end of the HQ device can set-up an open end condition and thus sustain resonance within the device. The imaginary acoustic impedance was measured to confirm the attenuation mechanism of the HQ device as well as to verify some previously mentioned phenomenon in Chapter 4.1 such as the added mass effect of the HQ device and that the attenuation scales with the relative diameter ratio due to a change in the acoustic volume velocity, ultimately changing the acoustic impedance of the HQ device. The reflection coefficient of the HQ device was measured

in order to determine the possibility of the acoustic energy simply being reflected back to the source. However, it was measured that for both a QWR and an HQ device, the acoustic reflection coefficient at the targeted frequency of attenuation is very low. This indicates that the mechanism of attenuation relies on trapping acoustic energy which is used to sustain the acoustic resonance within these reactive damping devices.

Finally, CAA simulations were conducted to verify the experimentally determined trends and to better visualize the attenuation phenomenon. The experimental domain was modelled in ANSYS Fluent and a straight pipe base case was utilized as a point of validation to compare to the experimental results. The simulation was successful at self-coupling the acoustic natural frequency of the piping system with the simulated 150 Hz pulse signal excitation source and the 5^{th} acoustic mode of the open-open pipe was accurately materialized within simulation. The HQ device was then added to the simulation domain and the same square pulse excitation source was utilized. Several static pressure monitors were placed along the length of the HQ device in order to compare the time signals of the simulated monitors to that of the experimentally determined values. The results agreed quite well with one another with discrepancy arising for the higher order harmonics of the system. The HQ device was self-coupled with the main piping system such that the open-end condition was naturally created at each end of the HQ device without input as a forced boundary condition. The HQ device exhibited a standing wave with the second acoustic mode of an open-open pipe in both the simulation and the experiments. The particle velocity contours were visualized and it was seen that the particle velocity was equal in magnitude and 180 degrees out of phase between both ends of the HQ device.

Chapter 6

Passive Damping of a Travelling Wave System

Although the severity of damage sustained from a resonant piping system is severe, there exists practical scenarios where acoustic resonance is not initiated. For scenarios where the blade passage frequency of a centrifugal pump or compressor does not coincide with one of the natural acoustic frequencies of the adjacent piping systems, the pressure pulsations which materialize will still propagate through the piping system however, a standing waveform will not be present. It is quite common to find this scenario of acoustic pressure pulsations propagating through a piping system which is not coupled, and the following chapter will study the case of the travelling wave scenario. The total length of the piping system was altered such that the 150 Hz frequency of interest was an anti-resonant frequency as opposed to the preceding chapter where it was a resonant frequency. The same frequency of excitation was studied (150 Hz) for the following experiments so that consistency in the HQ device parameters could be maintained.

To avoid repetition of content and to maintain brevity, some of the parameters tested in Chapter 4 which remained consistent with Chapter 6 such as the normalization of the diameter ratio with transmission loss, implementation of multiple devices and the effects

of mean flow velocity/directionality are not presented as they were not necessarily dependant on the acoustics of the system. However, there does exist some parameters which showed a considerable difference between the resonant and travelling wave systems. This chapter will compare the effect of the relative diameter ratio on the acoustic performance of the HQ device for both a resonant and travelling wave piping system. This chapter will also highlight the change in performance caused by the placement of an HQ device in proximity to other piping components.

6.1 Relative Diameter Ratio (d/D) & Proximity to Adjacent Piping Components

The effect of the relative diameter ratio between the HQ device and the main piping system was first studied in order to determine if there is a difference in attenuation achieved for an HQ device implemented into a resonant or travelling wave piping system. The transmission loss was measured for an HQ device applied to a travelling wave piping system and compared to the values which were obtained under resonant conditions as seen in Figure 6.1. A similar trend was observed to that of the change of axial location on the transmission loss in Chapter 4.2 - Figure 4.5, such that there was no significant change in the transmission loss peak of the targeted type I mechanism. This result is exemplary of the inherent feature of transmission loss measurements such that it is independent of the end terminations and source impedance, thus characterizing the transmission loss is identical for both a resonant and travelling wave piping system.

It was thus required that the comparison of the diameter ratio was investigated in terms of insertion loss so that this trend could be further clarified. HQ devices of d/D = 0.125 and 0.25 were studied for both a resonant and travelling wave piping system and the measured insertion loss is seen in Figure 6.2. The comparison is made also for several axial locations, corresponding to the distance measured from the open end to that

of the nearest HQ junction. When comparing the resonant system tests to that of the travelling wave system, the maximum attenuation achieved for the same sized HQ device is significantly greater when applied to a resonant system, provided it is well placed. The increase in attenuation is as much as 6 dB for d/D=0.25 and almost 8 dB for d/D=0.125. Considering the fluctuating acoustic pressure at the acoustic pressure antinode during resonance is much larger then that observed in the travelling wave system, the extent to which the HQ device is excited is observed to be dependant on this factor. This can also be seen for the case where the device is poorly placed along the axial location of the resonant system. It is clear that the attenuation is significantly reduced with a lower attenuation being achieved in the resonant system if placed at the acoustic pressure node when compared to the same HQ device placed in a travelling wave system.

It is also evident from Figure 6.2 that the volatility of an HQ device placed at different locations along a quarter wavelength is decreased for the application to a travelling wave system. This is due to the fact that there is no standing waveform present within the piping system, and so the travelling wave phenomenon causes similar values of fluctuating acoustic pressure at each of the locations along the quarter wavelength, yielding very similar values of attenuation at the tested locations. However, this conjecture is only true when there is no constructive interference present within the piping system. With the addition of an HQ device into a piping system, a new boundary condition is introduced into the piping system at the point of insertion and so the investigation of the HQ device in proximity to other piping components was carried out to determine this effect, if any. The HQ device was relocated so that one end condition of the piping system was an integer multiple of $\frac{\lambda}{2}$ distance away. Figure 6.3 shows the measured insertion loss of HQ devices placed at locations surrounding and including the λ distance away from the end termination. Interestingly enough, it was observed that a minimum in the insertion loss is present such that a sharp decrease in attenuation is present, even when moving a distance of $\frac{\lambda}{8}$ away from the λ position. To further investigate this to ensure this trend is

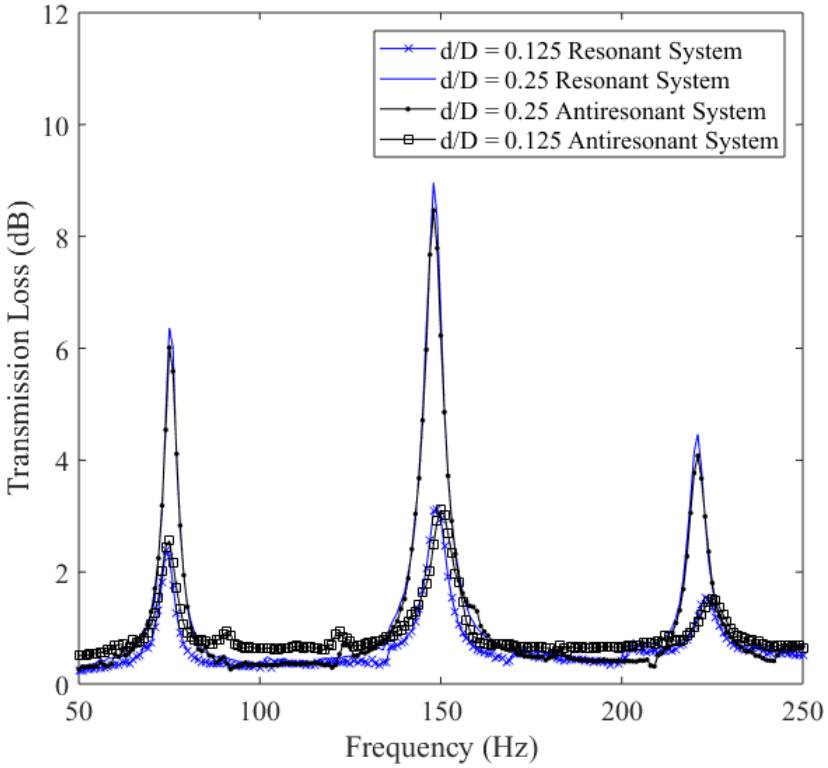

Figure 6.1: Change in transmission loss for HQ devices applied to a resonant and travelling wave piping system

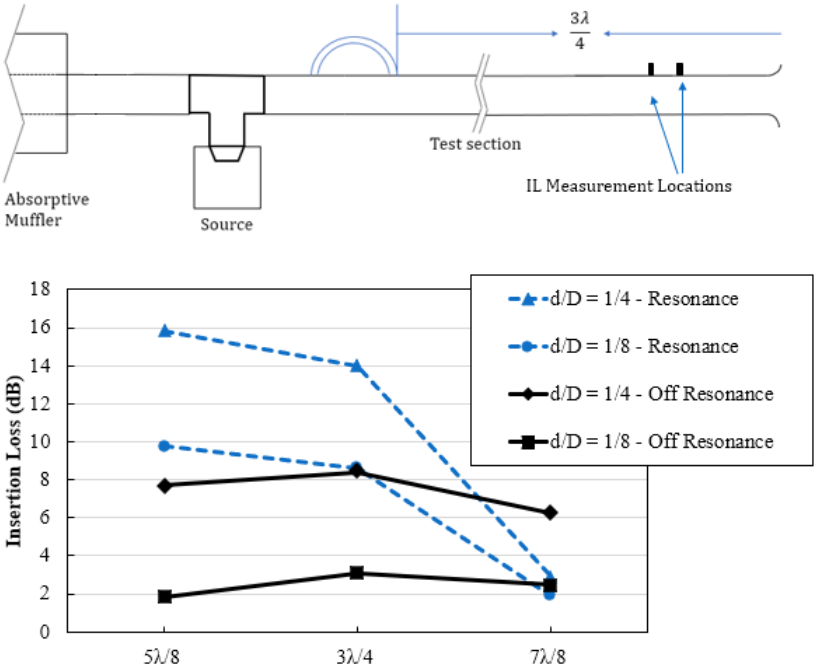

Figure 6.2: Resonant and travelling wave piping system comparison for insertion loss of an HQ device at multiple locations along the pipeline axis

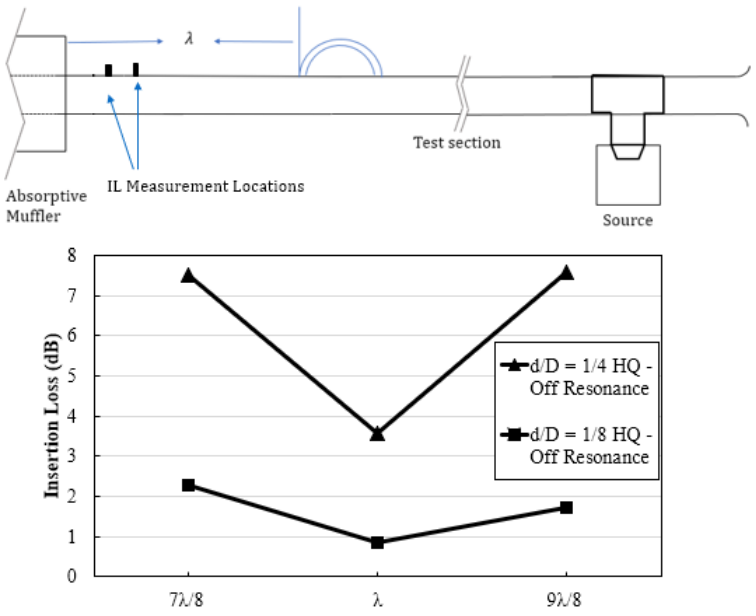

Figure 6.3: Change in insertion loss with HQ device placement for multiple locations along a travelling wave piping system including an end termination located at a multiple of $\frac{\lambda}{2}$ away

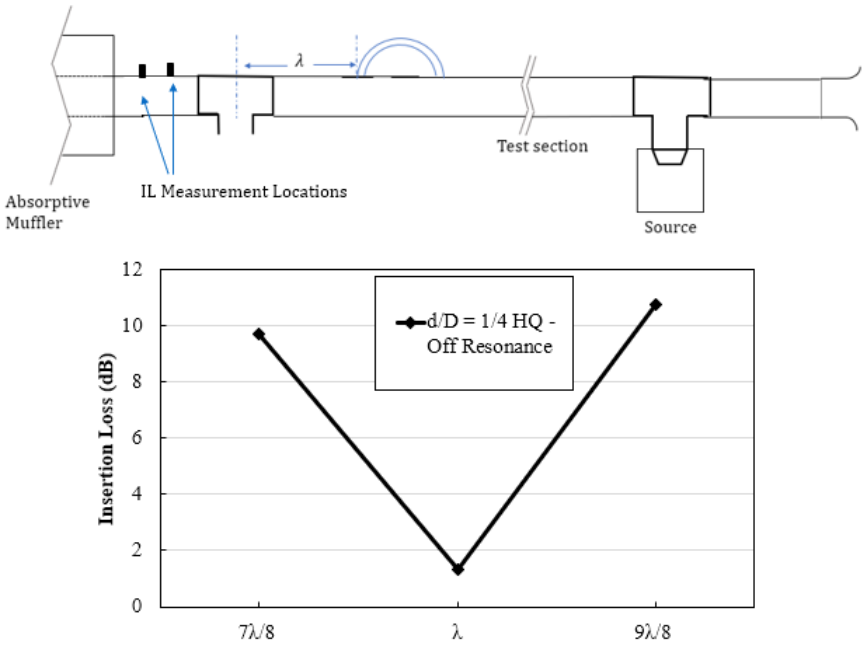

Figure 6.4: Change in insertion loss with HQ device placement for multiple locations along a travelling wave piping system including an open T-connection located at a multiple of $\frac{\lambda}{2}$ away

not an anomaly, the HQ device was then moved to a position which was not at an integer multiple of $\frac{\lambda}{2}$ away from the end condition. Additionally, an open-ended T-connection was added at a distance of λ away from the HQ device as shown in Figure 6.4 to see if another type of boundary condition (with a different value of acoustic reflection) would still exhibit the same behaviour. It was clear that the same trend was present with a different piping component, such that situating it a distance of λ away from the HQ device caused a large decrease in the attenuation achieved.

It is also interesting to note, that the insertion loss had dropped to different values for each of these aforementioned cases. It was noted that the open ended boundary condition at the t-section yielded a slightly different decrease in insertion loss than that observed from the absorptive muffler end condition. These cases reinforce the understanding that the HQ device placement in proximity to other piping components is an issue if constructive interference can take place. This constructive interference will take place if sufficient reflections are present, the length is not significantly large between the HQ device and the piping component and finally, that the length is a integer multiple of $\frac{\lambda}{2}$. For industrial applications of an HQ device to an travelling wave piping system, it is crucial to properly apply these findings in order to ensure the efficient installation and operation of the HQ device such that the materialization of constructive interference can be avoided.

6.2 Summary and Conclusions

The study of an HQ device applied to a travelling wave piping system was compared to that of a resonant system. Several of the trends previously outlined in Chapter 4 remained consistent and so a focus was placed on the change in attenuation between the two systems when maintaining a consistent value of d/D. It was noted that a well placed HQ device in a resonant piping system will achieve larger values of attenuation than that

of the same HQ device placed in a travelling wave system. This is due to the ability of a resonant system to more strongly excite the mechanism of the HQ device whereby the fluctuating acoustic pressure is greater at the antinode in the resonant system compared to that observed in the travelling wave system. The effect of placing an HQ device at different axial locations along a travelling wave piping system was found to be much less sensitive, such that the measured insertion loss was relatively consistent. The major concern for the application of an HQ device to a travelling wave system was found to be the relative distance between the HQ device and the adjacent piping components. If the reflections provided by the end termination or piping components is large enough, the length is relatively small and the length is some integer multiple of $\frac{\lambda}{2}$ then constructive interference may materialize which was seen to significantly decrease the attenuation performance of the device. This provides some preliminary guideline for the application of the HQ device to a travelling wave piping system.

Chapter 7

Conclusions

7.1 Summary and Conclusions

The current thesis performed an extensive experimental study on the application of HQ tubes to pressure pulsations in piping systems for both resonant and travelling systems. The investigation of the relative diameter ratio between the HQ device and main piping system showed that even for larger sized piping systems, the transmission loss normalizes linearly with the relative diameter ratio, a practical advantage for implementation in industry. The attenuation of HQ devices with lower diameter ratios ranging from d/D=1/12 - 1/2 were studied and were found to be quite effective in attenuating the acoustic pressure pulsations. The shift in the total acoustic response of the piping system was characterized in terms of the change in the fluid volume ratio between the HQ device and the main pipeline. An effective length formula was developed in order to quantify the shift in the adjacent resonant frequencies of the natural acoustic response. This analytical formula was successful in quantifying the shift in the total acoustic response caused by HQ devices with a larger d/D ratio as well as the addition of multiple HQ devices. The axial location of a HQ device along the piping system was seen to have a significant effect on the attenuation of an HQ device for a resonant piping system. A

small well placed HQ device with d/D=0.125 was seen to exhibit more attenuation than a poorly placed large HQ device with d/D=0.25. The acoustic pressure antinode was seen to exhibit the most attenuation while the acoustic pressure node yielded low values of attenuation. The large value of fluctuating acoustic pressure at the acoustic pressure antinode more easily excites the mechanism of the HQ device, yielding better acoustic performance. The implementation of multiple HQ devices was thoroughly investigated and it was found that a large HQ device can be divided into multiple smaller devices with a total equivalent fluid volume and achieve nearly identical values of insertion loss. It was also found that multiple devices placed at multiple locations along the axis of the pipeline can still achieve similar values of attenuation, provided they are at the same relative location along the standing wave. The mean flow effect on the attenuation of the HQ device was investigated with a particular focus on Mach numbers below 0.15 as this was not yet studied in the literature to date. It was found that the mean flow effect was much less pronounced for the aforementioned range of Mach numbers in comparison to the larger range of flow velocities previously studied. It was also noted for the first time that the directionality of the incident acoustic propagating wave relative to the mean flow direction showed some differences in attenuation. A downstream propagating acoustic wave observed decreasing attenuation with the increase of the mean flow while an upstream propagating wave showed increasing acoustic performance with the increase in mean flow.

The subsequent chapter of this thesis consisted of clarifying the underlying mechanism of attenuation of an HQ device implemented into a resonant system. Acoustic pressure measurements were experimentally obtained within the HQ device at several axial locations along the device. It was noted that the acoustic pressure was highly sensitive to the location along the HQ device such that the $L_3/4$ distances away from the HQ device ends yielded an acoustic pressure antinode while the centre location of the HQ device was an acoustic pressure node. The second acoustic mode of an open-open pipe was seen

to materialize within the HQ device such that the open end condition was satisfied by means of acoustic pressure phase measurement. The acoustic pressure phase between the HQ device end and the main piping system was seen to be 90 degrees, the same timing which a QWR relies on to maintain the open end boundary condition to sustain resonance within the reactive damping device. The mechanism of the HQ device under resonant conditions is seen to be similar to that of a side branch resonator whereby acoustic energy is extracted from the main piping system resonance and is trapped within the resonance of the auxiliary system: the HQ device. The excitation of higher order acoustic modes of the HQ device was exhibited when changing the length of the HQ device. It was noted that a decrease in attenuation was achieved with increasing length of the HQ device which was due to the added damping caused by the higher order modes as well as the additional visco-thermal attenuation caused by the increased length of the HQ device. The specific acoustic impedance ratio was measured for a straight pipe during resonance and additionally, with attached HQ devices of varying d/D ratios. It was noted that the HQ device induces an effective travelling wave peak into the main piping system, causing the shift in the total response of the system as well as a mechanism for absorption of acoustic energy. This change in the acoustic impedance was seen to become larger with the increase of the relative diameter ratio of the HQ device, indicating that the change in acoustic particle velocity at the ends of the HQ device is responsible for the increased impedance and acoustic attenuation. It was also seen that the acoustic reflection from both the QWR and the HQ device was very low at the targeted frequency of attenuation such that very little acoustic energy was reflected back to the source. This further solidified the mechanism of attenuation of the HQ device under resonant conditions to be the trapping of energy to within the HQ device to sustain it's own resonant mechanism.

CAA simulations were carried out in order to further consolidate the mechanism of attenuation of the HQ device under resonant conditions. The CAA simulations also allowed for visualization of the acoustic pressure distribution along the HQ device and

the acoustic particle velocity contours within the HQ device. The validation efforts between the experimental acoustic resonance of a straight pipe were successful such that the CAA simulation was able to self couple the acoustic excitation source with the fifth acoustic mode of the piping system. A clear standing wave was formed within the piping system with a good agreement with the experimental measurements. The HQ device was then added to the simulation domain and validation efforts were taken to compare the acoustic pressure time signals experimentally measured within the HQ device to that monitored within the simulation. The results of the CAA simulation were supportive and conclusive to that found in the experiments whereby the self-coupling of the HQ device was achieved and the second acoustic mode of an open-open pipe was seen to materialize within the HQ device. The open-end conditions at the ends of the HQ device was not forced, and were naturally present within the simulation whereby the phasing of 90 degrees was present between the acoustic pressure signal in the main piping system and with that of the end of the HQ device. The relative phasing of the acoustic particle velocity of the HQ device was verified at the ends of the HQ device such that the 180 degree condition is present to satisfy the second acoustic mode of the open-open pipe.

Finally, the HQ device was additionally applied to a travelling wave system whereby the main piping system natural frequencies were not coupled with the acoustic excitation source. It was shown that a well placed HQ device in a resonant system can achieve significantly more attenuation then a HQ device of equal diameter ratio placed in a travelling wave system. The effect of HQ device placement along the axial location of the piping system was found to have less effect when placed in a travelling wave system due to the fact that the acoustic pressure is not changing significantly along the axis of the piping system. The attenuation was noted to be relatively constant as the HQ device was placed at different locations however, there was a special case observed where there was a sharp decrease in attenuation. If the HQ device was placed at an integer multiple of $\frac{\lambda}{2}$ distance away from an adjacent piping component or end condition, constructive

interference could materialize if the length between components was sufficiently small and proved that enough acoustic reflection was present from the boundary. This was the cause of the sharp decrease in attenuation of the HQ device and can be avoided in industrial applications to improve the effectiveness of the device.

7.2 Research Contributions

The thesis in-hand presents a fundamental understanding of the passive damping mechanism of HQ devices for pressure pulsations in piping systems. Several experiments were conducted to advance the knowledge of the acoustics of the HQ device and the following contributions were achieved:

(i) The relative diameter ratio was experimentally proven for the first time to be a good normalization parameter for the measured transmission loss of an HQ device.

(ii) The change in the relative fluid volume ratio of the HQ device relative to the main piping system was quantified and analytically explained using an effective length analogy. The effective length successfully accounted for the change in the total acoustic response of the piping system when implementing various sized HQ devices and multiple devices.

(iii) The mechanism of attenuation of the HQ device was experimentally clarified for the application to a resonant system and further solidified and visualized utilizing CAA simulations.

(iv) Practical considerations for both resonant and travelling wave systems were clarified for applying HQ devices to piping systems.

7.3 Recommendations for Future Work

The work within this thesis focuses on the Mechanism of attenuation of an HQ device applied to an open air loop. The recommendations for future work would be to further validate this concept in a different medium such as water in order to prove the feasibility of the application as well as to understand the possible scaling of attenuation with density, speed of sound and elevated pressure of the medium. For future work, the HQ device could also be applied to other types of resonant systems such as flow excited acoustic resonance of cylinders or single cavities applied to the transverse acoustic modes in a rectangular duct or enclosure.

7.4 Supporting Publications

Journal articles (1)

(i) Lato T., and Mohany A., Passive damping of pressure pulsations in pipelines using Herschel-Quincke tubes, Journal of Sound and Vibration, (Accepted - Minor Revisions. Reference Number: JSV-D-18-01812), 2018.

Referred Conference proceedings (1)

(i) Lato T., and Mohany A., Control of Resonant Excitation in Piping Systems, 9th International Symposium on Fluid-Structure Interactions, Flow-Sound Interactions, Flow-Induced Vibration & Noise, Toronto, 2018.

Bibliography

[1] M Gabbani, R Sejnoha, BA Surette, and E Kohn. Out-reactor bundle endplate fatigue tests: Design evaluation. In *Proceedings of the Canadian Nuclear Society 15, Montréal, Canada*, 1994.

[2] Atef M Mohany. *Flow-sound interaction mechanisms of a single and two tandem cylinders in cross-flow*. ProQuest, 2007.

[3] Nadim Arafa and Atef Mohany. Flow-excited acoustic resonance of isolated cylinders in cross-flow. *Journal of Pressure Vessel Technology*, 138(1):011302, 2016.

[4] Mahmoud Shaaban and Atef Mohany. Passive control of flow-excited acoustic resonance in rectangular cavities using upstream mounted blocks. *Experiments in Fluids*, 56(4):72, 2015.

[5] Ahmed Omer, Nadim Arafa, Atef Mohany, and Marwan Hassan. The effect of upstream edge geometry on the acoustic resonance excitation in shallow rectangular cavities. *International Journal of Aeroacoustics*, 15(3):253–275, 2016.

[6] D. Rockwell and E. Naudascher. Review - Self-sustaining oscillations of flow past cavities. *ASME Transactions Journal of Fluids Engineering*, 100:152–165, June 1978.

[7] RM Baldwin and H Ri Simmons. Flow-induced vibration in safety relief valves. *Journal of pressure vessel technology*, 108(3):267–272, 1986.

[8] KE Widell. Governing valve vibration in a large steam turbine. *Practical Experiences With Flow-Induced Vibrations, E. Naudascher, ed., Springer-Verlag, Berlin*, pages 320–323, 1980.

[9] Tsutomu Shioyama, Daisuke Asakura, Tsuyoshi Kobayashi, Takashi Iseki, and Hideo Hosaka. Coupling vibrations between pipe wall and internal higher-order acoustic wave caused by valve choking. *Transactions of the Japan Society of Mechanical Engineers, Part C*, 61(589):3450–3455, 1995.

[10] Koichi Yonezawa, Ryohei Ogawa, Kanako Ogi, Tomofumi Takino, Yoshinobu Tsujimoto, Takahide Endo, Kenichi Tezuka, Ryo Morita, and Fumio Inada. Flow-induced vibration of a steam control valve. *Journal of Fluids and Structures*, 35:76–88, 2012.

[11] Christopher E Brennen. *Hydrodynamics of pumps*. Cambridge University Press, 2011.

[12] M Morgenroth and DS Weaver. Sound generation by a centrifugal pump at blade passing frequency. *Journal of turbomachinery*, 120(4):736–743, 1998.

[13] R Brownell, R Flack, and G Kostrowsky. Flow visualization in the tongue region of a centrifugal pump. *J. Therm. Eng*, 4(2):35–45, 1985.

[14] Jens Keller, J Parrondo, R Barrio, Joaquín Fernández, and E Blanco. Effects of the pump-circuit acoustic coupling on the blade-passing frequency perturbations. *Applied Acoustics*, 76:150–156, 2014.

[15] Gustav Kirchhoff. Ueber den einfluss der wärmeleitung in einem gase auf die schallbewegung. *Annalen der Physik*, 210(6):177–193, 1868.

[16] Werner Zielke. Frequency-dependent friction in transient pipe flow. *Journal of basic engineering*, 90(1):109–115, 1968.

[17] E Dokumaci. Sound transmission in narrow pipes with superimposed uniform mean flow and acoustic modelling of automobile catalytic converters. *Journal of Sound and vibration*, 182(5):799–808, 1995.

[18] MS Howe. The damping of sound by wall turbulent shear layers. *The Journal of the Acoustical Society of America*, 98(3):1723–1730, 1995.

[19] MCAM Peters, Avraham Hirschberg, AJ Reijnen, and APJ Wijnands. Damping and reflection coefficient measurements for an open pipe at low mach and low helmholtz numbers. *Journal of Fluid Mechanics*, 256:499–534, 1993.

[20] Burns Anderson, Marwan Hassan, and Atef Mohany. Modelling of fluidelastic instability in a square inline tube array including the boundary layer effect. *Journal of Fluids and Structures*, 48:362–375, 2014.

[21] G Rzentkowski and S Zbroja. Experimental characterization of centrifugal pumps as an acoustic source at the blade-passing frequency. *Journal of fluids and structures*, 14(4):529–558, 2000.

[22] V Chatoorgoon and Qizhao Li. A study of acoustic wave damping in water-filled pipes with zero flow and turbulent flow. *Nuclear Engineering and Design*, 239(11):2326–2332, 2009.

[23] A Mohany and M Hassan. Modelling of fuel bundle vibration and the associated fretting wear in a candu fuel channel. *Nuclear Engineering and Design*, 264:214–222, 2013.

[24] XY Huang and DS Weaver. On the active control of shear layer oscillations across a cavity in the presence of pipeline acoustic resonance. *Journal of Fluids and Structures*, 5(2):207–219, 1991.

[25] Benjamin J Zimmer, Stanley P Lipshitz, Kirsten A Morris, John Vanderkooy, and Edmund E Obasi. An improved acoustic model for active noise control in a duct. *Journal of dynamic systems, measurement, and control*, 125(3):382–395, 2003.

[26] Samir Ziada. Control of fluid-structure-sound interaction mechanisms by means of synthetic jets. *JSME International Journal Series C Mechanical Systems, Machine Elements and Manufacturing*, 46(3):873–880, 2003.

[27] R Burdisso and J Smith. Control of inlet noise from turbofan engines using herschel-quincke waveguides. In *6th Aeroacoustics Conference and Exhibit*, page 1994, 2000.

[28] Dan Zhao and Aimee S Morgans. Tuned passive control of combustion instabilities using multiple helmholtz resonators. *Journal of sound and vibration*, 320(4-5):744–757, 2009.

[29] Vidya Sagar and ML Munjal. Analysis and design guidelines for fork muffler with h-connection. *Applied Acoustics*, 125:49–58, 2017.

[30] William M Ihde. Tuning stubs to silence large air handling systems. *Noise Control Engineering*, 5(3):131–136, 1975.

[31] W Neise and GH Koopmann. Reduction of centrifugal fan noise by use of resonators. *Journal of Sound and Vibration*, 73(2):297–308, 1980.

[32] Omar Sadek, Mahmoud Shaaban, and Atef Mohany. Suppression of acoustic resonance in piping system using passive control devices. *Journal of Canadian Acoustic*, 42(3):58–59, 2014.

[33] M Abdelmwgoud, M Shaaban, N Arafa, K Sachedina, A Mohany, and M Hassan. Use of helmholtz resonators to suppress acoustic pressure pulsations in pipelines. In *37th Annual Conference of the Canadian Nuclear Society, Niagara Falls, Canada*, 2017.

[34] Karim Sachedina, Atef Mohany, and Marwan Hassan. Suppression of acoustic resonance in pipelines using helmholtz resonators. In *Proceedings of the 9th International Symposium on Fluid-Structure Interactions, Flow-Sound Interactions, Flow-Induced Vibration Noise, Toronto, Canada*, 2018.

[35] Raphaël F Hallez. *Investigation of the herschel-quincke tube concept as a noise control device for turbofan engines*. PhD thesis, Virginia Tech, 2001.

[36] Lori Ann Brady. *Application of the herschel-quincke tube concept to higher-order acoustic modes in two-dimensional ducts*. PhD thesis, Virginia Tech, 2002.

[37] John FW Herschel. Lxiii. on the absorption of light by coloured media, viewed in connexion with the undulatory theory. *Philosophical Magazine Series 3*, 3(18):401–412, 1833.

[38] Georg Quincke. Ueber interferenzapparate für schallwellen. *Annalen der Physik*, 204(6):177–192, 1866.

[39] GW Stewart. The theory of the herschel-quincke tube. *Physical Review*, 31(4):696, 1928.

[40] A Selamet, NS Dickey, and JM Novak. The herschel–quincke tube: a theoretical, computational, and experimental investigation. *The Journal of the Acoustical Society of America*, 96(5):3177–3185, 1994.

[41] Ahmet Selamet and Paul M Radavich. Effect of expansion chamber on the resonance frequency of side branches and herschel-quincke tubes. *ASME NCA*, 22:127–132, 1996.

[42] A Selamet and V Easwaran. Modified herschel–quincke tube: Attenuation and resonance for n-duct configuration. *The Journal of the Acoustical Society of America*, 102(1):164–169, 1997.

[43] Steve Griffin, Steve Huybrechts, and Steven A Lane. An adaptive herschel-quincke tube. *Journal of intelligent material systems and structures*, 10(12):956–961, 1999.

[44] Jose S Alonso, Ricardo A Burdisso, Douglas Ivers, and Hwa W Kwan. Adaptive concepts for herschel–quincke waveguides. *Journal of Vibration and Acoustics*, 135(3):031016, 2013.

[45] AJ Torregrosa, A Broatch, and R Payri. A study of the influence of mean flow on the acoustic performance of herschel–quincke tubes. *The Journal of the Acoustical Society of America*, 107(4):1874–1879, 2000.

[46] ML Munjal. Acoustics of ducts and mufflers with application to exhaust and ventilation design, 1987.

[47] Mikael Karlsson, Ragnar Glav, and Mats Åbom. The herschel–quincke tube: The attenuation conditions and their sensitivity to mean flow. *The Journal of the Acoustical Society of America*, 124(2):723–732, 2008.

[48] Douglas H Keefe and Arthur H Benade. Wave propagation in strongly curved ducts. *The Journal of the Acoustical Society of America*, 74(1):320–332, 1983.

[49] Michael Mark James. *Fundamental Studies of the Herschel-Quinke Tube Concept with Mode Measurements*. PhD thesis, Virginia Tech, 2003.

[50] Z Tao and AF Seybert. A review of current techniques for measuring muffler transmission loss. Technical report, SAE Technical Paper, 2003.

[51] ML Munjal and AG Doige. Theory of a two source-location method for direct experimental evaluation of the four-pole parameters of an aeroacoustic element. *Journal of Sound and Vibration*, 141(2):323–333, 1990.

[52] E ASTM. 1050-90. standard test method for impedance and absorption of acoustical

materials using a tube, two microphones, and a digital frequency analysis system. *American Society for Testing and Materials, Philadelphia, PA*, 1990.

[53] KS Andersen. Analyzing muffler performance using the transfer matrix method. In *COMSOL Conf., Hannover*, 2008.

[54] Finn Jacobsen. Propagation of sound waves in ducts. 2000.

[55] Harold Levine and Julian Schwinger. On the radiation of sound from an unflanged circular pipe. *Physical review*, 73(4):383, 1948.

[56] S Rao Singiresu et al. *Mechanical vibrations*. Addison Wesley, 1995.

[57] TK Caughey and MEJ O'kelly. Effect of damping on the natural frequencies of linear dynamic systems. *The Journal of the Acoustical Society of America*, 33(11):1458–1461, 1961.

[58] CD Field and FR Fricke. Theory and applications of quarter-wave resonators: A prelude to their use for attenuating noise entering buildings through ventilation openings. *Applied Acoustics*, 53(1-3):117–132, 1998.

[59] Lawrence E Kinsler, Austin R Frey, Alan B Coppens, and James V Sanders. Fundamentals of acoustics. *Fundamentals of Acoustics, 4th Edition, Wiley-VCH*, page 560, 1999.